

# **Actuator-Work Concepts Applied to Morphing and Conventional Aerodynamic Control Devices**

by

**Christopher O. Johnston**

Thesis Submitted to the Faculty of the  
Virginia Polytechnic Institute and State University  
in partial fulfillment of the requirements for the degree of

Master of Science

in

Aerospace Engineering

Dr. William H. Mason, Chair  
Dr. Daniel J. Inman  
Dr. Harry H. Robertshaw

November 14, 2003  
Blacksburg, Virginia

Keywords: morphing aircraft, aerodynamics, thin airfoil theory

Copyright 2003, Christopher O. Johnston

# Abstract

The research presented in this thesis examines the use of an estimated “actuator work” value as a performance parameter for the comparison of various aerodynamic control device configurations. This estimated “actuator work,” or practical work as it will be referred to as in this thesis, is based on the aerodynamic and structural resistance to a control surface deflection. It is meant to represent the actuator energy cost required to deflect a general configuration of conventional or unconventional control surface. Thin airfoil theory is used to predict the aerodynamic load distribution required for this work calculation. The details of applying thin airfoil theory to many different types of control surface arrangements are presented. Convenient equations for the aerodynamic load distributions and aerodynamic coefficients are obtained. Using the developed practical work equations, and considering only the aerodynamic load component, the practical work required for a given change in lift is compared between different control surface arrangements. For single control surface cases, it is found that a quadratic (morphing) trailing edge flap requires less practical work than a linear flap of the same size. As the angle of attack at which the change in lift occurs increases, the benefit of the quadratic flap becomes greater. For multiple control surface cases, it is necessary to determine the set of control deflections that require the minimum practical work for a given change in lift. For small values of the initial angle of attack, it is found that a two-segment quadratic trailing edge flap (MTE) requires more work than a two-segment linear flap (TETAB). But, above a small value of angle of attack, the MTE case becomes superior to the TETAB case. Similar results are found when a 1-DOF static aeroelastic model is included in the calculation. The minimum work control deflections for the aeroelastic cases are shown to be strongly dependent on the dynamic pressure.

# Acknowledgements

I would like to thank Dr. Mason for his generous guidance and support. Without his high standards and insightful criticism, the quality of this work would be greatly reduced. I would also like to thank Dr. Inman and Dr. Robertshaw for their suggestions and help. Also, the rest of the “morphing” group deserves my thanks for their willingness to discuss many of the problems confronted in this work. In particular, I would like to thank Dr. Bae for reviewing this manuscript and providing suggestions. Last but not least, I would like to thank my parents for their wisdom and support.

# Table of Contents

<b>Chapter 1</b>	<b>Introduction and Overview of Morphing Aircraft</b>	<b>1</b>
1.1	Motivation . . . . .	1
1.2	Overview of Morphing. . . . .	2
1.3	Past Morphing Research . . . . .	3
1.4	Overview of Thesis . . . . .	8
<b>Chapter 2</b>	<b>Actuator Work for an Aerodynamic Control Device</b>	<b>9</b>
2.1	Introduction . . . . .	9
2.2	Calculating the Work Required by an Actuator to Operate an Aerodynamic Control Devices . . . . .	9
2.3	The Work Required to Overcome the Aerodynamic and Structural Forces . . . . .	12
2.4	The Practical Work for an Aerodynamic Control Device . . . . .	14
2.5	Chapter Summary . . . . .	19
<b>Chapter 3</b>	<b>An Analysis of Control Surface Aerodynamic Characteristics Using Thin Airfoil Theory</b>	<b>20</b>
3.1	Introduction . . . . .	20
3.2	A Review of Thin Airfoil Theory . . . . .	21
3.3	Modeling an Airfoil with a Trailing-Edge Flap . . . . .	22
3.4	Modeling an NACA 4-Digit Camberline . . . . .	26
3.5	Influence of a Leading-Edge Flap on a Flapped Airfoil . . . . .	31
3.6	Modeling a Two-Segment Trailing-Edge Flap . . . . .	33

3.7	Modeling a Morphing Trailing-Edge Device . . . . .	35
3.8	Trim Considerations . . . . .	41
3.9	Chapter Summary . . . . .	43
<b>Chapter 4 The Minimum Aerodynamic Work for an Airfoil Geometry Change</b>		<b>44</b>
4.1	Introduction . . . . .	44
4.2	Minimum Work Control Deflections Required for a Single $\Delta C_l$ Away from an Initially Flat Airfoil . . . . .	45
4.3	Minimum Work Control Deflections Required for a Single $\Delta C_l$ on an Airfoil with an Initial $\alpha$ . . . . .	52
4.4	Minimum Work Control Deflections for Multiple $\Delta C_l$ 's . . . . .	55
4.5	The Minimum Work for a LETE Configuration . . . . .	56
4.6	Chapter Summary . . . . .	59
<b>Chapter 5 The Effect of Aeroelasticity on the Required Aerodynamic Work</b>		<b>60</b>
5.1	Introduction . . . . .	60
5.2	Aeroelastic Considerations . . . . .	60
5.3	Required Work for Single Control Surface Cases . . . . .	65
5.4	Required Work for Multiple Control Surface Cases . . . . .	68
5.5	Chapter Summary . . . . .	71
<b>Chapter 6 Conclusions</b>		<b>72</b>
6.1	Brief Summary of Thesis . . . . .	72
6.2	Contributions . . . . .	74
6.3	Future Work . . . . .	75
<b>References</b>		<b>76</b>
<b>Appendix A</b>		<b>81</b>

# List of Figures

1.1	Reasons for Variable Sweep Applications [Kress 1983] . . . . .	3
1.2	$L/D_{MAX}$ and $C_{D0}$ vs. Sweep [Kress 1983] . . . . .	4
1.3	AFTI/F-111 Layout [Smith 1990] . . . . .	5
1.4	Influence of variable camber on the $L/D$ [Monner 2001] . . . . .	6
2.1	Example layout of control devices on an airfoil and the resulting $\Delta p$ distribution. . . . .	10
2.2	The possible variations of $I$ with $\tau$ . . . . .	16
2.3	Analogy for the interaction of work for linked control surfaces . . . . .	18
3.1	Geometric representation of a flapped-airfoil . . . . .	48
3.2	Example load distribution . . . . .	49
3.3	The work per-unit length for a flapped-airfoil . . . . .	50
3.4	NACA camberline representation . . . . .	51
3.5	Load distribution validation . . . . .	29
3.6	Work per-unit length for a variable camber NACA airfoil . . . . .	30
3.7	Aerodynamic work required to go from a flat airfoil to a cambered or flapped airfoil. . . . .	31
3.8	Airfoil with a leading and trailing edge flap . . . . .	31
3.9	Load distribution comparison of a LE and TE flap. . . . .	32
3.10	Airfoil with a two-segment trailing-edge flap . . . . .	33
3.11	Load distribution for a two-segment trailing edge flap . . . . .	35
3.12	Representation of the morphing trailing edge device . . . . .	36
3.13	A comparison of the trailing-edge camberline shapes required for a $C_l = 0.1$ . . . . .	39
3.14	A comparison of the trailing-edge load distribution required for a $C_l = 0$ . . . . .	39
3.15	A comparison of the work per-unit length required for a $C_l = 0.1$ . . . . .	40
3.16	A comparison of the required work for a $\Delta C_l = 0.1$ . . . . .	40
3.17	Effect of control deflections on the trimmed $C_L$ of a stable configuration . . . . .	43
4.1	Work integrands for a TETAB airfoil . . . . .	46

4.2	Work integrands for a TETAB airfoil . . . . .	48
4.3	Minimum work values for various control surface arrangements . . . . .	49
4.4	Minimum work values for various ratios of control surface size . . . . .	49
4.5	Minimum work ratio of deflections for the case shown in Figure 4.4 . . . . .	50
4.6	Minimum work values for various ratios of control surface size with trim constraint . . .	52
4.7	Minimum work deflections corresponding to Figure 4.6 . . . . .	52
4.8	The effect of a constant $\alpha$ on the minimum required work . . . . .	54
4.9	Minimum work control deflection variation with a constant $\alpha$ . . . . .	54
4.10	Minimum work values with an initial $\alpha$ and allowing $\alpha$ to vary . . . . .	55
4.11	Variation of desired lift coefficients . . . . .	56
4.12	The influence of the second $\Delta C_l$ on the minimum work . . . . .	56
4.13	Work required to achieve $C_{l,1} = 0$ , $C_{l,2} = 0.1$ and $C_{l,3} = 0$ . . . . .	58
4.14	Load distributions at state 2. . . . .	58
4.15	Load distributions at state 3. . . . .	59
5.1	Flexible airfoil representation . . . . .	61
5.2	Example load distributions including aeroelastic effects . . . . .	62
5.3	Roll rate achieved for a constant aileron deflection [Anderson, <i>et al.</i> 1997] . . . . .	64
5.4	Aileron deflection required for a constant roll rate [Anderson, <i>et al.</i> 1997] . . . . .	64
5.5	Control surface deflections required for a constant roll rate [Anderson, <i>et al.</i> 1997] . . .	65
5.6	The effect of dynamic pressure on the required aerodynamic work for a given $\Delta C_l q c$ . . . . .	66
5.7	The effect of dynamic pressure on the deflection angle for a given $\Delta C_l q c$ . . . . .	67
5.8	The effect of dynamic pressure on the wing deformation angle for a given $\Delta C_l q c$ . . . . .	67
5.9	The effect of dynamic pressure on the work for a given $\Delta C_l q c$ at $\alpha_0 = 1$ degree . . . . .	68
5.10	The effect of dynamic pressure on the required work with multiple control surfaces . . . . .	69
5.11	The effect of dynamic pressure on the deformation with multiple control surfaces . . . . .	69
5.12	The effect of dynamic pressure on the minimum work control deflections . . . . .	70
5.13	The effect of dynamic pressure on the minimum work control deflections . . . . .	70

# Nomenclature

- $\alpha$  = angle of attack  
 $a$  = flap-to-chord ratio  
 $A_n$  = Fourier coefficients used to represent the load distribution, defined in Eqs. (3.3 – 3.5)  
 $\beta$  = general control surface deflection  
 $c$  = chord length  
 $C_l$  = airfoil lift coefficient ( $l/qc$ )  
 $C_M$  = airfoil pitching moment coefficient ( $m/qc^2$ )  
 $C$  = force resisting a control surface motion at a point  $x$ , defined in Eq. (2.6)  
 $\delta$  = control surface deflection angle (used in Chapter 3)  
 $f$  =  $\Delta z/\beta$ , represents the  $\Delta z$  per-unit deflection of  $\beta$  along the chord  
 $F$  = structural force resisting a control surface deflection  
 $\gamma$  = vorticity or load distribution ( $\Delta C_p = 2\gamma/U$ )  
 $\eta$  = represents the cost of negative work relative to positive work, defined in Eq. (2.10)  
 $I$  = integrand of the  $\overline{W}$  equation, defined in Eq. (2.11)  
 $k$  =  $x$  location of the flap hinge line (Figure 3.1)  
 $K$  = distribution of internal structural forces per-unit  $\beta$   
 $l$  = total airfoil lift  
 $m$  = pitching moment about the  $1/4$  chord point  
 $M$  = magnitude of maximum camber for a NACA camberline  
 $\Delta p$  = difference between the pressure on the upper and lower airfoil surface  
 $P$  = location of maximum camber for a NACA camberline  
 $q$  = dynamic pressure ( $1/2 \rho U^2$ )  
 $Q$  = defined in Eqs. (2.12 and 2.18), represents the hinge moment for a linear control surface  
 $\rho$  = density of air  
 $\tau$  = nondimensional time used to define the path between the initial and final states  
 $\theta$  = defined in Eq. (3.2), represents the location  $x$  along the airfoil chord

$U$  = free-stream velocity

$W$  = practical actuator work, defined in Eq. (2.10)

$\bar{W}$  = basic actuator work, defined in Eq. (2.9)

$\bar{w}$  = basic work per-unit length, defined in Eq. (2.8)

### Superscripts

+ = positive component

- = absolute value of the negative component

### Subscripts

$a$  = additional load distribution

$b$  = basic load distribution

$A$  = control surface  $A$

$B$  = control surface  $B$

$D$  = divergence

LE = leading edge

$R$  = reversal

TE = trailing edge

# Chapter 1

## Introduction and Overview of Morphing Aircraft

### 1.1 Motivation

The modern aircraft designer is faced with increasingly conflicting design requirements. Designing for efficient subsonic and supersonic cruise, high maneuverability, and low radar signature requires many trade-offs [Waaland 1991]. This leads to an aircraft that, at a given flight condition, is not as good as an aircraft designed specifically for that condition. If an aircraft has the ability to continuously transform into the design that is optimal for its current flight condition, its mission capability and superiority over hostile aircraft will be unmatched [Herbst 1973, 1980 and 1983]. For military applications this has become the motivating factor in the development of variable geometry aircraft, or as they are called today, morphing aircraft.

The current military interest in unmanned air vehicles (UAVs) has been a strong motivating factor in the research devoted to morphing aircraft [Fulghum 2003]. The removal of the pilot from the system means that human limitations no longer need to be considered, and also allows for the removal of the volume required for the crew station. This allows for new aircraft concepts with extremely high maneuverability and very long flight times. Morphing can be used to achieve optimal performance over this wide range of conditions. According to Fulghum [2003], “by 2027 UAVs may have morphing airframes that can optimize their shape for various missions and flight

conditions.” He also mentions the use of shape memory alloys (SMAs) for actuating the morphing structure.

The recent development of smart materials such as SMAs has been a driving factor in the recent interest in morphing aircraft. For years aerodynamicists have recognized the benefits of a bird’s ability to manipulate its wings for various flight regimes [Tucker 1970]. But mimicking this ability with aircraft has not been successful, mainly because of the structural considerations. It is possible that smart materials will finally enable the difficult combination of lightweight, flexibility, and strength in an aircraft structure [Wlezien *et al.* 1998].

## 1.2 Overview of Morphing

There are two main categories of morphing: mission morphing and flight-control morphing. Mission morphing is usually defined as a large change in an aircraft’s geometry to optimize itself for a changing flight regime. Flight-control morphing is generally thought of as a smooth, unhinged change in an aircraft’s geometry for the purpose of control or maneuvering. In many cases, there is not a clear distinction between mission and flight-control morphing. For example, a smooth trailing-edge control surface on a wing could be used for both minimizing drag for various flight conditions as well as acting as an efficient aileron. It is curious that in defining mission and flight-control morphing, only flight-control morphing required a smooth or unhinged change in geometry.

The Wright Brothers were the first to use morphing, in the form of wing warping, on their early gliders as well as on the Wright Flyer [Culick 2003]. This was an example of flight-control morphing, which was used to perform roll maneuvers and allow the airplane to turn. This method of control was not chosen for its performance benefits, but instead because it was the easiest to implement on a relatively flexible wing. As aircraft became heavier and wings became stiffer, wing warping was no longer practical and it soon gave way to ailerons.

An early case of mission morphing was NACA’s X-5 variable sweep aircraft, which began in 1948. This aircraft had the ability to change the wing sweep-angle during flight to optimize its transonic performance [Kress 1983]. Many variable sweep aircraft followed the X-5 program in both the U.S. and abroad. The most recent U.S. variable sweep design, from the late 1970s, is the Rockwell B-1 Bomber.

### 1.3 Past Morphing Research

As mentioned above, other than the wing warping used by the Wright Brothers, the first use of morphing was in variable sweep wing aircraft. Figure 1.1 [Kress 1983] shows the reasons for the use of variable sweep in U.S. aircraft. This figure shows that, excluding the X-5, all of these aircraft used variable sweep for low takeoff and landing speeds, delaying the transonic drag rise, supersonic drag, and minimum design weight. Morphing in these cases allowed the aircraft to fly effectively at low speeds as well as at transonic and supersonic speeds. Figure 1.2 shows how a sweep change affects the  $L/D$  and  $C_{D0}$ . This clearly shows the penalty resulting from being restricted to a single sweep angle as speeds approach the transonic regime.

	X-5	XF10F-1	F-111	F-14	B-1
Low Takeoff and Landing Speeds		X	X	X	X
Subsonic Cruise			X	X	X
Transonic Characteristics	X				
- L/D				X	X
- Drag Rise		X	X	X	X
- Buffet Onset and Intensity				X	
Maneuvering CLmax				X	
Supersonic Drag		X	X	X	X
Wing Design Load Relief				X	
Research	X				
Minimum Design Weight		X	X	X	X

Figure 1.1: Reasons for Variable Sweep Applications [Kress 1983]

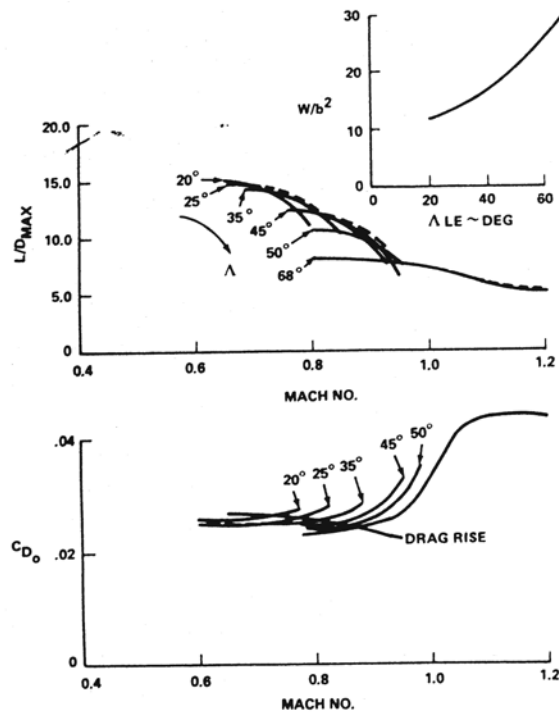


Figure 1.2:  $L/D_{MAX}$  and  $C_{D0}$  vs. Sweep [Kress 1983]

The Advanced Fighter Technology Integration (AFTI) F-111 was a joint Air Force, NASA, and Boeing project in the early 1980s to develop a smooth variable camber aircraft. As shown in Figure 1.3, this aircraft used six independent trailing edge sections and two leading edge sections for both control and wing shape optimization [Smith 1990]. Electro-hydraulic rotary actuators and a flexible composite skin were used to achieve smooth camber variation. The variable camber capability was utilized through a control system consisting of four operating modes. The Maneuver Camber Control (MCC) mode selected the best leading and trailing edge camber combinations for maximum  $L/D$  as a function of flight condition. This system used wind-tunnel data stored in tables with lift coefficient, wing sweep, and Mach number as the lookup parameters. Cruise Camber Control (CCC) mode was designed to maximize velocity at constant altitude and throttle setting. This closed-loop mode performed an iterative process of changing the trailing edge camber until maximum velocity was achieved. Maneuver Load Control (MLC) mode measured the wing-root bending moment and adjusted the camber on the outboard wing to concentrate the loading towards the root. This allows the wing weight to be decreased for a given  $g$  capability. The Maneuver Enhancement/Gust Alleviation (MEGA) mode used the variable leading and trailing edge camber capability to quicken aircraft response [Bonnema 1988, Smith 1987]. The predicted benefits of these control modes were a 20% increase in range, a 15%

increase in maximum ceiling, and a 20% increase in subsonic sustained turn rate [Smith 1986]. Whether these goals were ever achieved has not been published. Smith [1990] does present a comparison of the F-111 with the variable camber wing and with a conventional wing. An 8% reduction in drag at the design point and a 20% reduction at off-design points were shown.

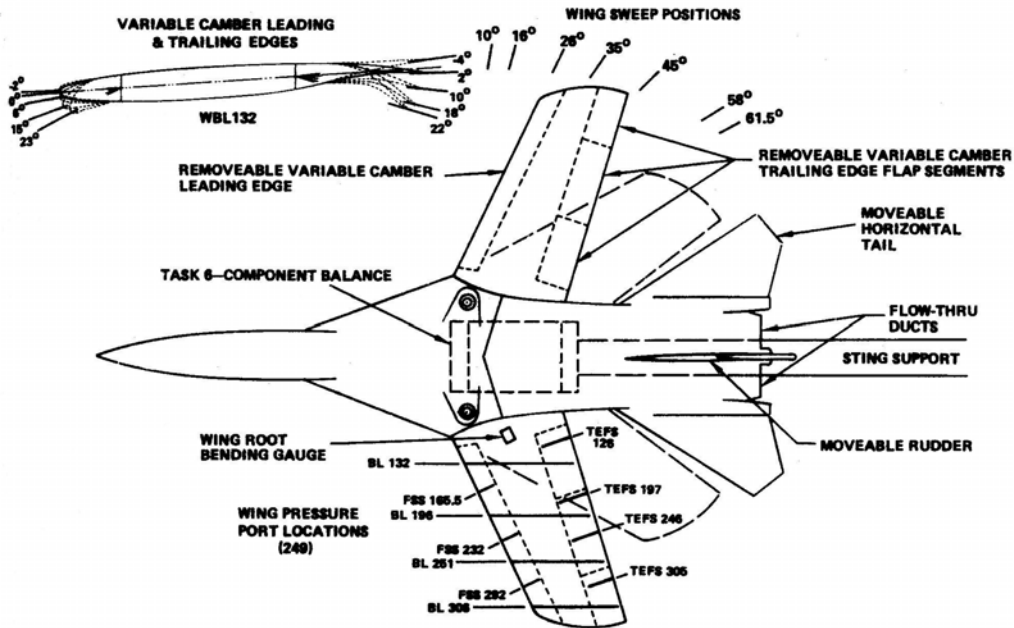


Figure 1.3: AFTI/F-111 Layout [Smith 1990]

Many researchers have studied the use of variable camber, similar to that of the AFTI/F-111, on transport aircraft. The main objective of this research has been to increase the  $L/D$  over a wide range of lift coefficients as shown in Figure 1.4 [Monner 2001]. It is seen that not only does variable camber have the ability to increase the range of lift coefficients over which low drag is obtained, but it is also able to decrease the minimum drag point (drag at the design point) because structural load restrictions are decreased [Szodruch 1985, Renken 1985]. The structural load restrictions are decreased because variable camber allows for the aerodynamic loads to be distributed in a way that minimizes the root bending moment on the wing.

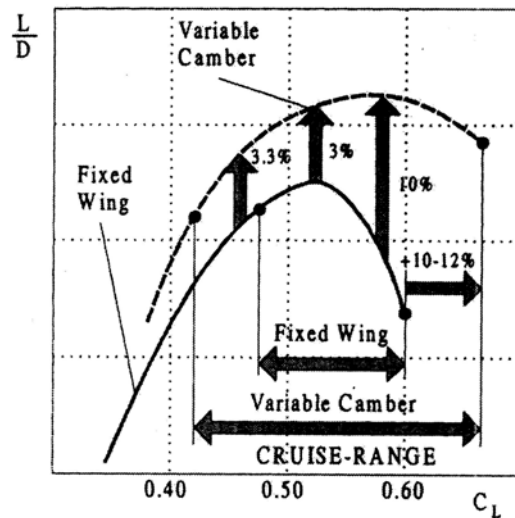


Figure 1.4: Influence of variable camber on  $L/D$  [Monner 2001]

Greff [1990] discusses the ability of variable camber to improve the operational flexibility of an aircraft by delaying the buffet boundary. He also mentions that variable camber will allow the same wing to be used optimally on many different aircraft. Spillman [1992] emphasizes the use of independent control of camber along the span to tailor spanloads to various flight conditions. He discusses the importance of separating the lift due to incidence to that due to camber. This idea is important when considering various flight conditions where different angles of attack and control deflections are required. Martins [1996, 1997, and 2000] followed the work of Greff and Spillman by implementing a formal optimization scheme to a variable camber transport aircraft. A vortex lattice method coupled with a strip boundary layer analysis was used for the aerodynamic predictions. The optimization procedure used is discussed in Martins [1996].

A topic of recent interest is the amount of work required to overcome the aerodynamic forces for control surface deflections. Pettit *et al.* [2001] presented a model to compute the aerodynamic work for an entire aircraft configuration. A modified lifting line combined with conformal mapping was used for the aerodynamic analysis. There was a brief mention of reversible and irreversible work in the presentation of some of his work results. He called the reversible work the work required if the work provided by the airstream is able to be captured and stored as usable work. The irreversible work was the total work if the work provided by the airstream could not be captured. It will be shown in this thesis that the distinction between reversible and irreversible work is not this simple, and it actually depends on how the wing is actuated.

Henderson *et al.* [2001] briefly discusses aerodynamic work in his study of adaptive control surfaces. A comparison is presented of the work required for a wing to deflect a full-span flap 1-degree for different planforms. His conclusion was that high aspect ratio wings are favorable for low aerodynamic work. This conclusion is not directly applicable to this study because the comparison was made with a constant flap deflection, and not a constant  $\Delta C_l$  between the different cases.

Prock *et al.* [2002] presented the first entire paper devoted to investigating aerodynamic work. This paper emphasized the effect of aeroelasticity on the required work. It was shown that for a simple flapped-airfoil with a torsional spring, there is a dynamic pressure where the flap can be deflected with no required work. This deflection results in a negative change in lift because it occurs at a dynamic pressure larger than the reversal dynamic pressure. He also investigated the distribution of trailing edge deflections for a 3-D wing including aeroelastic effects. This showed that the ability to distribute control deflections along the span reduced the required work by concentrating deflections in regions of greatest effectiveness. All cases involved the work required to produce lift away from an initially flat wing. It will be shown in this thesis that the work away from an initially flat (non-lifting) wing is significantly different than that away from an initially lifting wing.

Gern *et al.* [2002] investigated the actuation energy considering both the structural and aerodynamic work values. A vortex lattice method was used for the aerodynamic work while a NASTRAN model calculated the structural work. This analysis showed that camber and twist actuation was able to obtain larger rolling moments because of their reduced aeroelastic influence. At low dynamic pressures, it was shown that the flap required significantly less aerodynamic work because there was no structural work component. As the dynamic pressure increases though, the flap effectiveness is decreased as the aileron reversal condition is approached resulting in large deflections to maintain the given roll-rate. The twist and camber actuation schemes are not as adversely effected by aeroelastics. Therefore, as the dynamic pressure increases, the required twist and camber deflections decrease resulting in a decrease in the structural work.

Forster *et al.* [2003] analyzed trailing-edge morphing and conventional flaps using thin airfoil theory. Aeroelastic effects were included using a spring at the shear center of the airfoil. It was

shown that a morphing trailing edge device could reduce the aerodynamic work by deflecting like a conventional flap-tab combination.

## 1.4 Overview of Thesis

This thesis investigates the actuator work required for conventional and morphing control devices. A fundamental analytic study is made using incompressible, inviscid aerodynamics. Chapter 2 begins by discussing the force components that contribute to the required actuator work for a general aerodynamic control device. A method of calculating the actuator work is derived considering linear structural and aerodynamic force components. The difference between positive and negative actuator work is discussed and incorporated in the work derivation. Because of the difference between positive and negative work, it is emphasized that the structural and aerodynamic work must be considered together.

Chapter 3 reviews and extends thin airfoil theory for use as the aerodynamic model for the work calculation derived in Chapter 2. This theory is used instead of a more accurate numerical method because it provides an analytic representation of the aerodynamic load distribution and force coefficients. The theory is applied to an airfoil with a trailing-edge flap, an NACA camberline, a leading edge flap, a two-segment trailing edge flap (TETAB), and a morphing trailing edge flap (MTE). It is shown that the morphing flap requires less aerodynamic work than a standard flapped airfoil. The addition of a trim constraint is discussed at the end of this chapter.

Chapter 4 uses the work model developed in Chapter 2 to find the control deflections required for the minimum aerodynamic work. An analytic solution is obtained for the minimum work control deflections for a two-segment trailing edge flap and a morphing flap to obtain a  $\Delta C_l$  away from an initially flat ( $\alpha = 0$ ) configuration. The effect of an initial  $C_l$  on the required work is investigated and shown to dramatically effect the minimum work control deflections. The morphing trailing edge flap is shown to be superior to the two-segment trailing edge flap as the initial  $C_l$  is increased. The minimum work control deflections for two  $\Delta C_l$ 's are investigated and shown to be related to those for a single  $\Delta C_l$ . For the initially flat case, an analytic solution for these deflections is obtained. Chapter 5 extends the analysis of Chapter 4 to include static aeroelastic effects.

# Chapter 2

## Actuator Work for an Aerodynamic Control Device

### 2.1 Introduction

This chapter examines the concept and calculation of the mechanical work required to operate an aerodynamic control device. A general theory will be presented that accounts for both the aerodynamic and structural resistance to a change in airfoil geometry. This theory will assume that both of these components are linear with respect to the parameter representing the geometry change. The concept of negative actuator work will be discussed and its implications to the required actuator work will be included in the theory. Results using the procedure discussed in this chapter will be presented and discussed in the following chapters.

### 2.2 Calculating the Work Required by an Actuator to Operate an Aerodynamic Control Device

Consider a layout of control devices on an airfoil as shown in Figure 2.1. Here, three control devices are shown, a morphing flap (A) and a trailing edge flap-tab combination (B and C). The figure shows that each surface is actuated by a separate actuator, a fact that will be shown to be important. Note that Figure 2.1 shows only the camberline of the airfoil, and not the distribution

of thickness. Thickness will be neglected in this analysis because, to the first order, it does not contribute to lift. Now, it is desired to calculate the mechanical work required by the actuators to achieve a change in  $\beta_A$ ,  $\beta_B$ , and  $\beta_C$ ; where the  $\beta$ 's represent the state of each control device (in these cases they represent the deflection angle). This calculation requires knowledge of the forces acting on the actuator during the change from the initial  $\beta$  value to the final  $\beta$  value, and the details of the change in geometry implied by a change in  $\beta$ .

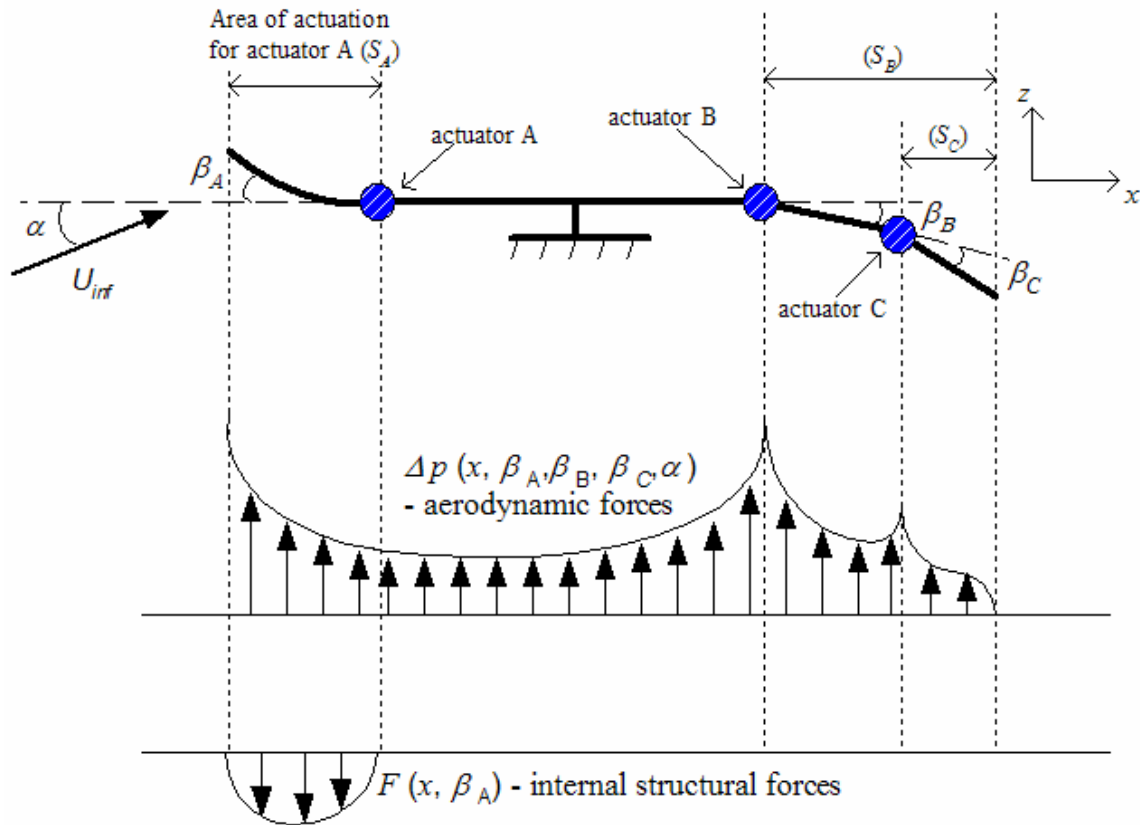


Figure 2.1: Example layout of control devices on an airfoil and the resulting  $\Delta p$  distribution

The forces resisting a change in  $\beta$  are the aerodynamic forces, internal structural forces, and inertial forces. The aerodynamic forces on an airfoil consist of both a lift and drag component. The present analysis ignores the viscous drag component, which produces a negligible net force in the direction of actuation. In general though, viscous effects have a significant influence on the normal (pressure) force, especially when the  $\beta$ 's become large, so we assume that the  $\beta$ 's remain small in this analysis. Another assumption that will be used throughout this analysis is that the shape change occurs slowly enough so that the unsteady component of the aerodynamic forces

can be ignored. Quasi-steady aerodynamics are therefore assumed. The assumption of a slow shape change process also allows us to neglect inertial forces.

With these assumptions on the magnitude and rate of change of  $\beta$ , the aerodynamic forces may be calculated with classical steady thin airfoil theory. These details will be presented in Chapter 3. Thus, in this analysis the pressure distribution, or more specifically the  $\Delta p$  distribution, is assumed to be linear with respect to the  $\beta$ 's. This linearity allows the  $\Delta p$  distribution to be separated into components resulting from each of the control surfaces and the angle of attack ( $\alpha$ ). Therefore, linear superposition of pressures can be used, and the pressure distribution can be written as

$$\Delta p(x) = \sum_{n=1}^N \Delta p_{\beta_n}(x) \beta_n + \Delta p_{\alpha}(x) \alpha \quad (2.1)$$

where  $\Delta p_{\beta_n}$  and  $\Delta p_{\alpha}$  are the derivatives of  $\Delta p$  with respect to  $\beta_n$  and  $\alpha$ , with the subscript  $n$  representing one of the  $N$  control surfaces. For the configuration shown in Figure 2.1,  $N=3$  and control surfaces A, B, and C correspond to  $n = 1, 2,$  and  $3$ .

The internal structural forces acting on an aerodynamic control device depend on the details of the structure being deformed. In many cases, such as the conventional flap-tab combination shown in Figure 2.1, a hinge is used so that no internal structural forces resist a change in  $\beta$ . The focus of this study is not on the calculation of the structural force component. This is because unlike the aerodynamic force, which depends only on the external shape of the airfoil (or in this case, the camberline), the structural force depends on the details of the internal structure. Nevertheless, an approximate model will be considered by assuming an elastic material and recalling the restriction that  $\beta$  remain small. The distribution of the actuator force required to overcome the internal structural forces will be represented as

$$F(x) = \sum_{n=1}^N K_n(x) (\beta_n - \beta_{0n}) \quad (2.2)$$

where  $K_n$  is the distribution of internal forces per-unit  $\beta_n$ , and  $\beta_{0n}$  is the value of  $\beta_n$  at which the structure is undeformed (or unstrained). This model is simplified in that it does not account for the camberline deformation caused by the aerodynamic forces. This is accepted because the structure aeroelastics are not the focus of this analysis. It should be mentioned that because each control surface has been defined to be actuated by only one actuator, the actuator must be

distributed or some type of mechanism must be attached to the actuator to obtain shapes such as the morphing flap (A) in Figure 2.1.

Once all of the internal and external forces are known as a function of  $\beta$  (or  $\beta$ 's) and  $x$ , it is necessary to specify the distance that each actuator moves the control surface between the initial and final states. Figure 2.1 labels an “area of actuation” ( $S$ ) for each of the actuators. This area of actuation refers to the length of the chord that is displaced or moved by the actuator. Over this area of actuation, a function  $f(x)$  is defined for each actuator which represents the  $\Delta z(x)$  produced per-unit  $\beta$  of that control surface. The correct definition of  $f(x)$  is important to correctly calculate the aerodynamic work, especially for configurations such as the trailing edge flap-tab combination shown in Figure 2.1. For this case, the area of actuation of actuator B ( $S_B$ ) overlaps that of actuator C ( $S_C$ ). This means that the  $\Delta z(x)$  produced per-unit  $\beta_C$  must be taken relative to  $\beta_B$ , which is implied in the definition of  $\beta_C$  in Figure 2.1.

## 2.3 The Work Required to Overcome the Aerodynamic and Structural Forces

The previous section discussed the assumptions resulting in a linear representation of aerodynamic and structural forces with respect to the control parameter  $\beta$ . The deflection at each point along the chord is defined in  $f(x)$ , where

$$\Delta z(x) = f(x)\beta \quad (2.3)$$

which is zero for points not in the area of actuation and non-zero for points in the area of actuation. Because the work is calculated for a change in state, it is necessary to define the path between the initial and final state. This is done by relating  $\beta$  linearly to a nondimensional time  $\tau$  as

$$\beta(\tau) = (\beta_2 - \beta_1)\tau + \beta_1 \quad (2.4)$$

where  $0 \leq \tau \leq 1$ , and  $\beta_1$  and  $\beta_2$  are the values of  $\beta$  at the initial and final state.

The general equation for mechanical work ( $\overline{W}$ ) can be written as

$$\overline{W} = \int_{r_1}^{r_2} C(r) \cdot dr \quad (2.5)$$

where  $C$  is the force acting on a point that is being moved from location  $r_1$  to a location  $r_2$  along a path  $r$ . To apply Eq. (2.5) to a point  $x$  on an airfoil, the force per-unit length  $C$  is written as ( $\beta_0$  from Eq. 2.2 is assumed to be zero for brevity)

$$C(x, \tau) = \{\Delta p_\beta(x)\beta(\tau) + \Delta p_\alpha(x)\alpha(\tau) + K(x)\beta(\tau)\} \quad (2.6)$$

where  $\beta(\tau)$  is defined in Eq. (2.4) and  $\alpha(\tau)$  is represented in the same form. The  $dr$  term at point  $x$  is written as

$$dr = f(x) \frac{d\beta}{d\tau} d\tau \quad (2.7)$$

where  $f(x)$  is defined in Eq. (2.3). Substituting Eqs. (2.6) and (2.7) into Eq. (2.5) results in the following expression for the work per-unit length ( $\bar{w}$ ) at point  $x$ :

$$\bar{w}(x, \alpha_1, \alpha_2, \beta_1, \beta_2) = -\int_0^1 \{\Delta p_\beta(x)\beta(\tau) + \Delta p_\alpha(x)\alpha(\tau) + K(x)\beta(\tau)\} f(x) \frac{d\beta}{d\tau} d\tau \quad (2.8)$$

where the negative sign is added so that the work is positive when the actuator is required to provide a force in the direction of  $dr$ . Integrating Eq. (2.8) across the chord results in the following equation for the total work required by the actuator:

$$\bar{W}(\alpha_1, \alpha_2, \beta_1, \beta_2) = -\int_0^1 \int_0^c \{\Delta p_\beta(x)\beta(\tau) + \Delta p_\alpha(x)\alpha(\tau) + K(x)\beta(\tau)\} f(x) \frac{d\beta}{d\tau} dx d\tau \quad (2.9)$$

Although Eq. (2.9) is mathematically correct, its practical usefulness is limited. To understand this, it is necessary to discuss the meaning of the sign of the required actuator work. As mentioned, a positive work value from Eq. (2.9) means that the actuator must provide a force in the direction of its actuation motion. A negative value means that the actuator must provide a force in the direction opposite to its motion. These two types of actuation work are fundamentally different. To see this, consider a flapped airfoil at zero degrees  $\alpha$  with the flap changing from -20 degrees to 20 degrees deflection (assume no structural work). Evaluating Eq. (2.9) for this case results in a  $\bar{W}$  equal to zero. This does not seem intuitively correct because it is known that some positive work should be required for this geometry change. What has happened is the negative work required to go from -20 degrees to 0 degrees has cancelled the positive work required to go from 0 degrees to 20 degrees. Allowing these terms to cancel each other assumes that the negative work is collected and used to produce positive work. Although this is not impossible, it is a restrictive and impractical assumption. A more practical equation will be developed in the next section that only calculates the positive work.

## 2.4 The Practical Work Required for an Aerodynamic Control Device

The previous section mentioned that the outer integral of Eq. (2.9) allows for the cancellation of positive and negative work, which was shown to produce work values that clearly do not represent the required work. The issue that must be addressed here is the cost of the actuator work, because what we are really interested in is the amount of energy that must be supplied to the actuator. This topic has been widely studied by biologists to determine the muscle efficiencies of different types of animal motion [Nieslon 1972, Blikhan 1994, Tucker 1975]. The cost of negative work for a muscle was investigated by Abbot *et al* [1952] by measuring the oxygen consumption of humans performing positive and negative work. In this case, the oxygen consumption can be considered a measure of the work supplied to the actuator, or the cost. It was found that the oxygen required for negative work is considerably less than that of positive work. For the problem of determining the energy supplied to an actuator, it is conceivable that the cost of negative work is also small compared to the cost of positive work. This statement is difficult to justify for conventional actuators, for which it is difficult to find information connecting the required input energy to the output force and displacement. Most of the information found for conventional actuators is concerned only with the maximum available force, which is used to size the actuators for the maximum allowable hinge moment of the control surface [Raymond and Chenoweth 1993].

For this study, we will label  $W$  the practical work, which accounts for the difference in negative and positive work. The practical work will be defined as

$$W = \overline{W}^+ + \eta \overline{W}^- \quad (2.10)$$

where  $\overline{W}^+$  and  $\overline{W}^-$  are the absolute values of the positive and negative work terms. These terms are obtained by separating the outer integral in Eq. (2.9) into segments that calculate only positive or negative work (this will be discussed in detail below). The  $\eta$  term in Eq. (2.10) is a coefficient that represents the cost of negative work relative to positive work. If there is no cost required for the actuator to perform negative work, then  $\eta = 0$ . If the cost of positive and negative work are equal, then  $\eta = 1$ .

The remainder of this study will assume a value of  $\eta = 0$ , or that the cost of negative work is negligible so that  $W = \overline{W}^+$ . Applying the following development to nonzero values of  $\eta$  is straightforward, the only difference is the negative component of  $\overline{W}$  is calculated in addition to the positive component calculated in the following procedure. To calculate the positive component of  $\overline{W}$ , we first rewrite the inner integral of Eq. (2.9) as

$$\begin{aligned} I(\tau) &= -\int_0^c (\Delta p_\beta(x)\beta(\tau) + \Delta p_\alpha(x)\alpha(\tau) + K(x)\beta(\tau))f(x) \frac{d\beta}{d\tau} dx \\ &= -\left\{ (Q_\beta + Q_s)[(\beta_2 - \beta_1)\tau + \beta_1] + Q_\alpha[(\alpha_2 - \alpha_1)\tau + \alpha_1] \right\} (\beta_2 - \beta_1) \end{aligned} \quad (2.11)$$

where

$$\begin{aligned} Q_\beta &= \int_0^c \Delta p_\beta(x) f(x) dx \\ Q_\alpha &= \int_0^c \Delta p_\alpha(x) f(x) dx \\ Q_s &= \int_0^c K(x) f(x) dx \end{aligned} \quad (2.12)$$

If  $f(x)$  is a linear function of  $x$ , as is the case for a conventional flap, then  $Q$  represents the hinge moment per-unit  $\beta$  or  $\alpha$ . To determine if  $I(\tau)$  changes from positive to negative, it is evaluated at  $\tau$  equal to zero and one. The 4 possible variations of  $I(\tau)$  are shown in Figure 2.2. Case (C) occurs if  $I(\tau=0)$  and  $I(\tau=1)$  are  $\geq 0$ , which results in  $W = \overline{W}$  because there is no negative work. Case (D) occurs if  $I(\tau=0)$  and  $I(\tau=1)$  are  $\leq 0$ , then  $W = 0$  because there is no positive work. For cases (A) and (B), where one of the  $I(\tau)$  values is positive and one is negative, the outer integral of Eq. (2.9) must be broken up into two parts. The value of  $\tau$  at which to break up the integral is determined by setting Eq. (2.11) equal to zero and solving for  $\tau$ .

$$\tau_0 = -\frac{(Q_\beta + Q_s)\beta_1 + Q_\alpha\alpha_1}{(Q_\beta + Q_s)(\beta_2 - \beta_1) + Q_\alpha(\alpha_2 - \alpha_1)} \quad (2.13)$$

If  $I(\tau=0)$  is  $\geq 0$  and  $I(\tau=1)$  is  $\leq 0$ , corresponding to case (A) in Figure 2.2, the correct expression for the aerodynamic work is

$$\begin{aligned} W(\alpha_1, \alpha_2, \beta_1, \beta_2) &= -\int_0^{\tau_0} \int_0^c (\Delta p_\beta(x)\beta(\tau) + \Delta p_\alpha(x)\alpha(\tau) + K(x)\beta(\tau))f(x, \kappa) \frac{d\beta}{d\tau} dx d\tau \\ &= -\left\{ (Q_\beta + Q_s)[(\beta_2 - \beta_1)\tau_0^2 / 2 + \beta_1\tau_0] + Q_\alpha[(\alpha_2 - \alpha_1)\tau_0^2 / 2 + \alpha_1\tau_0] \right\} (\beta_2 - \beta_1) \end{aligned} \quad (2.14)$$

where the contribution from  $\tau$  equal to  $\tau_0$  and one is zero. If  $I(\tau=0)$  is  $\leq 0$  and  $I(\tau=1)$  is  $\geq 0$ , corresponding to case (B) in Figure 2.2, the correct expression for the aerodynamic work is

$$W(\alpha_1, \alpha_2, \beta_1, \beta_2) = - \int_{\tau_0}^1 \int_0^c (\Delta p_\beta(x) \beta(\tau) + \Delta p_\alpha(x) \alpha(\tau) + K(x) \beta(\tau)) f(x) \frac{d\beta}{d\tau} dx d\tau$$

$$= - \left\{ (Q_\beta + Q_s) \left[ (\beta_2 - \beta_1) (1 - \tau_0^2) / 2 + \beta_1 (1 - \tau_0) \right] + Q_\alpha \left[ (\alpha_2 - \alpha_1) (1 - \tau_0^2) / 2 + \alpha_1 (1 - \tau_0) \right] \right\} \quad (2.15)$$

where the contribution from  $\tau$  equal to zero and  $\tau_0$  is zero.

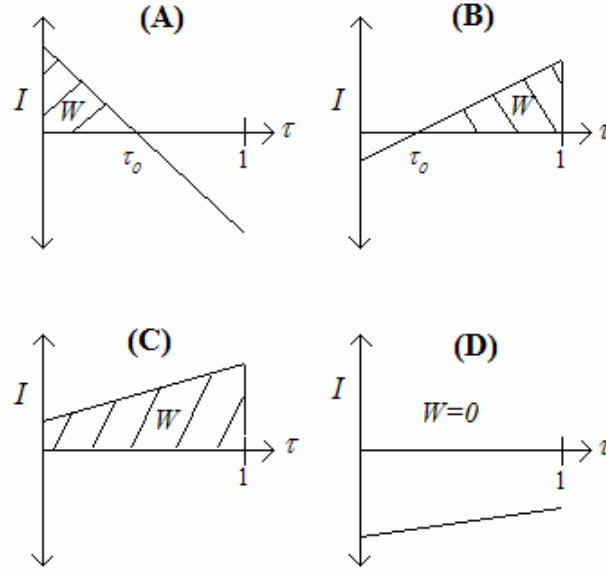


Figure 2.2: The possible variations of  $I$  with  $\tau$

Eq. (2.9) was derived for an airfoil that has only one control parameter changing between the initial and final points. In many cases it is desired to calculate the work required to deflect multiple control surfaces, as shown in Figure 2.1. For an airfoil with  $N$  control surfaces, the position of the  $n^{\text{th}}$  control surface ( $\beta_n$ ) between the initial and final points is written as

$$\beta_n(\tau) = (\beta_{n_2} - \beta_{n_1}) \tau + \beta_{n_1}$$

Ignoring the positive-negative work issues discussed above, the generalization of Eq. (2.9) can be written for the work required for the  $m^{\text{th}}$  control surface as

$$\bar{W}_m = - \int_0^1 \int_0^c \left\{ \sum_{n=1}^N (\Delta p_{\beta_n}(x) + K_n(x)) \beta_n(\tau) \right\} f_m(x) \left( \frac{d\beta_m}{d\tau} \right) dx d\tau \quad (2.16)$$

where  $\Delta p_{\beta_n}$  represents the derivative of the  $\Delta p$  distribution with the  $\beta_n^{\text{th}}$  control surface and  $K_n(x)$  is the structural force term defined in Eq. (2.2). An expression must be obtained, as was done in

the single control parameter case, which only accounts for positive work. As in the single control case, the inner integral of Eq. (2.16) can be written as

$$\begin{aligned}
I_m(\tau) &= - \int_0^c \left( \sum_{n=1}^N [(\Delta p_{\beta_n}(x) + K_n(x))\beta_n(\tau)] + \Delta p_{\alpha}(x)\alpha(\tau) \right) f_m(x) \frac{d\beta_m}{d\tau} dx \\
&= - \left\{ \sum_{n=1}^N \left\{ (Q_{m,n} + S_{m,n}) [(\beta_{n_2} - \beta_{n_1})\tau + \beta_{n_1}] \right\} + Q_{m,\alpha} [(\alpha_2 - \alpha_1)\tau + \alpha_1] \right\} (\beta_{m_2} - \beta_{m_1})
\end{aligned} \tag{2.17}$$

where

$$\begin{aligned}
Q_{m,n} &= \int_0^c \Delta p_{\beta_n}(x) f_m(x) dx \\
Q_{m,\alpha} &= \int_0^c \Delta p_{\alpha}(x) f_m(x) dx \\
S_{m,n} &= \int_0^c K_n(x) f_m(x) dx
\end{aligned} \tag{2.18}$$

If  $I_m(\tau=0)$  and  $I_m(\tau=1)$  are  $\geq 0$ , then  $W_m = \overline{W}_m$ . If  $I_m(\tau=0)$  and  $I_m(\tau=1)$  are  $\leq 0$ , then  $W_m = 0$ . If  $I_m(\tau=0)$  and  $I_m(\tau=1)$  have different signs, the value of  $\tau$  at which  $I_m$  changes sign ( $\tau_{0m}$ ) is found by setting  $I_m(\tau)$  equal to zero

$$\tau_{0m} = - \frac{\sum_{n=1}^N (Q_{m,n} + S_{m,n})\beta_{n_1} + Q_{m,\alpha}\alpha_1}{\sum_{n=1}^N (Q_{m,n} + S_{m,n})(\beta_{n_2} - \beta_{n_1}) + Q_{m,\alpha}(\alpha_2 - \alpha_1)} \tag{2.19}$$

For the case where  $I_m(\tau=0)$  is  $\geq 0$  and  $I_m(\tau=1)$  is  $\leq 0$  (case (A) in Figure 2.2),  $W_m$  is written as

$$\begin{aligned}
W_m &= - \int_0^{\tau_{0m}} \int_0^c \left\{ \sum_{n=1}^N (\Delta p_{\beta_n}(x) + K_n(x))\beta_n(\tau) \right\} + \Delta p_{\alpha}(x)\alpha(\tau) \left\} f_m(x) \left( \frac{d\beta_m}{d\tau} \right) dx d\tau \\
&= - \left\{ \sum_{n=1}^N \left\{ (Q_{m,n} + S_{m,n}) [(\beta_{n_2} - \beta_{n_1})\tau_{0m}^2 / 2 + \beta_{n_1}\tau_{0m}] \right\} + Q_{m,\alpha} [(\alpha_2 - \alpha_1)\tau_{0m}^2 / 2 + \alpha_1\tau_{0m}] \right\} (\beta_{m_2} - \beta_{m_1})
\end{aligned} \tag{2.20}$$

For the case where  $I_m(\tau=0)$  is  $\leq 0$  and  $I_m(\tau=1)$  is  $\geq 0$  (case (B) in Figure 2.2),  $W_m$  is written as

$$\begin{aligned}
W_m &= - \int_{\tau_{0m}}^1 \int_0^c \left\{ \sum_{n=1}^N (\Delta p_{\beta_n}(x) + K_n(x))\beta_n(\tau) \right\} + \Delta p_{\alpha}(x)\alpha(\tau) \left\} f_m(x) \left( \frac{d\beta_m}{d\tau} \right) dx d\tau \\
&= - \left\{ \sum_{n=1}^N \left\{ (Q_{m,n} + S_{m,n}) [(\beta_{n_2} - \beta_{n_1})(1 - \tau_{0m}^2) / 2 + \beta_{n_1}(1 - \tau_{0m})] \right\} + Q_{m,\alpha} [(\alpha_2 - \alpha_1)(1 - \tau_{0m}^2) / 2 + \alpha_1(1 - \tau_{0m})] \right\} (\beta_{m_2} - \beta_{m_1})
\end{aligned} \tag{2.21}$$

Once the work required for each control surface ( $W_m$ ) is calculated, the work for the entire system is obtained by the following summation

$$W = \sum_{m=1}^N W_m \quad (2.22)$$

where  $W_m$  is the work required for the  $m^{\text{th}}$  control surface. It should be noticed that the work is calculated separately for each control surface, or actuator, and then added together. This assumes that each control surface is actuated independently. If this is not true and the control surfaces are linked, then  $I_m$  and  $\tau_0$  should be calculated for the combination of linked control surfaces. This would mean that a single area of actuation be used that includes each control surface being linked together. This is important because if they are linked, for example a linked leading and trailing flap, then at each value of  $\tau$  the positive and negative work values can cancel. To clarify the difference in the work calculated for linked actuators, consider an analogy of two weights ( $a$  and  $b$ ) being moved vertically as shown in Figure 2.3. If both  $a$  and  $b$  weigh the same, it is easy to imagine that an infinitesimal disturbance (assuming no friction in the system) will cause the two weights to move from their initial to final  $z$  values. This means no work is required. But, if the bar connecting the two weights is removed, work will have to be exerted to move weight  $a$  up, but not to move weight  $b$  down (which requires negative work). This shows clearly the reason for subtracting positive and negative work if the control surfaces are linked, and not if they are independent.

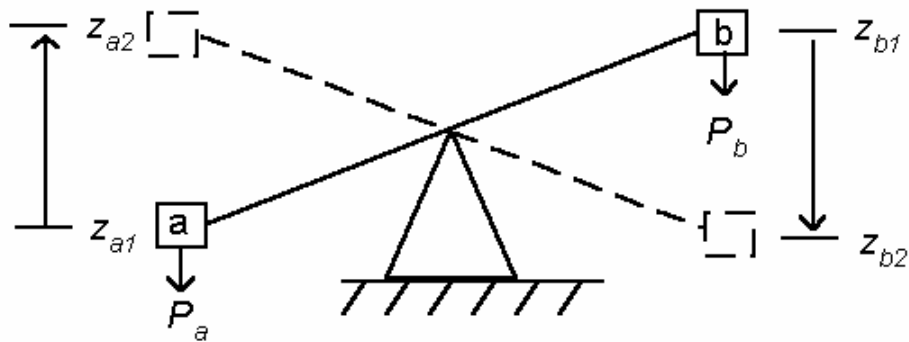


Figure 2.3: Analogy for the interaction of work for linked control surfaces

To conclude, it should be mentioned that although the structural forces have been considered throughout this chapter, the remainder of the chapters will assume that there is no structural resistance or that  $K = 0$ . The reason for carrying the structural term throughout this chapter is that if there is a structural force, and it is desired to calculate the required actuator work, the aerodynamic and structural forces acting on the actuator *must* be considered together. This fact is

a result of the assumption that negative work requires negligible actuator effort. The main effect of the presence of structural work is that the negative aerodynamic work, which is ignored if there is no structure, becomes useful and is able to cancel some of the positive work required to deform the structure.

## 2.5 Chapter Summary

This chapter presented a method of calculating the mechanical work required from actuators to operate an aerodynamic control device. It is argued that it is really desired to calculate the energy “cost” of actuating an aerodynamic control device, and not the required mechanical work. This leads to calculation of the practical work ( $W$ ), which is related to the straightforward work ( $\bar{W}$ ) through Eq. (2.10). The term  $\eta$  in Eq. (2.10), which represents the difference in the cost of positive and negative work, defines the relationship between  $\bar{W}$  and  $W$ . The remainder of this study will use a value of  $\eta = 0$ , which implies that energy required by an actuator to perform negative work is zero. An important consequence of treating negative and positive work differently is that the structural and aerodynamic work calculations cannot be performed independently.

# Chapter 3

## An Analysis of Control Surface Aerodynamic Characteristics Using Thin Airfoil Theory

### 3.1 Introduction

This chapter provides the theoretical aerodynamic loading distributions for various airfoil control devices using thin airfoil theory. This theory is subject to the usual limitations of thin airfoil theory. For example, it cannot predict drag or flow separation, which restricts the theory's ability to compare these effects for various control devices. But, this does not limit the theory's ability to compare control devices at low to moderate deflections, whereat the change in viscous drag and the likelihood of flow separation should be small.

We will begin by reviewing thin airfoil theory and its application to a flapped airfoil and a 4-digit NACA camberline (Sections 3.2 – 3.4). With the goal of making a work comparison, other control devices (leading edge-trailing edge, trailing edge-tab, and morphing trailing edge configuration) are modeled in Sections 3.5 through 3.7. Section 3.8 describes the addition of the trim requirement to connect the 2-D airfoil studies to a complete aircraft.

## 3.2 A Review of Thin Airfoil Theory

Thin airfoil theory assumes that the aerodynamic properties of an airfoil are functions of its mean camber line, angle of attack, and thickness envelope\*. The lifting properties of an airfoil are modeled as a vortex sheet placed on the chord line. The chordwise distribution of the strength for this vortex sheet is obtained by requiring that the velocity induced by the vortices be tangent to the mean camber line and that the vortex strength at the trailing edge of the airfoil is zero (Kutta condition). Because the slope of the mean camber line of most airfoils is small, the flow tangency condition is met by projecting the slope of the mean camber line onto the chord line [Munk 1923].

The vorticity distribution can be represented by a Fourier series as

$$\gamma(\theta) = 2U_\infty \left( A_0 \left[ \frac{1 + \cos \theta}{\sin \theta} \right] + \sum_{n=1}^{\infty} A_n \sin n\theta \right) \quad (3.1)$$

where

$$0 \leq \theta \leq \pi$$

$$x = \frac{c}{2} (1 - \cos \theta) \quad (3.2)$$

$$A_0 = \alpha - \frac{1}{\pi} \int_0^\pi \frac{dz}{dx} d\theta \quad (3.3)$$

$$A_1 = \frac{2}{\pi} \int_0^\pi \frac{dz}{dx} \cos(\theta) d\theta \quad (3.4)$$

$$A_2 = \frac{2}{\pi} \int_0^\pi \frac{dz}{dx} \cos(2\theta) d\theta \quad (3.5)$$

By representing the vorticity distribution as a Fourier series, the aerodynamic coefficients of the airfoil can be written as [Glauert 1947]

$$C_l = \pi(2A_0 + A_1) \quad (3.6)$$

$$C_{M_0} = -\frac{\pi}{2} \left( A_0 + A_1 - \frac{A_2}{2} \right) \quad (3.7)$$

---

\* Note that to the first order thickness does not contribute to lift.

$$C_{M_{\frac{1}{4}c}} = \frac{\pi}{4}(A_2 - A_1) \quad (3.8)$$

It is convenient to separate Eq. (3.1) into terms that are dependent and independent of angle of attack. The term dependent upon angle of attack is called the additional load distribution ( $\gamma_a$ ), and is seen to be the first term in Eq. (3.1).

$$\gamma_a(\theta) = 2U_\infty A_0 \left[ \frac{1 + \cos \theta}{\sin \theta} \right] \quad (3.9)$$

Eq. (3.9) will always produce a singularity at the leading edge because the airfoil is modeled as being infinitely thin. Theodorsen [1931] recognized that the most efficient flow around an airfoil would occur when  $\gamma_a$  equaled zero, and proposed the “ideal angle of attack” ( $\alpha_i$ ) as the angle of attack when this occurred. From Eqs. (3.3) and (3.9) it is found that

$$\alpha_i = \frac{1}{\pi} \int_0^\pi \frac{dz}{dx} d\theta \quad (3.10)$$

The term that is independent of angle of attack, called the basic load distribution ( $\gamma_b$ ), represented by the infinite series term in Eq. (3.1), can be shown to converge to the following integral [Allen 1943]:

$$\gamma_b(\theta) = 2U_\infty \sum_1^\infty A_n \sin n\theta = \frac{2U_\infty}{\pi} \int_0^\pi \frac{\frac{dz}{dx}(\theta_0) \sin \theta}{\cos \theta_0 - \cos \theta} d\theta_0 \quad (3.11)$$

If  $dz/dx$  is finite, the basic load distribution will always be zero at the leading edge<sup>†</sup>. So, if the additional load distribution is zero, the load (vortex strength) at the leading edge will also be zero. Because the vortex strength at the leading edge is zero at the ideal angle of attack, the flow will enter the leading edge smoothly, and as Theodorsen suggested, most efficiently. This also means that  $\alpha_i$  is the angle of attack at which thin airfoil theory is the most accurate because the small disturbance assumption is not violated at the leading edge.

### 3.3 Modeling an Airfoil with a Trailing-Edge Flap

The governing equations of thin airfoil theory were derived with the assumption that the slope of the mean camber line was small, therefore allowing the small angle approximation to be used.

---

<sup>†</sup> For NACA 6-digit series airfoils the design load at the leading edge is finite, resulting in a logarithmic singularity for the camberline slope  $dz/dx$  at the leading edge.

For the flapped-airfoil shown in Figure 3.1, the small angle approximation greatly simplifies the expression for the mean camber line and the subsequent analysis.

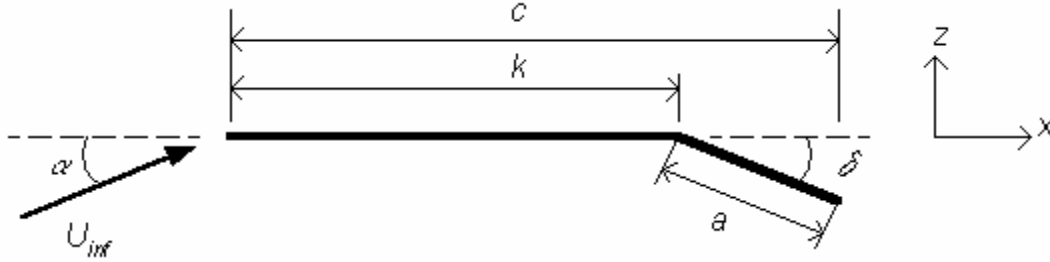


Figure 3.1: Geometric representation of a flapped-airfoil

From Figure 3.1,  $c$  may be written as

$$c = k + a \cos \delta \approx k + a \quad (3.12)$$

The flap deflection causes a slope discontinuity in the mean camber line, resulting in the following two equations for  $z$

$$\begin{aligned} 0 \leq x \leq k \\ z = 0 \end{aligned} \quad (3.13)$$

and

$$\begin{aligned} k \leq x \leq c \\ z = -(x - k) \tan \delta \\ \approx -(x - k) \delta \end{aligned} \quad (3.14)$$

Eq. (3.2) shows the transformation from  $x$  to  $\theta$ , which was used in Eqs. (3.3 - 3.5) to find the coefficients of the Fourier series. The location of the discontinuity transformed into its  $\theta$  representation is

$$\theta_B = \cos^{-1} \left( 1 - \frac{2k}{c} \right) \quad (3.15)$$

With the geometric parameters defined, the Fourier coefficients from Eqs. (3.3 - 3.5) are obtained as follows

$$\begin{aligned} A_0 &= \alpha - \frac{1}{\pi} \int_0^\pi \frac{dz}{dx} d\theta = \alpha - \frac{1}{\pi} \left( \int_{\theta_B}^\pi (-\delta) d\theta \right) \\ &= \alpha + \frac{1}{\pi} \delta (\pi - \theta_B) \end{aligned} \quad (3.16)$$

$$\begin{aligned}
A_1 &= \frac{2}{\pi} \int_0^\pi \frac{dz}{dx} \cos \theta d\theta = \frac{2}{\pi} \left( - \int_{\theta_B}^\pi [\delta \cos \theta] d\theta \right) \\
&= \frac{2\delta}{\pi} \sin(\theta_B)
\end{aligned} \tag{3.17}$$

$$\begin{aligned}
A_2 &= \frac{2}{\pi} \int_0^\pi \frac{dz}{dx} \cos(2\theta) d\theta = \frac{2}{\pi} \left( - \int_{\theta_B}^\pi [\delta \cos(2\theta)] d\theta \right) \\
&= \frac{\delta}{\pi} \sin(2\theta_B)
\end{aligned} \tag{3.18}$$

Combining Eqs. (3.16 – 3.18) with Eqs. (3.6) and (3.8) results in an analytic solution for the lift and pitching moment coefficients of an airfoil with a given  $\delta$  and  $a$ .

The load distribution is obtained by evaluating Eqs. (3.9) and (3.11) with the camber line given in Eqs. (3.13) and (3.14). Because a singularity ( $\theta_0 = \theta$ ) lies within the range of integration, Eq. (3.11) is an improper integral. The Cauchy Principle Value is obtained by separating the integral into two integrals and using a limiting process, which leads to

$$\gamma_b(\theta) = \frac{2U_\infty}{\pi} \lim_{\varepsilon \rightarrow 0} \left[ \int_0^{\theta-\varepsilon} \frac{\frac{dz}{dx}(\theta_0) \sin \theta}{\cos \theta_0 - \cos \theta} d\theta_0 + \int_{\theta+\varepsilon}^\pi \frac{\frac{dz}{dx}(\theta_0) \sin \theta}{\cos \theta_0 - \cos \theta} d\theta_0 \right] \tag{3.19}$$

With  $dz/dx$  equal to a constant, Eq. (3.11) can be evaluated in the form [Gradshteyn 1965]

$$\int \frac{d\theta}{a + b \cos \theta} = \frac{1}{\sqrt{b^2 - a^2}} \ln \left( \frac{\sqrt{b^2 - a^2} \tan(\theta/2) + a + b}{\sqrt{b^2 - a^2} \tan(\theta/2) - a - b} \right) \tag{3.20}$$

where  $a = -\cos \theta$  and  $b = 1$  for our case. Applying Eq. (3.19) to (3.20) leads to the final expression for the basic load distribution due to the flap deflection ( $\delta$ ).

$$\gamma_b(\theta) = \frac{2U_\infty \delta}{\pi} \ln \left( \frac{\sin \theta \tan(\theta_B/2) - \cos \theta + 1}{\sin \theta \tan(\theta_B/2) + \cos \theta - 1} \right) \tag{3.21}$$

Eq. (3.21) is equivalent to the solution obtained by Spence [1958] although it is not identical in form. Combining Eqs. (3.9) and (3.16) results in the equation for the additional load distribution.

$$\gamma_a(\theta) = 2U_\infty \left( \alpha + \delta \left( 1 - \frac{\theta_B}{\pi} \right) \right) \left[ \frac{1 + \cos \theta}{\sin \theta} \right] \tag{3.22}$$

Notice that, as expected with linear theory, both  $\gamma_b$  and  $\gamma_a$  are linear with respect to  $\delta$ . Fig. 3.2 shows an example load distribution (note that  $\Delta C_p = 2\gamma/U_{inf}$ ). The singularity at  $k$  (or  $\theta_B$ ) is a result of the step change in the camber line slope. It should also be observed that although the

airfoil is at zero incidence, there is a leading edge singularity. As mentioned previously, this will be true unless the airfoil is at its ideal angle of attack, meaning  $A_0$  equals zero.

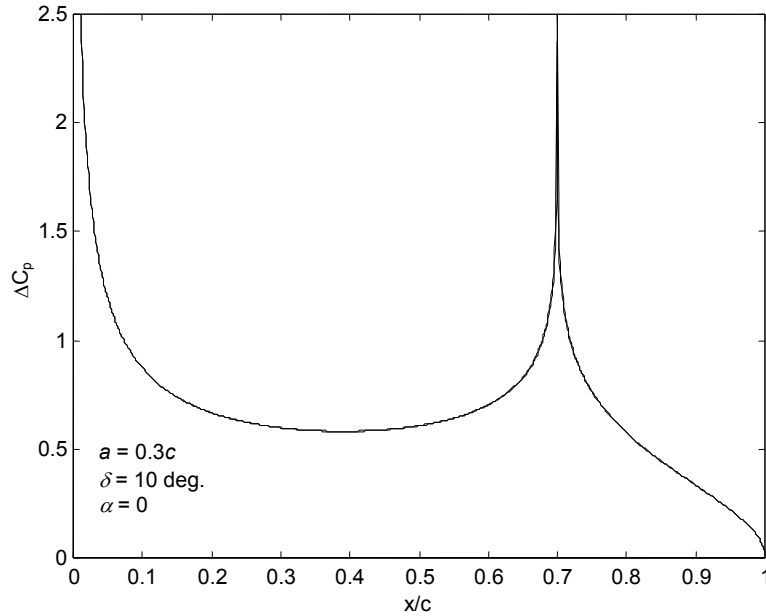


Figure 3.2: Example load distribution

To apply the aerodynamic work equations (Eq. (2.13-2.15) for the single control surface) developed in the previous chapter, we set  $\beta = \delta$ . The  $\Delta p_\beta$  and  $\Delta p_\alpha$  functions required for the work equations are obtained from Eqs. (3.21) and (3.22) as

$$\Delta p_\delta(\theta) = \frac{2\rho U_\infty^2}{\pi} \left\{ \ln \left( \frac{\sin \theta \tan(\theta_B/2) - \cos \theta + 1}{\sin \theta \tan(\theta_B/2) + \cos \theta - 1} \right) + (\pi - \theta_B) \left[ \frac{1 + \cos \theta}{\sin \theta} \right] \right\} \quad (3.23)$$

$$\Delta p_\alpha(\theta) = 2\rho U_\infty^2 \left[ \frac{1 + \cos \theta}{\sin \theta} \right] \quad (3.24)$$

where the first term in Eq. (3.23) is the basic load distribution and the second term is part of the additional load distribution. Eq. (3.24) is due entirely to the additional load distribution. The  $f(x)$  term required for the work equations for a flapped-airfoil is (using Eq. (3.1) to transform from  $x$  to  $\theta$ )

$$\begin{aligned} 0 &\leq \theta \leq \theta_B \\ f(\theta) &= 0 \\ \theta_B &\leq \theta \leq \pi \\ f(\theta) &= -0.5(\cos \theta_B - \cos \theta) \end{aligned} \quad (3.25)$$

Figure 3.3 shows the integrands of the work due to the basic and additional load distributions. It is seen that the contribution of the additional load distribution to the work is smaller than the contribution from the basic load at  $\alpha$  equal to zero.

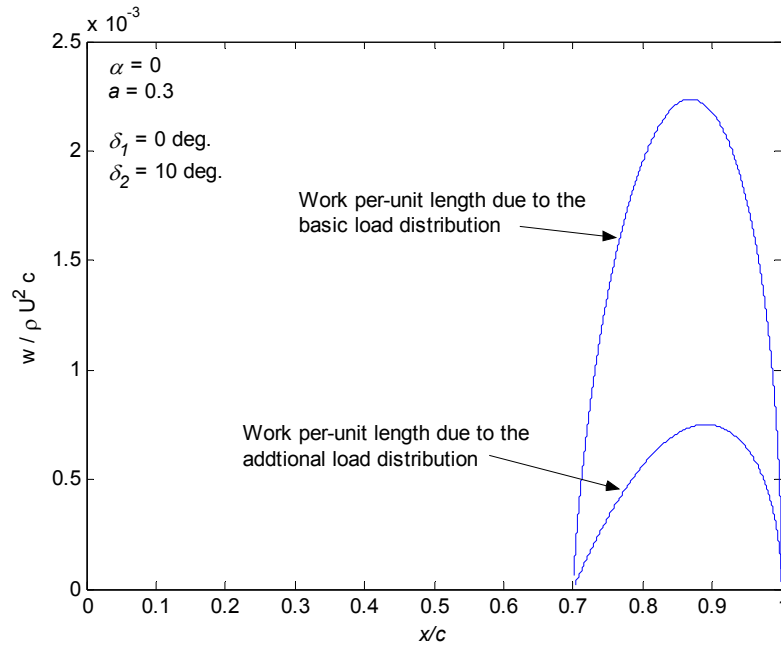


Figure 3.3: The work per-unit length for a flapped-airfoil

### 3.4 Modeling an NACA 4-Digit Camberline

For a variable-camber morphing airfoil, camber changes can be modeled as an NACA 4-digit camberline with a variable magnitude and location of maximum camber. Using the NACA convention, an NACA  $MPXX$  airfoil has a magnitude of maximum camber  $M$  (in percent chord), maximum camber location  $P$  (in tenths of the chord), and maximum thickness  $XX$  (in percent chord). The first two of these parameters are shown in Fig. 3.4 (ignoring thickness).

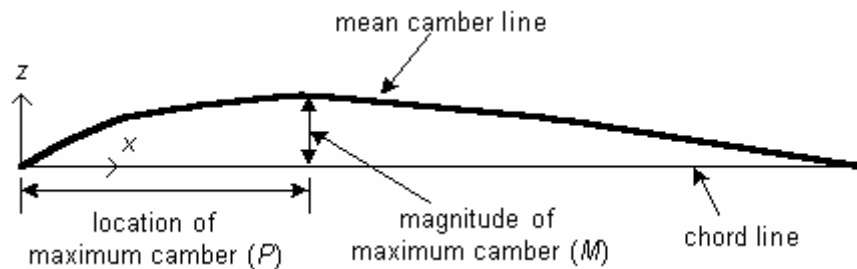


Figure 3.4: NACA camberline representation

The equations for the mean camber line of an NACA  $mpXX$  are as follows [Abbot and Von Doenhoff 1959]:

$$\begin{aligned}
M &= 0.01m \\
P &= 0.1p \\
0 &\leq \frac{x}{c} \leq P \\
\frac{z}{c} &= \frac{M}{P^2} \left[ 2P \left( \frac{x}{c} \right) - \left( \frac{x}{c} \right)^2 \right]
\end{aligned} \tag{3.26}$$

$$\begin{aligned}
P &\leq \frac{x}{c} \leq 1 \\
\frac{z}{c} &= \frac{M}{(1-P)^2} \left[ 1 - 2P + 2P \left( \frac{x}{c} \right) - \left( \frac{x}{c} \right)^2 \right]
\end{aligned} \tag{3.27}$$

Eq. (3.1) is used again to transform between  $x$  to  $\theta$ . The location of the transition between Eq. (3.26) and (3.27) is found from Eq. (3.28) to be

$$\cos \theta_B = 1 - \frac{2P}{c} \tag{3.28}$$

Applying Eqs. (3.2 – 3.4) results in the following

$$\begin{aligned}
A_0 &= \alpha - \frac{1}{\pi} \int_0^\pi \frac{dz}{dx} d\theta = \alpha - \frac{1}{\pi} \left[ \left( \frac{2M}{P^2} \right) \int_0^{\theta_B} \left( P - \frac{1}{2} + \frac{\cos \theta}{2} \right) d\theta + \left( \frac{2M}{(1-P)^2} \right) \int_{\theta_B}^\pi \left( P - \frac{1}{2} + \frac{\cos \theta}{2} \right) d\theta \right] \\
&= \alpha - \frac{2M}{\pi P^2} \left[ P\theta_B - \frac{\theta_B}{2} + \frac{\sin \theta_B}{2} \right] - \frac{2M}{\pi(1-P)^2} \left[ P(\pi - \theta_B) - \frac{1}{2}(\pi - \theta_B) - \left( \frac{\sin \theta_B}{2} \right) \right]
\end{aligned} \tag{3.29}$$

$$\begin{aligned}
A_1 &= \frac{2}{\pi} \int_0^\pi \frac{dz}{dx} \cos \theta d\theta = \frac{2}{\pi} \left[ \left( \frac{2M}{P^2} \right) \int_0^{\theta_B} \left( P - \frac{1}{2} + \frac{\cos \theta}{2} \right) \cos \theta d\theta + \left( \frac{2M}{(1-P)^2} \right) \int_{\theta_B}^\pi \left( P - \frac{1}{2} + \frac{\cos \theta}{2} \right) \cos \theta d\theta \right] \\
&= \frac{2}{\pi} \left\{ \frac{2M}{P^2} \left[ \left( P - \frac{1}{2} \right) \sin \theta_B + \frac{1}{4} \theta_B + \frac{1}{8} \sin(2\theta_B) \right] \right. \\
&\quad \left. + \frac{2M}{(1-P)^2} \left[ \left( P - \frac{1}{2} \right) (-\sin \theta_B) + \frac{1}{4} (\pi - \theta_B) - \frac{1}{8} (\sin(2\theta_B)) \right] \right\}
\end{aligned} \tag{3.30}$$

$$\begin{aligned}
A_2 &= \frac{2}{\pi} \int_0^\pi \frac{dz}{dx} \cos(2\theta) d\theta = \frac{2}{\pi} \left[ \left( \frac{2M}{P^2} \right) \int_0^{\theta_B} \left( P - \frac{1}{2} + \frac{\cos \theta}{2} \right) \cos(2\theta) d\theta + \left( \frac{2M}{(1-P)^2} \right) \int_{\theta_B}^\pi \left( P - \frac{1}{2} + \frac{\cos \theta}{2} \right) \cos(2\theta) d\theta \right] \\
&= \frac{2}{\pi} \left\{ \frac{2M}{P^2} \left[ \left( P - \frac{1}{2} \right) \frac{1}{2} \sin(2\theta_B) + \frac{1}{2} \left( \frac{\sin \theta_B}{2} + \frac{\sin(3\theta_B)}{6} \right) \right] \right. \\
&\quad \left. + \frac{2M}{(1-P)^2} \left[ \left( -\frac{1}{2} \sin(2\theta_B) \left( P - \frac{1}{2} \right) - \frac{1}{2} \left( \frac{\sin \theta_B}{2} + \frac{\sin(3\theta_B)}{6} \right) \right) \right] \right\}
\end{aligned} \tag{3.31}$$

Combining Eqs. (3.29 – 3.31) with Eqs. (3.5) and (3.7) results in closed form solutions for the lift and pitching moment coefficients for an NACA airfoil with a given  $M$  and  $P$ .

The load distribution for the NACA camberline is found in a manner similar to that for the flapped-airfoil. The main difference for the NACA camberline is that the camberline slope varies all the way along the chord. And two separate equations define the camberline. To apply Eq. (3.11), the derivatives of Eqs. (3.26) and (3.27) are represented in terms of  $\theta$  through Eq. (3.1) as

$$0 \leq \theta \leq \theta_B$$

$$\frac{dz}{dx}(\theta) = M(T_1 + S_1 \cos \theta) \quad (3.32)$$

$$\theta_B \leq \theta \leq \pi$$

$$\frac{dz}{dx}(\theta) = M(T_2 + S_2 \cos \theta) \quad (3.33)$$

where

$$T_1 = \frac{2}{P^2}(P - 0.5)$$

$$S_1 = \frac{1}{P^2}$$

$$T_2 = \frac{2}{(1-P)^2}(P - 0.5)$$

$$S_2 = \frac{1}{(1-P)^2} \quad (3.34)$$

The integral obtained by substituting Eqs. (3.32) and (2.33) into Eq. (3.11) is evaluated in the following form [Gradshteyn 1965]

$$\int \frac{T + S \cos \theta}{a + b \cos \theta} d\theta = \frac{S}{b} \theta + \frac{Tb - aS}{b} \frac{1}{\sqrt{b^2 - a^2}} \ln \left( \frac{\sqrt{b^2 - a^2} \tan(\theta/2) + a + b}{\sqrt{b^2 - a^2} \tan(\theta/2) - a - b} \right) \quad (3.35)$$

Obtaining the principal value using Eq. (3.35) for both sections of the camberline leads to the final equation for the basic load distribution

$$\gamma_b(\theta) = \frac{2U_\infty M}{\pi} \left\{ S_1 \theta_B \sin \theta + S_2 (\pi - \theta_B) \sin \theta + [T_1 - T_2 + (S_1 - S_2) \cos \theta] \ln \left( \frac{\sin \theta \tan(\theta_B/2) - \cos \theta + 1}{\sin \theta \tan(\theta_B/2) + \cos \theta - 1} \right) \right\} \quad (3.36)$$

The additional load distribution is found by combining Eqs. (3.9) and (3.29) to get the following

$$\gamma_a(\theta) = 2U_\infty \left\{ \alpha - \frac{2M}{\pi P^2} \left[ P\theta_B - \frac{\theta_B}{2} + \frac{\sin \theta_B}{2} \right] - \frac{2M}{\pi(1-P)^2} \left[ P(\pi - \theta_B) - \frac{1}{2}(\pi - \theta_B) - \left( \frac{\sin \theta_B}{2} \right) \right] \right\} \left[ \frac{1 + \cos \theta}{\sin \theta} \right] \quad (3.37)$$

Note that both  $\gamma_b$  and  $\gamma_a$  are linear with respect to  $M$ .

The load distributions represented by Eqs. (3.36) and (3.37) are compared to the results of Abbot and Von Doenhoff [1959] in Figure 3.5 (note that  $\Delta C_p = 2\gamma/U_{inf}$ ). There is a small but noticeable difference near the location of maximum camber ( $P$ ), likely because Abbot and Von Doenhoff used Pinkerton's [1936] empirically modified conformal mapping approach to determine the pressure distribution.

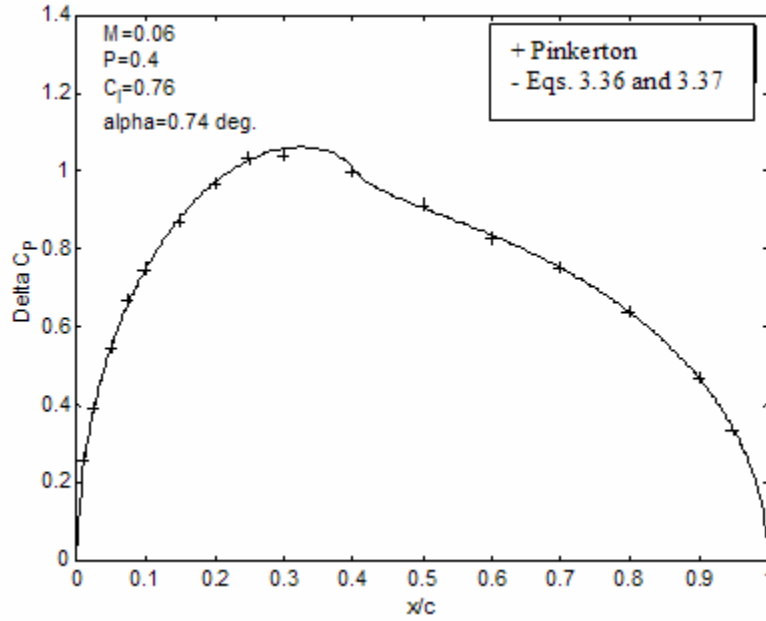


Figure 3.5: Load distribution validation

For a morphing NACA camberline, the work equations are applied with  $\beta = M$ . The  $\Delta p_\beta$  function is obtained from Eqs. (3.36) and (3.37) and is written separately for the basic and additional load distributions.

$$\Delta p_{b,M}(\theta, P) = \frac{2\rho U_\infty^2}{\pi} \left\{ S_1 \theta_B \sin \theta + S_2 (\pi - \theta_B) \sin \theta + [T_1 - T_2 + (S_1 - S_2) \cos \theta] \ln \left( \frac{\sin \theta \tan(\theta_B/2) - \cos \theta + 1}{\sin \theta \tan(\theta_B/2) + \cos \theta - 1} \right) \right\}$$

$$\Delta p_{a,M}(\theta, P) = 2\rho U_\infty^2 \left\{ \frac{2}{\pi P^2} \left[ P\theta_B - \frac{\theta_B}{2} + \frac{\sin \theta_B}{2} \right] - \frac{2}{\pi(1-P)^2} \left[ P(\pi - \theta_B) - \frac{1}{2}(\pi - \theta_B) - \left( \frac{\sin \theta_B}{2} \right) \right] \right\} \left[ \frac{1 + \cos \theta}{\sin \theta} \right] \quad (3.38)$$

The  $\Delta p_a$  term, given in Eq. (3.24) is the same for all thin airfoils regardless of the type of control surface and so it is not repeated here. The  $f(x)$  term for an NACA airfoil is

$$\begin{aligned}
 & 0 \leq \theta \leq \theta_B \\
 & f(\theta) = \frac{1}{P^2} \left[ P(1 - \cos \theta) - 0.25(1 - \cos \theta)^2 \right] \\
 & \theta_B \leq \theta \leq \pi \\
 & f(\theta) = \frac{1}{(1-P)^2} \left[ 1 - P - P \cos \theta - 0.25(1 - \cos \theta)^2 \right]
 \end{aligned} \tag{3.39}$$

Figure 3.6 shows the work per-unit length from Eq. (2.8) for various values of  $P$ . It is seen that the contribution of the basic load distribution to the work is similar for  $P$  equal to 0.3 and 0.7. For the additional load distribution, Figure 3.6 indicates that its contribution to the work changes from positive to negative as  $P$  moves past  $x/c$  equal to 0.5.

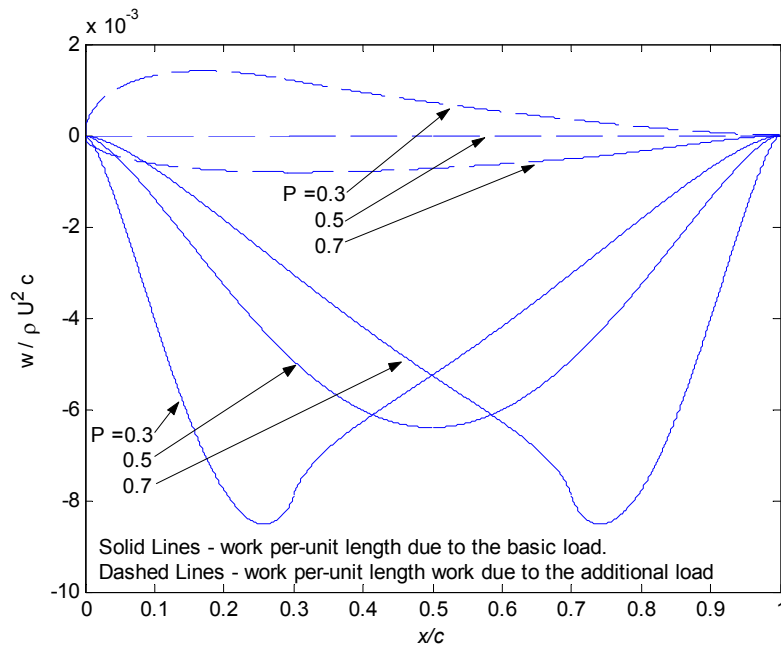


Figure 3.6: Work per-unit length for a variable camber NACA airfoil

Figure 3.7 compares the aerodynamic work required to go from an initially flat airfoil to a cambered or flapped airfoil at zero angle of attack. These are the work values ( $\overline{W}$ ) obtained from Eq. (2.9), therefore negative work values are included. If the practical aerodynamic work ( $W$ ) from Eqs. (2.13 - 2.15) was shown in Figure 3.7, the work required for all of the NACA cases would be zero because they are negative. If the work was calculated with an initial state equal to the final state used for Figure 3.7, then the required work for the NACA case would be the

negative of that shown in Figure 3.7. The required work for the flapped-airfoil would then be zero.

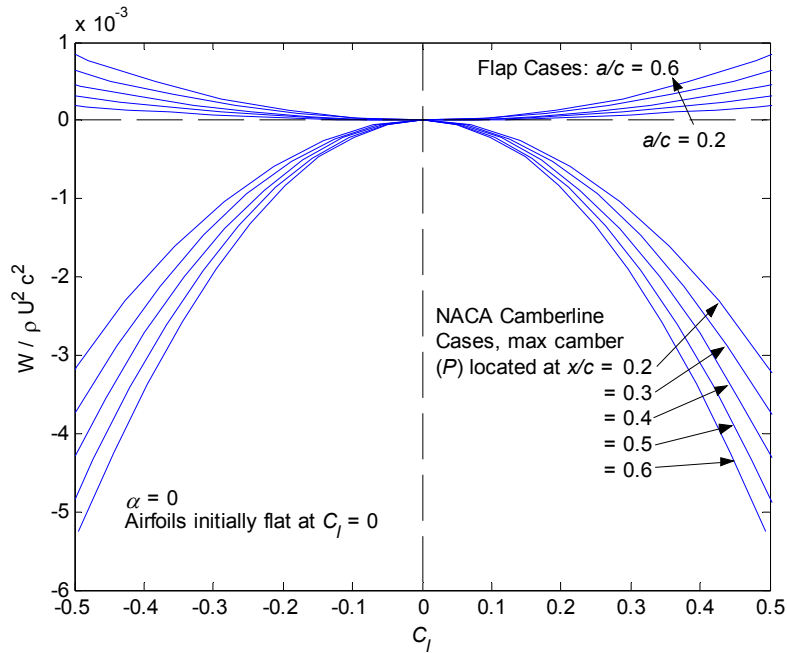


Figure 3.7: Aerodynamic work required to go from a flat airfoil to a cambered or flapped airfoil

### 3.5 Influence of a Leading-Edge Flap on a Flapped Airfoil

In Section 3.3 the aerodynamic characteristics of a flapped airfoil were determined using thin airfoil theory. Because thin airfoil theory is linear, superposition may be used to combine solutions of simple problems to handle more complex problems. This section will combine the flapped airfoil solution of Section 3.3 with a leading edge flap.

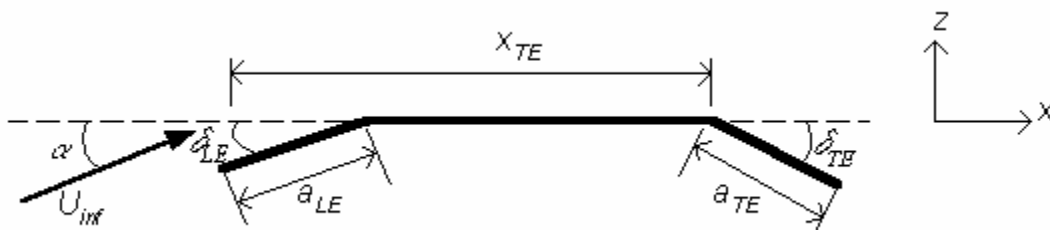


Figure 3.8: Airfoil with a leading and trailing edge flap

Figure 3.8 shows how the leading and trailing edge flap will be represented in this analysis. Following the analysis of Section 3.3, the Fourier coefficients are found to be

$$A_0 = \alpha - \frac{1}{\pi} \delta_{LE} \theta_{LE} + \frac{1}{\pi} \delta_{TE} (\pi - \theta_{TE}) \quad (3.40)$$

$$A_1 = \frac{2\delta_{LE}}{\pi} \sin \theta_{LE} + \frac{2\delta_{TE}}{\pi} \sin \theta_{TE} \quad (3.41)$$

$$A_2 = \frac{\delta_{LE}}{\pi} \sin(2\theta_{LE}) + \frac{\delta_{TE}}{\pi} \sin(2\theta_{TE}) \quad (3.42)$$

where

$$\theta_{LE} = \cos^{-1}(1 - 2a_{LE})$$

$$\theta_{TE} = \cos^{-1}(2a_{TE} - 1)$$

The basic and additional load distributions are found from Eqs. (3.9) and (3.11) to be

$$\gamma_b(\theta) = \frac{2U_\infty \delta_{LE}}{\pi} \ln \left( \frac{\sin \theta \tan(\theta_{LE}/2) - \cos \theta + 1}{\sin \theta \tan(\theta_{LE}/2) + \cos \theta - 1} \right) + \frac{2U_\infty \delta_{TE}}{\pi} \ln \left( \frac{\sin \theta \tan(\theta_{TE}/2) - \cos \theta + 1}{\sin \theta \tan(\theta_{TE}/2) + \cos \theta - 1} \right) \quad (3.43)$$

$$\gamma_a(\theta) = 2U_\infty \left\{ \alpha - \frac{1}{\pi} \delta_{LE} \theta_{LE} + \frac{1}{\pi} \delta_{TE} (\pi - \theta_{TE}) \right\} \left[ \frac{1 + \cos \theta}{\sin \theta} \right] \quad (3.44)$$

Figure 3.9 shows the components of Eqs. (3.43) and (3.44) due to the leading and trailing edge flaps. It is seen that a positive deflection of the leading edge flap causes negative lift.

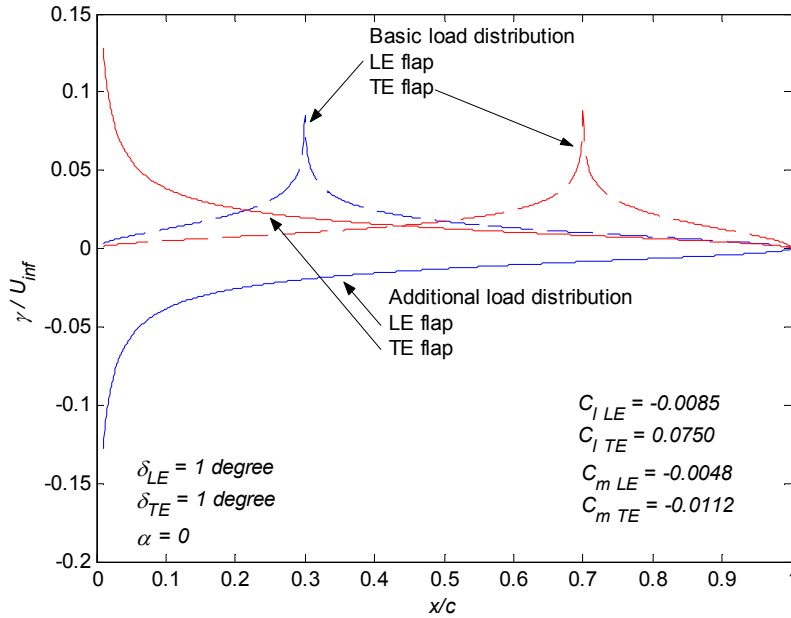


Figure 3.9: Load distribution comparison of a LE and TE flap

Section 2.4 developed the general aerodynamic work expressions for an airfoil with multiple control surfaces. For this case, with a leading and trailing edge flap combination,  $N=2$ ,  $\beta_1=\delta_{LE}$  and  $\beta_2=\delta_{TE}$ . The  $f$  functions for the work equations are as follows

$$\begin{aligned}
 &0 \leq \theta \leq \theta_{LE} \\
 &f_{LE}(\theta) = 0.5(\cos \theta_{LE} - \cos \theta) \\
 &f_{TE}(\theta) = 0 \\
 \\
 &\theta_{LE} \leq \theta \leq \theta_{TE} \\
 &f_{LE}(\theta) = f_{TE}(\theta) = 0 \\
 \\
 &\theta_{TE} \leq \theta \leq \pi \\
 &f_{LE}(\theta) = 0 \\
 &f_{TE}(\theta) = -0.5(\cos \theta_{TE} - \cos \theta)
 \end{aligned} \tag{3.45}$$

### 3.6 Modeling a Two-Segment Trailing-Edge Flap

This section discusses the modeling and influence of a trailing edge surface consisting of two straight line segments as shown in Figure 3.10.

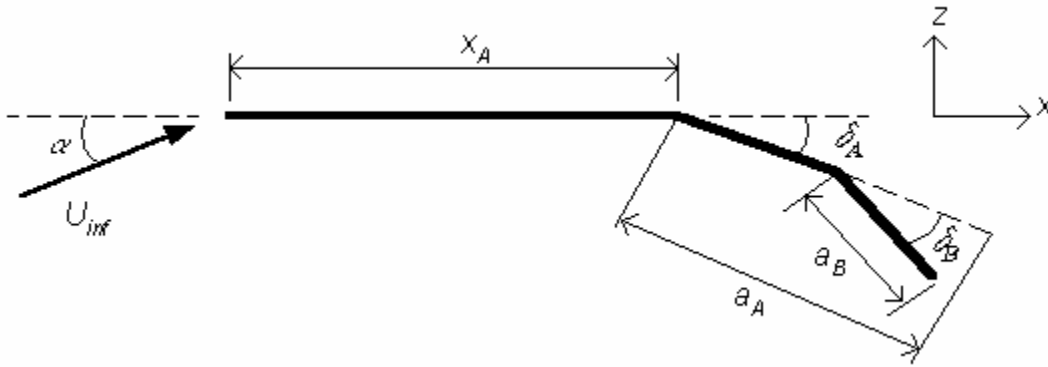


Figure 3.10: Airfoil with a two-segment trailing-edge flap

Following the analysis of Section 3.3, the Fourier coefficients for the lift and pitching moment coefficients (Eqs. (3.6) and (3.8)) are found to be

$$A_0 = \alpha + \frac{1}{\pi} \delta_A (\pi - \theta_A) + \frac{1}{\pi} \delta_B (\pi - \theta_B) \quad (3.46)$$

$$A_1 = \frac{2\delta_A}{\pi} \sin \theta_A + \frac{2\delta_B}{\pi} \sin \theta_B \quad (3.47)$$

$$A_2 = \frac{\delta_A}{\pi} \sin(2\theta_A) + \frac{\delta_B}{\pi} \sin(2\theta_B) \quad (3.48)$$

where

$$\theta_A = \cos^{-1}(2a_A - 1)$$

$$\theta_B = \cos^{-1}(2a_B - 1)$$

The basic and additional load distributions are found from Eqs. (3.9) and (3.11) to be

$$\gamma_b(\theta) = \frac{2U_\infty \delta_A}{\pi} \ln \left( \frac{\sin \theta \tan(\theta_A/2) - \cos \theta + 1}{\sin \theta \tan(\theta_A/2) + \cos \theta - 1} \right) + \frac{2U_\infty \delta_B}{\pi} \ln \left( \frac{\sin \theta \tan(\theta_B/2) - \cos \theta + 1}{\sin \theta \tan(\theta_B/2) + \cos \theta - 1} \right) \quad (3.49)$$

$$\gamma_a(\theta) = 2U_\infty \left\{ \alpha + \frac{1}{\pi} \delta_A (\pi - \theta_A) + \frac{1}{\pi} \delta_B (\pi - \theta_B) \right\} \left[ \frac{1 + \cos \theta}{\sin \theta} \right] \quad (3.50)$$

To apply the work equations developed in Section 2.4,  $N=2$ ,  $\beta_1=\delta_A$ ,  $\beta_2=\delta_B$ . Assuming an actuator for each of the hinge lines, the  $f$  functions are

$$0 \leq \theta \leq \theta_A$$

$$f_A(\theta, a_A) = f_B(\theta, a_B) = 0$$

$$\theta_A \leq \theta \leq \theta_B$$

$$f_A(\theta, a_A) = -0.5(\cos \theta_A - \cos \theta)$$

$$f_B(\theta, a_B) = 0$$

(3.51)

$$\theta_B \leq \theta \leq \pi$$

$$f_A(\theta, a_A) = -0.5(\cos \theta_A - \cos \theta)$$

$$f_B(\theta, a_B) = -0.5(\cos \theta_B - \cos \theta)$$

Notice that the area of actuation for flap A spans from  $\theta_A \leq \theta \leq \pi$ , and for flap B from  $\theta_B \leq \theta \leq \pi$ . These areas overlap because the deflection of flap A moves everything behind  $x_A$ , including flap B.

Figure 3.11 shows the components of the load distribution represented by Eqs. (3.49) and (3.50) due to the deflection of each flap. It is clear that this configuration is simply the combination of two trailing flaps. It is seen that each flap hinge-line produces a singularity. This is very undesirable from a viscous flow perspective.

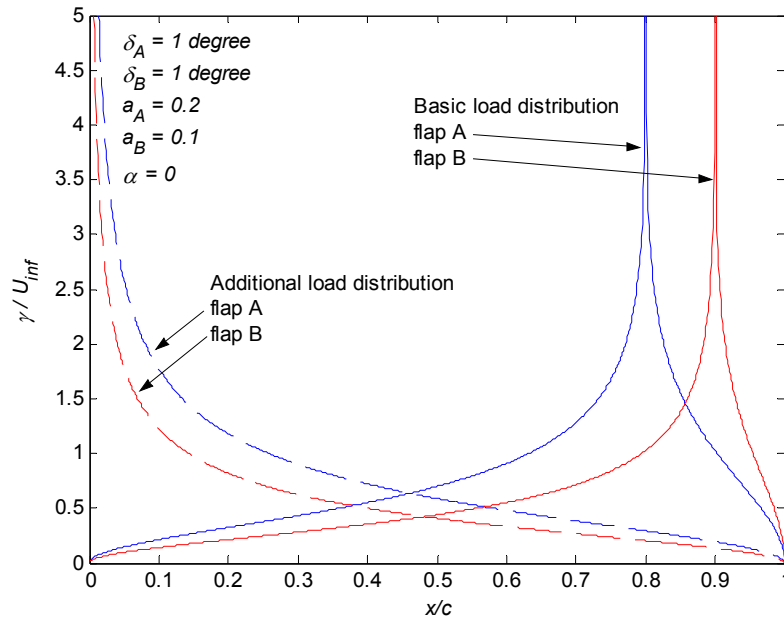


Figure 3.11: Load distribution for a two-segment trailing edge flap

### 3.7 Modeling a Morphing Trailing-Edge Device

The morphing trailing edge device modeled here is similar to the two-segment trailing edge flap except that the slope of the camber line is continuous. This continuous slope prevents any singularities from occurring in the basic load distribution. The single flap morphing case was studied by Sanders *et al.* [2003], who used a similar thin airfoil analysis to obtain an analytic representation of the load distribution. The expressions for these load distributions were not presented though. The results of this section were validated with the figures presented by Sanders *et al.* [2003].

Like the two-segment flap, the deflection of surface B is defined relative to surface A as shown in Figure 3.12. A quadratic curve defines both surfaces, with the coefficients determined by matching the desired deflections  $\delta_A$  and  $\delta_B$ . It is also required that the camberline be continuous and have a continuous slope. The resulting camberline equations are written as

$$0 \leq x \leq x_A$$

$$z(x) = 0$$

$$x_A \leq x \leq x_B$$

$$z(x) = a_1 x^2 + b_1 x + c_1 \quad (3.52)$$

$$x_B \leq x \leq 1$$

$$z(x) = a_2 x^2 + b_2 x + c_2$$

with

$$a_1 = \frac{-\delta_A}{2(x_B - x_A)}$$

$$a_2 = \frac{\delta_B}{2(x_B - 1)}$$

$$b_1 = \frac{-\delta_A x_A}{x_A - x_B}$$

$$b_2 = \frac{\delta_A - (\delta_A + \delta_B)x_B}{x_B - 1} \quad (3.53)$$

$$c_1 = \frac{-\delta_A x_A^2}{2(x_B - x_A)}$$

$$c_2 = \frac{-\delta_A(x_A + x_B - x_A x_B) + (\delta_A + \delta_B)x_B^2}{2(x_B - 1)}$$

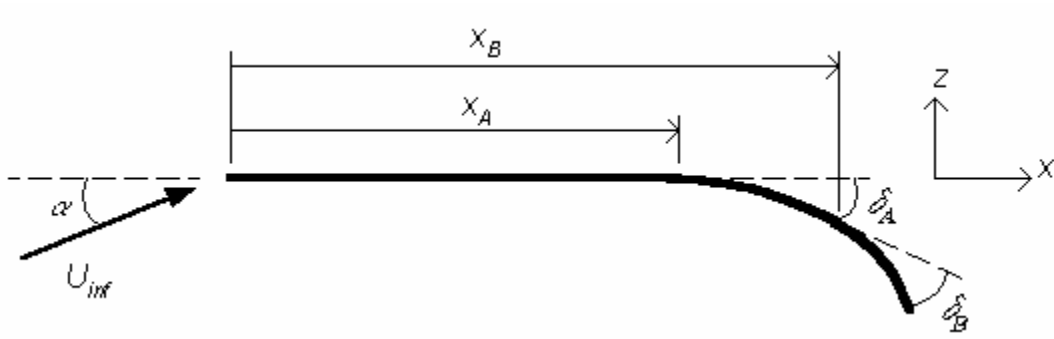


Figure 3.12: Representation of the morphing trailing edge device

The Fourier coefficients for the lift and pitching moment coefficients (Eqs. (3.6) and (3.8)) are found from Eqs. (3.3 – 3.5) to be

$$\begin{aligned}
A_0 &= \alpha - \frac{1}{\pi} \left[ (a_1 + b_1)(\theta_B - \theta_A) - a_1(\sin \theta_B - \sin \theta_A) \right. \\
&\quad \left. + (a_2 + b_2)(\pi - \theta_B) + a_2 \sin \theta_B \right] \\
A_1 &= \frac{2}{\pi} \left\{ (a_1 + b_1)(\sin \theta_B - \sin \theta_A) - 0.5a_1[(\theta_B - \theta_A) + 0.5(\sin 2\theta_B - \sin 2\theta_A)] \right. \\
&\quad \left. - (a_2 + b_2)\sin \theta_B - 0.5a_2[(\pi - \theta_B) - 0.5\sin 2\theta_B] \right\} \\
A_2 &= \frac{2}{\pi} \left[ 0.5(a_1 + b_1)(\sin 2\theta_B - \sin 2\theta_A) - a_1 \left( \frac{\sin \theta_B - \sin \theta_A}{2} + \frac{\sin 3\theta_B - \sin 3\theta_A}{6} \right) \right. \\
&\quad \left. - 0.5(a_2 + b_2)\sin 2\theta_B + a_2 \left( \frac{\sin \theta_B}{2} + \frac{\sin 3\theta_B}{6} \right) \right]
\end{aligned} \tag{3.54}$$

The basic and additional load distribution produced by each surface was found from Eq. (3.9) and (3.11), resulting in

$$\begin{aligned}
\Delta p_{b,A}(\theta) &= \frac{2\rho U_\infty^2}{\pi} \left\{ T_A(\theta_B - \theta_A)\sin \theta - [S_A + T_A \cos \theta] \ln \left( \frac{\sin \theta \tan(\theta_A/2) - \cos \theta + 1}{\sin \theta \tan(\theta_A/2) + \cos \theta - 1} \right) \right. \\
&\quad \left. + [S_A + T_A \cos \theta + 1] \ln \left( \frac{\sin \theta \tan(\theta_B/2) - \cos \theta + 1}{\sin \theta \tan(\theta_B/2) + \cos \theta - 1} \right) \right\} \\
\Delta p_{a,A}(\theta) &= -\frac{2\rho U_\infty^2}{\pi} [S_A(\theta_B - \theta_A) + T_A(\sin \theta_B - \sin \theta_A) + R_A(\pi - \theta_B)] \left[ \frac{1 + \cos \theta}{\sin \theta} \right] \\
\Delta p_{b,B}(\theta) &= \frac{2\rho U_\infty^2}{\pi} \left\{ T_B(\pi - \theta_B)\sin \theta - [S_B + T_B \cos \theta] \ln \left( \frac{\sin \theta \tan(\theta_B/2) - \cos \theta + 1}{\sin \theta \tan(\theta_B/2) + \cos \theta - 1} \right) \right\} \\
\Delta p_{a,B}(\theta) &= -\frac{2\rho U_\infty^2}{\pi} [T_B \sin \theta_B + R_B(\pi - \theta_B)] \left[ \frac{1 + \cos \theta}{\sin \theta} \right]
\end{aligned} \tag{3.55}$$

where

$$\begin{aligned}
S_A &= \frac{-0.5 + x_A}{x_B - x_A} \\
S_B &= \frac{-x_B + 0.5}{x_B - 1} \\
T_A &= \frac{0.5}{x_B - x_A} \\
T_B &= -\frac{0.5}{x_B - 1} \\
R_A &= -1 \\
R_B &= \frac{0.5 - x_B}{x_B - 1}
\end{aligned}$$

The  $f$  functions for the work calculation are:

$$\begin{aligned}
& 0 \leq \theta \leq \theta_A \\
& f_A(\theta) = f_B(\theta) = 0 \\
& \theta_A \leq \theta \leq \theta_B \\
& f_A(\theta) = -\frac{1}{8} \frac{1}{x_B - x_A} (1 - \cos \theta)^2 - \frac{1}{2} \frac{x_A}{x_A - x_B} (1 - \cos \theta) - \frac{1}{2} \frac{x_A^2}{x_B - x_A} \\
& f_B(\theta) = 0 \\
& \theta_B \leq \theta \leq \pi \\
& f_A(\theta) = -\frac{1}{2} (1 - \cos \theta) + \frac{1}{2} (x_B + x_A) \\
& f_B(\theta) = \frac{1}{8} \frac{1}{x_B - 1} (1 - \cos \theta)^2 - \frac{1}{2} \frac{x_B}{x_B - 1} (1 - \cos \theta) + \frac{0.5x_B^2}{x_B - 1}
\end{aligned} \tag{3.56}$$

where between  $\theta_B$  and  $\pi$ , the  $f$  function for flap A is linear and the  $f$  function for flap B is taken relative to this line. This assumes an actuator is located at  $x_A$  and  $x_B$ .

Figure 3.13 shows a comparison of the trailing edge shape required to achieve  $\Delta C_l$  equal to 0.1 for a conventional flap and a morphing single-degree of freedom flap (meaning  $\delta_A = 0$ ). It is seen that the morphing flap requires significantly less overall deflection than the conventional flap, although the required  $\delta$  is actually less for the conventional flap. Figure 3.14 shows the load distribution over the control surfaces corresponding to the trailing edge shapes shown in Figure 3.13. The distribution for the morphing case is seen to be centered further from the ‘‘hinge’’ than for the conventional case. This appears unfavorable from a work standpoint for the morphing case. Nevertheless, when these distributions are combined with the deflections in Figure 3.13, the morphing case is found to require 16% less work to achieve a  $\Delta C_l$  equal to 0.1. Figure 3.15 shows the distribution of the work per-unit length, which is obtained by combining Figures 3.13 and 3.14.

Figure 3.16 shows the effect of various flap to chord ratios and the effect of angle of attack on the required work. This indicates that the lower required work for the morphing case over the conventional case is a general characteristic of the single degree of freedom morphing camberline. Figure 3.16 also shows that  $\alpha$  has a larger effect on the required work for the conventional case than for the morphing case. This is because, as shown in Figure 3.13, the morphing case requires less overall deflection, and therefore the constant  $\alpha$ -dependent load distribution acting during the deflection produces a smaller work component.

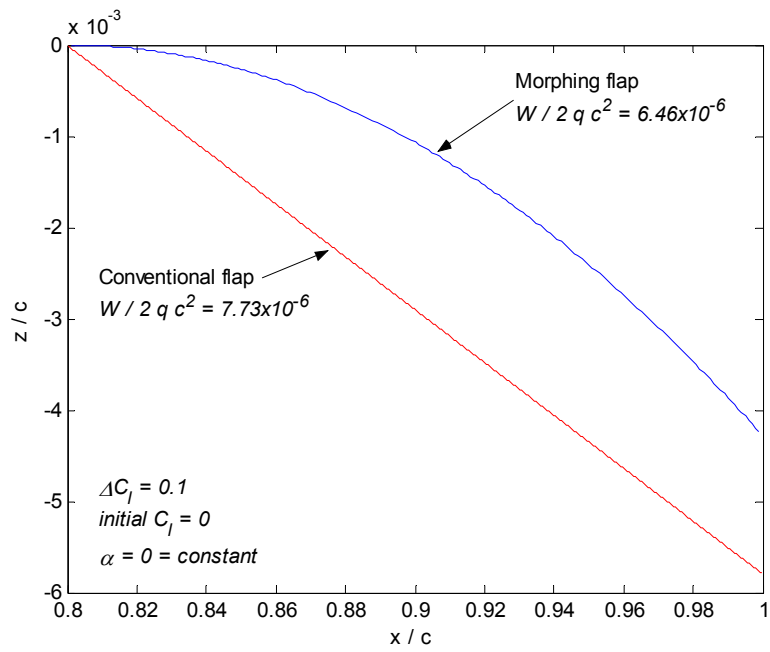


Figure 3.13: A comparison of the trailing-edge camberline shapes required for a  $C_l = 0.1$

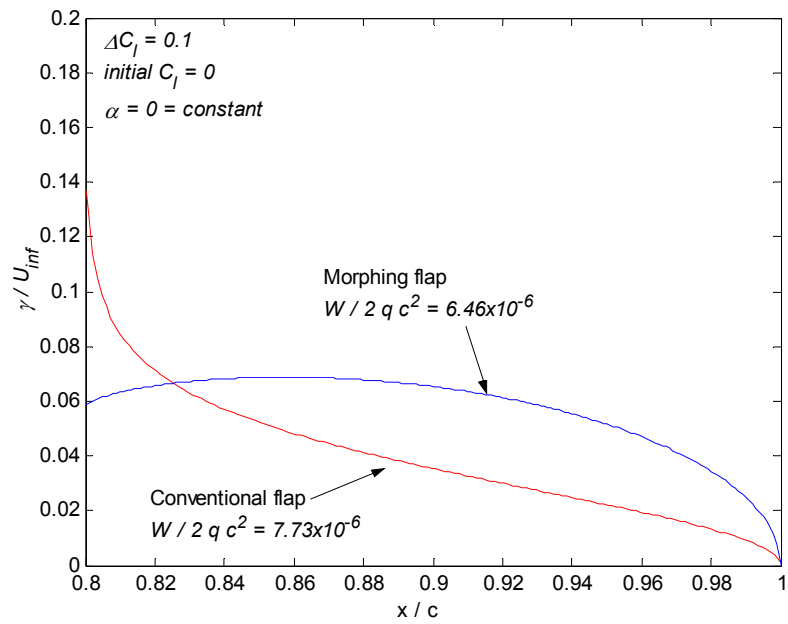


Figure 3.14: A comparison of the trailing-edge load distribution required for a  $C_l = 0.1$

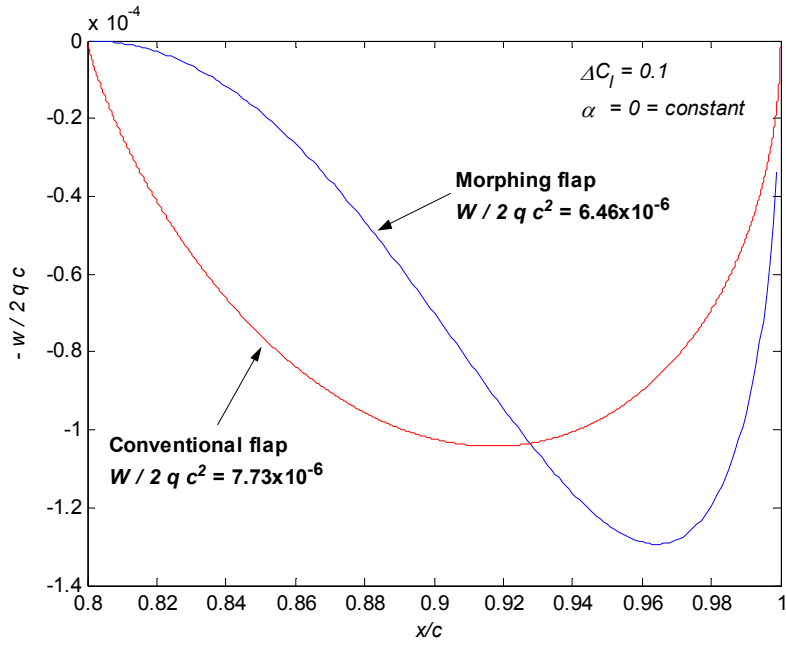


Figure 3.15: A comparison of the work per-unit length required for a  $C_l = 0.1$

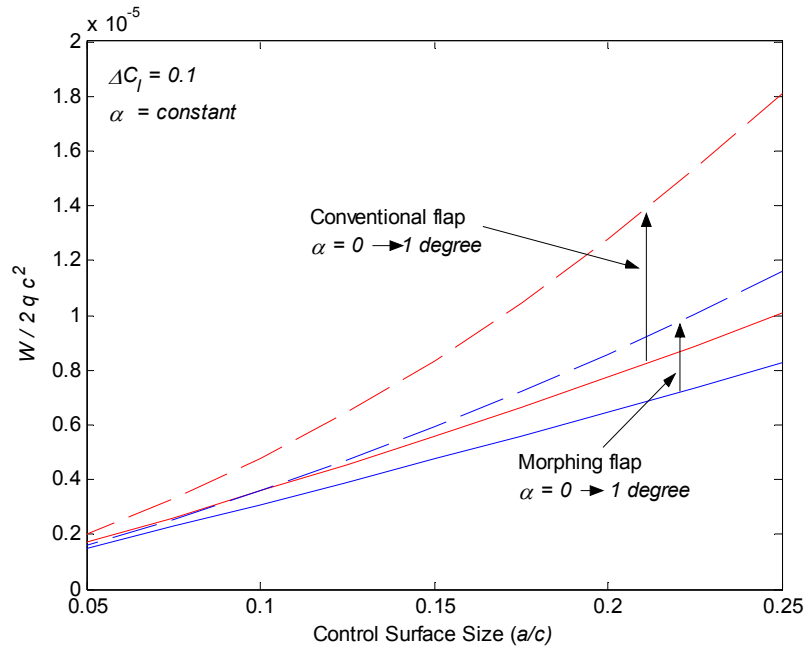


Figure 3.16: A comparison of the required work for a  $\Delta C_l = 0.1$

### 3.8 Trim Considerations

The aerodynamic work equations were developed with the freedom to allow  $\alpha$  to change between the initial and final state. This freedom in  $\alpha$  is desired because it allows an airfoil configuration to achieve a change in lift in a realistic manner. For an aircraft performing longitudinal maneuvers, the main purpose of the control surface is to produce the pitching moments required to change the aircraft's  $\alpha$ . It is primarily  $\alpha$  that produces the change in lift, while the control surfaces allow the aircraft to achieve and maintain that particular  $\alpha$ .

For the aerodynamic work calculations, it is required that the aircraft be trimmed at the initial and final state. To calculate the  $\beta_n$  values required to achieve trimmed flight at a given  $C_l$ , the following equations are used

$$C_l = C_{l_\alpha} \alpha + \sum_{n=1}^N C_{l_n} \beta_n \quad (3.57)$$

$$C_{M_{cg}} = C_{l_\alpha} (x_{cg}/c - 0.25) \alpha + \sum_{n=1}^N [C_{l_n} (x_{cg}/c - 0.25) + C_{M_n}] \beta_n$$

where the  $C_{M_n}$  is relative to the quarter chord and any camber or twist is represented through  $\beta_n$ .

Solving the equation  $C_{M_{cg}} = 0$  for  $\alpha$  and substituting this value into the  $C_l$  equation results in

$$C_l = - \left( \frac{\sum_{n=1}^N [C_{l_n} (x_{cg}/c - 0.25) + C_{M_n}] \beta_n}{(x_{cg}/c - 0.25)} \right) + \sum_{n=1}^N C_{l_n} \beta_n \quad (3.58)$$

$$= - \frac{\sum_{n=1}^N C_{M_n} \beta_n}{(x_{cg}/c - 0.25)}$$

which represents the trimmed  $C_l$ . It is seen from Eq. (3.58) that if  $N$  is greater than one, there are infinitely many combinations of  $\beta_n$  to achieve a given trimmed  $C_l$ .

From Eq. (3.58) the control deflections required for flight at the initial and final  $C_l$  value can be calculated. But, before these values are used in the previously developed aerodynamic work equations, one more issue must be discussed. Because the quasi-steady aerodynamic assumption has already been made, it is assumed that the control surfaces are deflected relatively slowly. This allows the additional assumption that the dynamic process of the  $\alpha$ -change is quasi static,

meaning  $C_M = 0$  throughout the process. This quasi-static process is understood by considering a small control surface increment away from a trimmed state, which causes a small nonzero pitching moment. This nonzero moment causes a small acceleration leading to a small pitch rate and change in  $\alpha$ . For a statically stable aircraft (meaning  $dC_M/d\alpha < 0$ ), a restoring pitching moment is created as  $\alpha$  changes which leads to a trimmed state ( $C_M = 0$ ) at an  $\alpha$  different from the initial value. This process is shown in Figure 3.17 for a configuration with a single control  $\beta$  initially trimmed at  $C_{L,t1}$ ,  $\alpha_1$  and  $\beta_1$  and then going to  $C_{L,t2}$ ,  $\alpha_2$  and  $\beta_2$ . This process is not possible for an unstable aircraft because the zero-lift pitching moment increment required to increase the trimmed  $C_L$  is in the opposite direction of the pitching moment required to rotate the aircraft to the trimmed  $\alpha$ .

Consider a flapped-airfoil with  $a = 0.2c$  and  $x_{cg} = 0$ . If it is desired to trim this configuration at a  $C_l$  of 0.1, Eq. (3.58) must be solved for  $\delta (= \beta)$ . This results in  $\delta = -2.23$  degrees, which trims the configuration at  $\alpha = 2.14$  degrees. Now, assume it is desired to change to a  $C_l$  equal to 0.3. The required  $\delta$  for this  $C_l$  is calculated as before, and is found to equal  $-6.71$  degrees with an  $\alpha$  of 6.42 degrees. To calculate the aerodynamic work required for this process, Eqs. (2.13-2.15) are applied with  $\beta_1 = \delta_1 = -2.23$  degrees,  $\beta_2 = \delta_2 = -6.71$  degrees,  $\alpha_1 = 2.14$  degrees, and  $\alpha_2 = 6.42$  degrees. As discussed previously, the assumption that  $\alpha$  changes linearly as the flap deflects restricts the work calculation to a stable aircraft with a flap being deflected slowly. If, for example, the flap was deflected suddenly, the entire deflection would occur at the initial  $\alpha$ , and therefore  $\alpha_2$  should not be used in the work calculation. For the current example, the work is  $5.41 \times 10^{-5} \rho U^2 c^2$  if  $\alpha$  changes linearly from the initial to final value as the flap deflects. If the flap is deflected entirely while the aircraft is at the initial  $\alpha$ , the aerodynamic work is  $8.3 \times 10^{-5} \rho U^2 c^2$ . The increase of aerodynamic work for the second case is a result of the reduction in the  $\alpha$ -dependent lift, which acts in the direction of the flap motion because the flap deflections are negative.

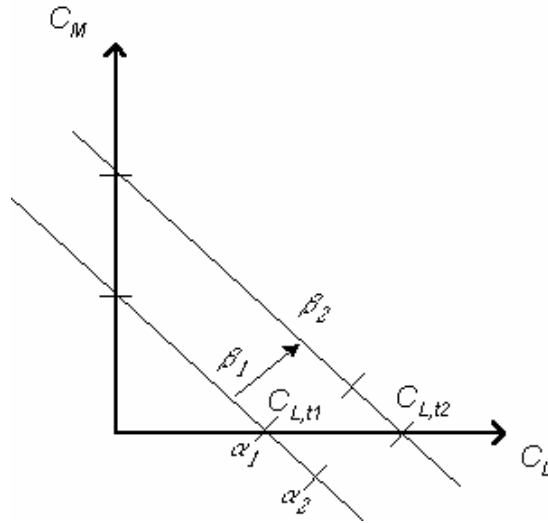


Figure 3.17: Effect of control deflections on the trimmed  $C_L$  of a stable configuration

### 3.9 Chapter Summary

Chapter 3 applies thin airfoil theory to various control surface configurations to provide an aerodynamic model for the work calculation discussed in Chapter 2. Along with the usual calculation of the aerodynamic coefficients using the first three Fourier coefficients (Eqs. (3.3 - 3.8)), analytic solutions for the load distribution are found using Eq. (3.11). The author is unaware of any previous analytic solutions to Eq. (3.11) for quadratic camberlines. These solutions are presented in Eqs. (3.38) and (3.55) for the NACA camberline and the morphing trailing-edge flap (MTE). Section 3.7 shows that less work is required to obtain a  $\Delta C_l$  with a single-surface morphing flap than with a conventional flap. Figures 3.13 – 3.15 show that this is true because the  $\Delta z$  required for the morphing flap is less than for the conventional flap. It is also shown that because the morphing flap requires less  $\Delta z$ , the influence of an  $\alpha$ -dependent load distribution on the work is less than that for a conventional flap.

# Chapter 4

## The Minimum Aerodynamic Work for an Airfoil Geometry Change

### 4.1 Introduction

The term aerodynamic work is defined in this thesis to mean the actuator work required to overcome the aerodynamic forces acting on an airfoil. As emphasized in Chapter 2, results considering just the aerodynamic component of the actuator work are meaningful only if there is no structural component. It is the author's opinion though that aerodynamic work is less intuitive than structural work, and therefore deserves to be studied independently of structural work. The current chapter does this by examining the control surface deflections that require the least amount of aerodynamic work for a given  $\Delta C_l$ . The minimum work deflections will also be examined for multiple  $C_l$  change cases to represent a flight path.

The thin airfoil theory aerodynamic models developed in Chapter 3 will be used for this investigation. Because of the  $C_l$  change constraint, which is linear with the control parameters ( $\beta_n$ ), only cases that have more than one control surface can be used for the optimization problem. This limits the investigation to the leading edge-trailing edge (LETE) flap airfoil, two-segment trailing edge (TETAB) flap airfoil, and the two-segment morphing trailing edge (MTE) airfoil. The TETAB and MTE cases are considered first in Sections 4.2 – 4.4 because of their similarities. The LETE configuration, which is a somewhat special case, is considered in Section 4.5. The effects of aeroelasticity will be investigated in the next chapter.

## 4.2 Minimum Work Control Deflections Required for a Single $\Delta C_l$ Away from an Initially Flat Airfoil

This section examines the control deflections for the minimum aerodynamic work required by an initially flat airfoil remaining at  $\alpha = 0$  to obtain a single  $\Delta C_l$  with the TETAB or MTE control configuration. Cases are examined that require that  $\alpha$  remain constant along with cases that allow  $\alpha$  to vary by considering the trim constraint discussed in Section 3.8. This simplified problem allows some insight to be gained into the nature of minimum work control deflections. To begin, it is helpful to examine the work equations developed in Chapter 2. In particular, the case of zero required work is investigated. With  $\beta_{m_1}$ ,  $\alpha_1$ , and  $\alpha_2$  all equal to zero, the integrands of the work equation ( $I_m$ ), Eq (2.17), can be written as

$$\begin{aligned} I_A(\tau) &= -\{Q_{A,A}\beta_{A_2} + Q_{A,B}\beta_{B_2}\}\beta_{A_2}\tau \\ I_B(\tau) &= -\{Q_{B,A}\beta_{A_2} + Q_{B,B}\beta_{B_2}\}\beta_{B_2}\tau \end{aligned} \quad (4.1)$$

where it is assumed that there are two control surface  $A$  and  $B$  (the letters  $A$  and  $B$  are used here instead of numbers 1 and 2 so that they are not confused with the states 1 and 2). It should be remembered that for conventional hinged control surfaces,  $Q_{m,n}$  can be thought of as the hinge moment acting on control surface  $m$  per unit deflection of control surface  $n$ . Since it desired to find the work required to obtain a desired  $C_l$ , one  $\beta$  can be written in terms of the other through the  $C_l$  equation. The  $C_l$  equation at state 2 is written as

$$C_l = C_{l_A}\beta_{A_2} + C_{l_B}\beta_{B_2}$$

so

$$\begin{aligned} \beta_{B_2} &= \frac{C_l - C_{l_A}\beta_{A_2}}{C_{l_B}} \\ &= k_1 - k_2\beta_{A_2} \end{aligned} \quad (4.2)$$

where

$$\begin{aligned} k_1 &= \frac{C_l}{C_{l_B}} \\ k_2 &= \frac{C_{l_A}}{C_{l_B}} \end{aligned}$$

From Eq. (4.1), it is seen that  $I_A(\tau = 0)$  and  $I_B(\tau = 0)$  will both be zero. Therefore, if zero required work is desired,  $I_A(\tau = 1)$  and  $I_B(\tau = 1)$  must be less than or equal to zero. If these equations

cannot be satisfied, then it is not possible to obtain with zero work the desired  $\Delta C_l$  with this control surface configuration. To examine these possibilities, Eq. (4.2) is substituted into Eq. (4.1) leading to

$$\begin{aligned}
 I_A(\tau=1) &= -Q_{A,A}\beta_{A_2}^2 - Q_{A,B}(k_1 - k_2\beta_{A_2})\beta_{A_2} \\
 &= (k_2Q_{A,B} - Q_{A,A})\beta_{A_2}^2 - Q_{A,B}k_1\beta_{A_2} \\
 I_B(\tau=1) &= -Q_{B,A}(k_1 - k_2\beta_{A_2})\beta_{A_2} - Q_{B,B}(k_1 - k_2\beta_{A_2})^2 \\
 &= (Q_{B,A}k_2 - Q_{B,B}k_2^2)\beta_{A_2}^2 + (2Q_{B,B}k_1k_2 - Q_{B,A}k_1)\beta_{A_2} - Q_{B,B}k_1^2
 \end{aligned} \tag{4.3}$$

The value or values of  $\beta_{A_2}$  that make  $I_A(\tau=1)$  and  $I_B(\tau=1)$  less than or equal to zero can be found by setting the equations in (4.3) equal to zero and solving each equation independently for  $\beta_{A_2}$ . Both equations in (4.3) are quadratic in  $\beta_{A_2}$ , which results in four total roots when both equations are solved independently. Two of these roots form the boundary of the “region of zero work,” if it exists. Plotting  $I_A(\tau=1)$  and  $I_B(\tau=1)$  allows the roots that form this boundary to be obtained by finding the region where both  $I_A(\tau=1)$  and  $I_B(\tau=1)$  are negative. An example of this is shown in Figure 4.1 for a TETAB airfoil with  $a_A = 0.2$  and  $a_B = 0.15$  (see Section 3.6 for definitions, note that  $\beta = \delta$  for this case) obtaining a  $\Delta C_l$  of 0.1. The roots for this example are 0 and 5.24 degrees for  $I_A(\tau=1)$  and 1.65 and 5.82 degrees for  $I_B(\tau=1)$ , where between the roots 5.24 and 5.82 degrees, zero work is required. It should be mentioned that this range of deflections is actually a region of the ratio of the deflections of the two control surfaces, which is constant for varying  $C_l$  values. This is because although one is solving for  $\beta_{A_2}$ ,  $\beta_{B_2}$  is implied through the  $C_l$  constraint (Eq. (4.2)).

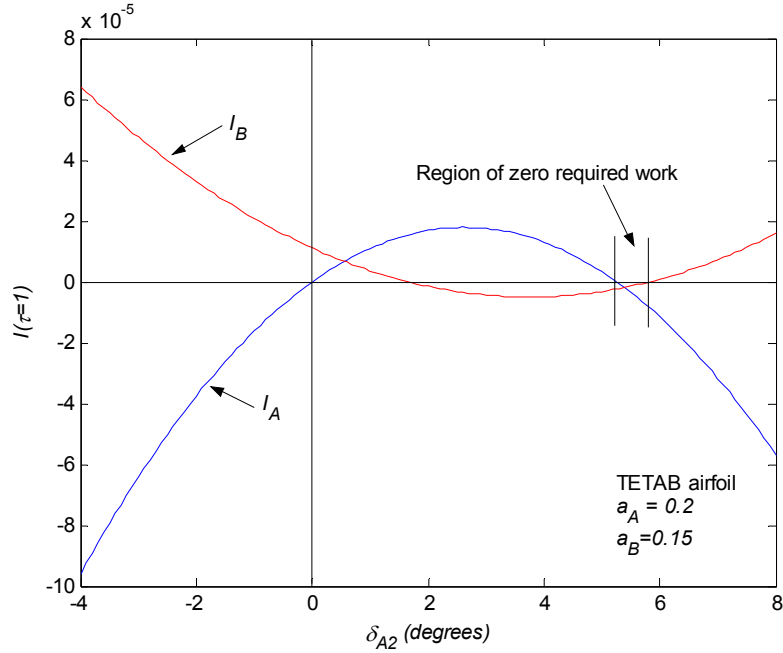


Figure 4.1: Work integrands for a TETAB airfoil

Figure 4.2 shows a plot of  $I(\tau = 1)$  for a TETAB airfoil with  $a_A = 0.2$  and  $a_B = 0.05$ . In this case, there is no region of zero work because at no  $\delta_{A_2}$  are both  $I_A(\tau = 1)$  and  $I_B(\tau = 1)$  less than or equal to zero. The value of  $\delta_{A_2}$  requiring the least aerodynamic work can be obtained from Figure 4.2 as the point where the sum of the positive  $I_A(\tau = 1)$  and  $I_B(\tau = 1)$  values is the smallest. In this case, this occurs at the point  $I_A(\tau = 1) = 0$ , where  $\delta_{A_2}$  is equal to 2.57 degrees. The reason for the minimum work point being at the point  $I_A(\tau = 1) = 0$  is a result of the  $I_A(\tau = 1)$  line having a steeper positive slope than the  $I_B(\tau = 1)$  line's negative slope around the intersection of the two lines. If the sum of the positive  $I_A(\tau = 1)$  and  $I_B(\tau = 1)$  values are taken at a small change in  $\delta_{A_2}$  to the left and right of the intersection of  $I_A(\tau = 1)$  and  $I_B(\tau = 1)$ , it is seen that this sum decreases until  $I_A(\tau = 1) = 0$ . This result holds for most two-section control surface configurations, including the TETAB and MTE configurations. The equation for  $I_A(\tau = 1) = 0$  is found from Eq. (4.3) to equal

$$\beta_{A_2} = -\frac{k_1 Q_{A,B}}{Q_{A,A} - k_2 Q_{A,B}} \quad (4.4)$$

which is therefore the solution for minimum work for an initially flat ( $C_l = 0$ ) two-segment control surface airfoil. If there is a region of zero work like in Figure 4.1, then Eq. (4.4) gives the

solution for the left hand border of the zero work region. Solving  $I_B(\tau = 1) = 0$  from Eq. (4.3) gives the right hand border of the zero work region.

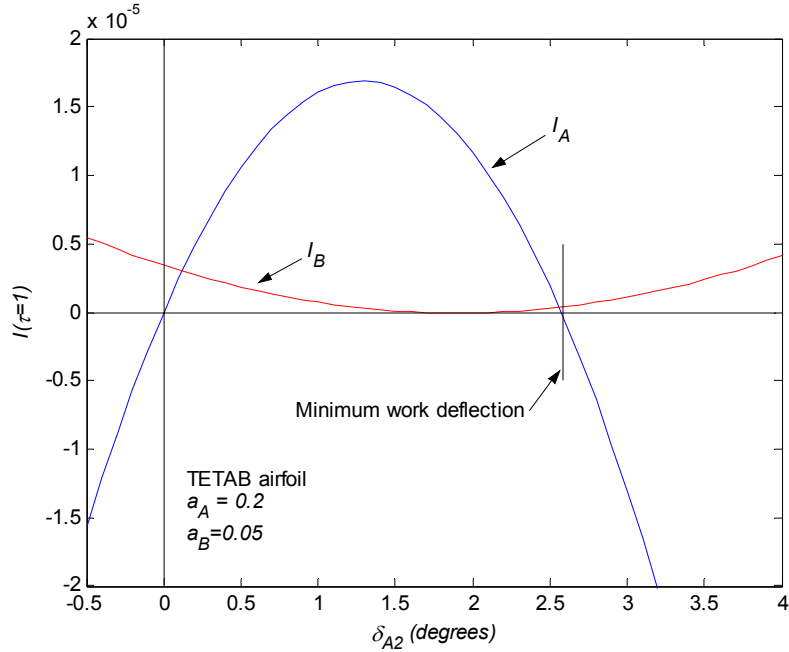


Figure 4.2: Work integrands for a TETAB airfoil

The solution shown in Eq. (4.4) was used (along with a numerical optimization scheme to assure the validity of Eq. (4.4)) to compare the minimum work values required for MTE and TETAB configurations to obtain a single  $\Delta C_l$  away from an initially flat airfoil. The LETE configuration was not considered because the deflection of the leading edge flap requires no positive work, leading to a trivial solution of  $W = 0$  by using the leading edge flap exclusively. This makes the LETE configuration ideal for a single  $\Delta C_l$ , but as will be shown in Section 4.5, a second  $\Delta C_l$  requires more work than both the MTE and TETAB cases. Figure 4.3 shows the work resulting from the minimum work deflections for the MTE and TETAB configuration with various control surface areas and  $a_B/a_A$  values. Although the MTE configuration is shown to require significantly more work than the TETAB configuration, it is still much lower than the value of  $12 \times 10^{-6} \rho U^2 c^2$  required by a single flap spanning 30% of the chord. Figure 4.4 shows the point from Figure 4.3 where  $x_A/c = 0.7$ . This shows a very different trend for varying  $a_B/a_A$  values between the MTE and TETAB cases. It is seen that beyond  $a_B/a_A$  equal to 0.55, the TETAB configuration requires no work while the MTE requires increasingly more.

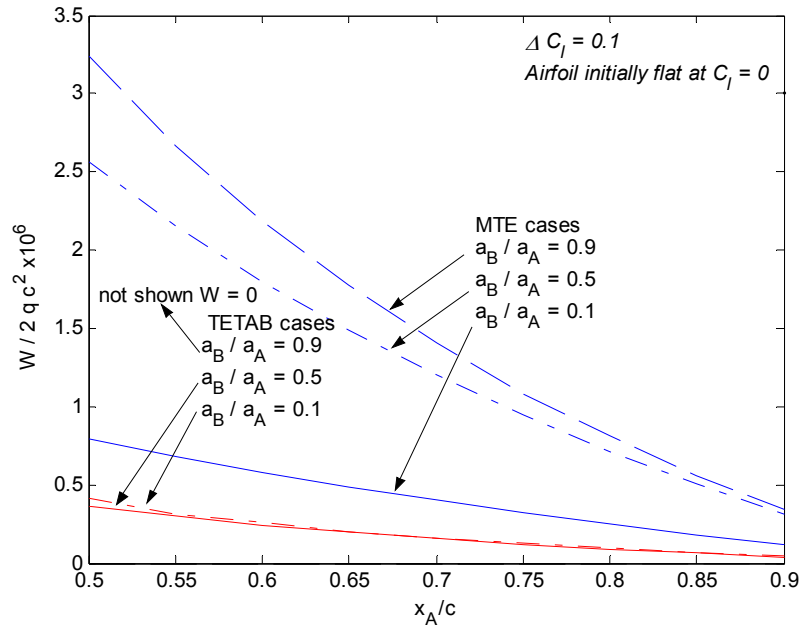


Figure 4.3: Minimum work values for various control surface arrangements

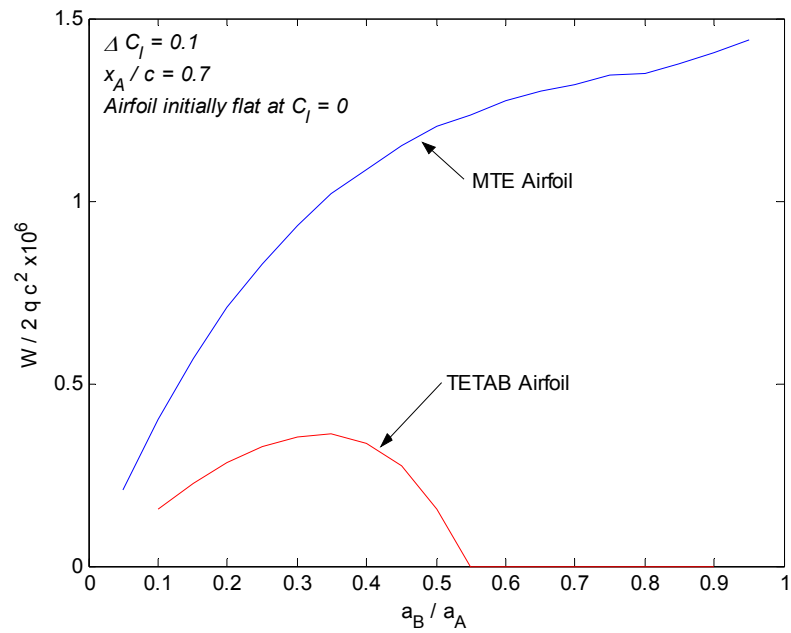


Figure 4.4: Minimum work values for various ratios of control surface size

Figure 4.5a shows the ratio of control deflections  $\delta_{A_2} / \delta_{B_2}$  corresponding to the minimum work values shown in Figure 4.4. Flap A is deflected positively (down) in all the cases shown. Figure

4.5b shows the resulting load distribution from the minimum work case corresponding to  $a_B/a_A$  in Figures 4.4 and 4.5a. As shown in Figure 4.4, the TETAB case requires no work. This is a result of the singularities present at the flap hinge lines. The MTE case does not benefit from these singularities and requires work to deflect flap B.

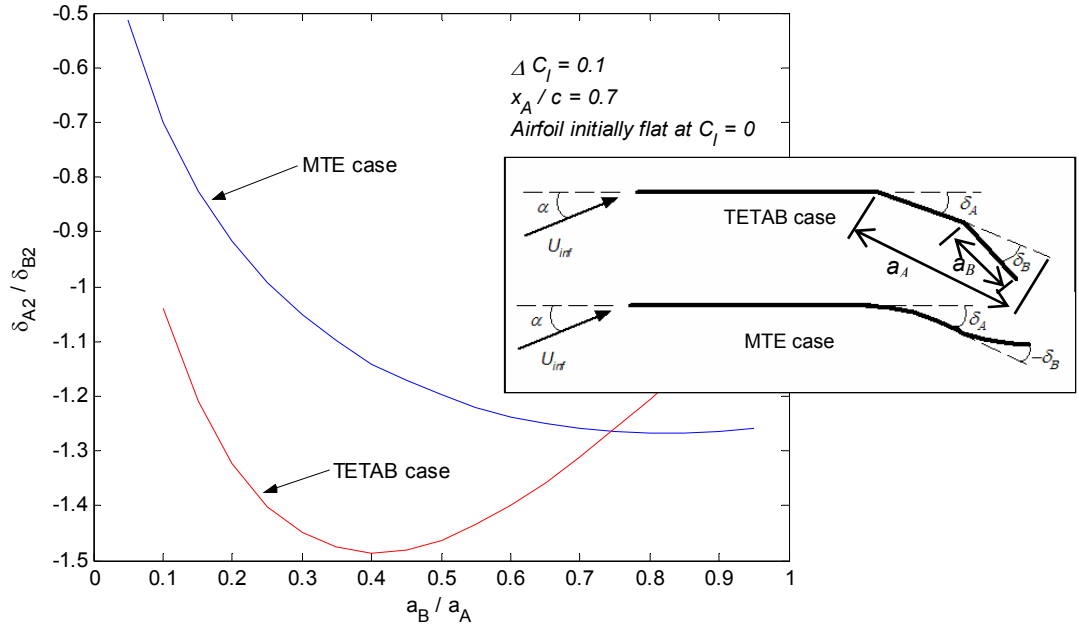


Figure 4.5a: Minimum work ratio of deflections for the case shown in Figure 4.4

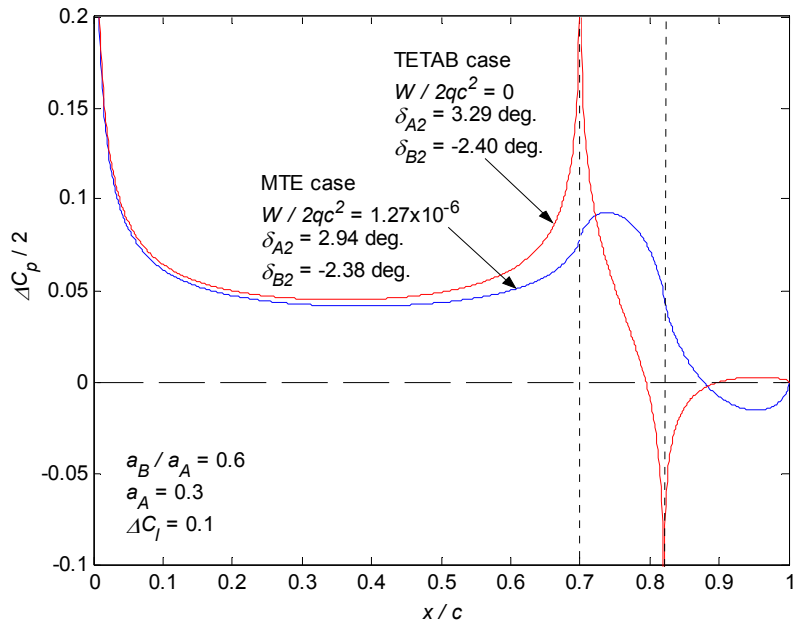


Figure 4.5b: Minimum work ratio of deflections for the case shown in Figure 4.4

The above analysis assumed  $\alpha$  remained zero between the initial and final point. Now it will be shown that enforcing the trim constraint discussed in Section 3.8 allows for the above analysis to be extended to the variable  $\alpha$  case. From Eq. (3.58), the trimmed control effectiveness of each control surface can be written as

$$C_{l,trim_n} = -\frac{C_{M_n}}{(x_{cg}/c - 0.25)} \quad (4.5)$$

where the trimmed  $\alpha$  per unit deflection of  $\beta_n$  is

$$\alpha_n = -\frac{C_{l_n}(x_{cg}/c - 0.25) + C_{M_n}}{2\pi(x_{cg}/c - 0.25)} \quad (4.6)$$

For the two-segment control surface cases analyzed previously,  $k_1$  and  $k_2$  from Eq. (4.2) are now written as

$$k_1 = \frac{C_l}{C_{l,trim_B}} = -\frac{(x_{cg}/c - 0.25)C_l}{C_{M_B}} \quad (4.7)$$

$$k_2 = \frac{C_{l_A}}{C_{l_B}} = \frac{C_{M_A}}{C_{M_B}}$$

Adding  $\alpha_A$  and  $\alpha_B$  from Eq. (4.6) to the additional load distribution for the calculation of the  $Q$  terms accounts for the change in the load distribution due to the change in  $\alpha$ . Using these  $Q$  terms and the  $k_1$  and  $k_2$  terms from Eq. (4.7), the minimum work control deflections can be found using Eq. (4.4).

Figure 4.6 shows the minimum work values for the MTE and TETAB configurations when  $\alpha$  is allowed to vary using the trim constraint. Figure 4.7 shows the ratio of control deflections corresponding to the cases presented in Figure 4.6. Comparing Figure 4.6 to Figure 4.4 it is seen that allowing the airfoil to obtain lift from  $\alpha$  greatly reduces the required work. If the configuration is neutrally stable, meaning  $x_{cg} = 0.25$ , Eq. 4.5 shows that the change in lift per unit deflection of each control surface becomes infinite. This means that the required deflection to achieve a change in lift becomes infinitely small, and therefore the required work goes to zero.

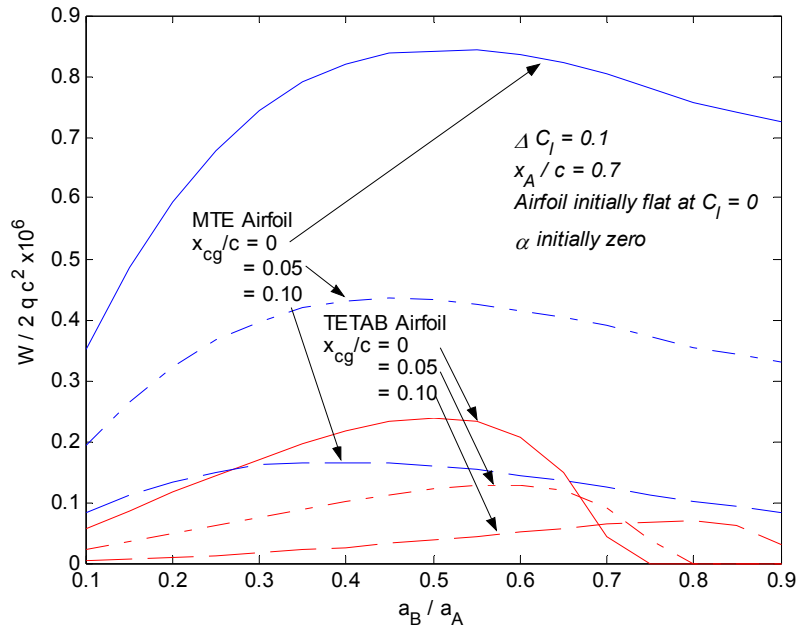


Figure 4.6: Minimum work values for various ratios of control surface size with trim constraint

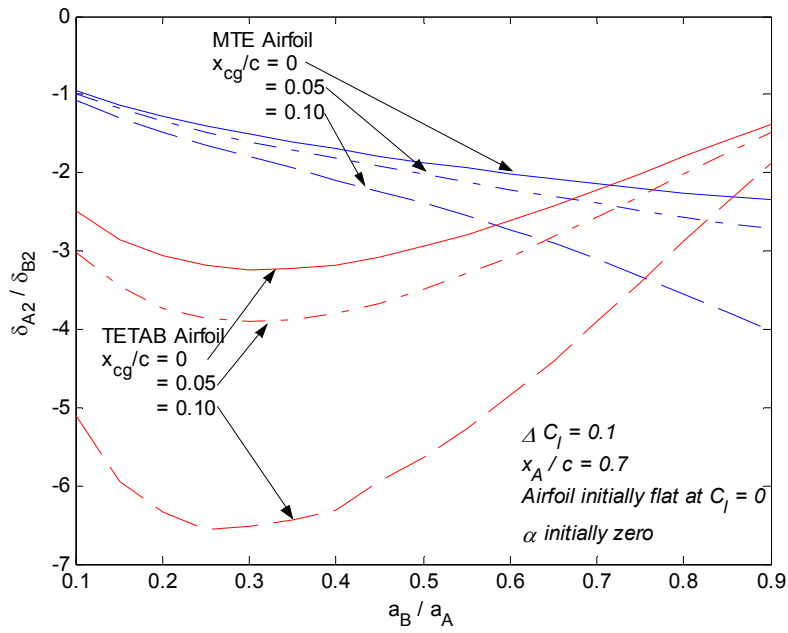


Figure 4.7: Minimum work deflections corresponding to Figure 4.6

### 4.3 Minimum Work Control Deflections Required for a Single $\Delta C_l$ on an Airfoil with an Initial $\alpha$

The previous analysis examined cases that were initially at zero degrees  $\alpha$  with no control deflections. This meant that there was no load component, which remained constant throughout the deflection process, acting on the airfoil. A more realistic analysis will now be carried out that considers a constant load component caused by an initial  $\alpha$ . The analytic treatment used above to find the minimum work deflections will not be pursued here. The fact that the initial load distribution is not zero implies that  $I_n(\tau=0)$  is not equal to zero, which makes any general treatment of the problem difficult. Instead, a numerical approach is used to find the minimum work deflections.

Figure 4.8 shows the influence of a constant  $\alpha$  on the minimum work control deflections. This figure shows that past an  $\alpha$  of about 0.5 degrees, the MTE case requires less work than the TETAB case. Figure 4.9 shows the minimum work control deflections corresponding to cases presented in Figure 4.8. It is seen that at an  $\alpha$  of about 0.8 degrees, the minimum work control deflections consist of the deflection of just flap B. This occurs because the load distribution due to  $\alpha$ , which is constant throughout the deflection process, begins to have a greater influence on the control surfaces than the load distributions caused by the control surfaces. This effect is beneficial for the MTE configuration because as was shown in Figure 3.15, the MTE configuration requires less overall deflection, or  $\Delta z$ , than the TETAB configuration. This is shown in Figure 4.9, where it is seen that the  $\delta$  values for the two cases are similar. Which, because a given  $\delta$  for the MTE case produces much less  $\Delta z$  than for the TETAB case, means that the  $\alpha$ -load distribution will have less influence on the minimum work for the MTE case.

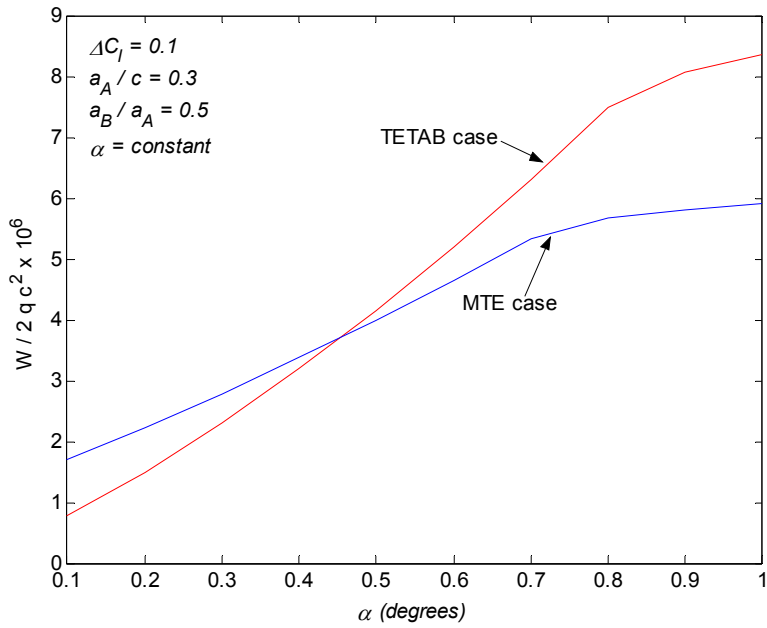


Figure 4.8: The effect of a constant  $\alpha$  on the minimum required work

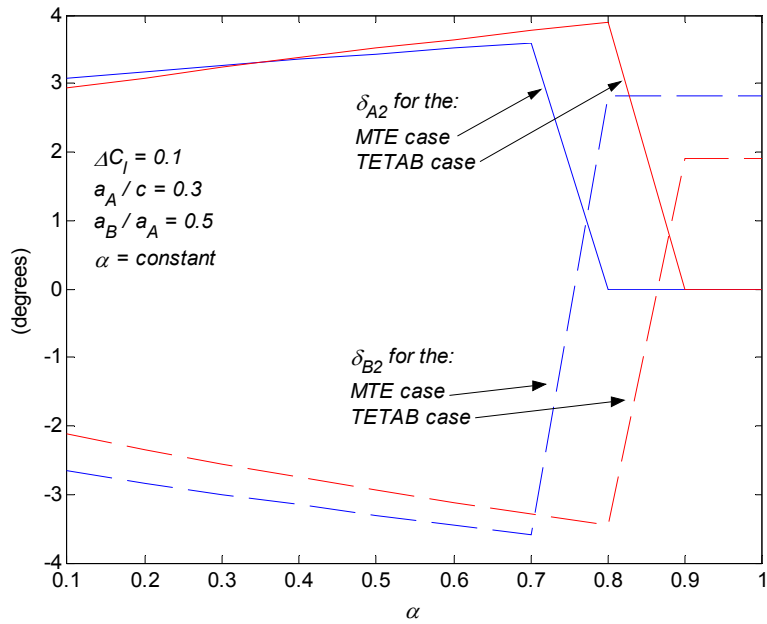


Figure 4.9: Minimum work control deflection variation with a constant  $\alpha$

The effect of enforcing the trim constraint and allowing  $\alpha$  to vary was shown in Section 4.2 to decrease the required work over the  $\alpha$ -fixed cases an amount depending on the c.g. location. For the current case where there is an initial trimmed  $C_l$ , this comparison is not as clear because it is

dependent on the control deflections required to obtain the initial trimmed  $C_l$ . Figure 4.10 shows the minimum work values for various initial trimmed  $C_l$ 's. The initial trimmed  $C_l$ 's were achieved with lift being distributed equally between the two control surfaces. Comparing the initial  $C_l = 0.1$  case with the  $\alpha$  equal 0.9 degree case of Figure 4.10 ( $\alpha = 0.9$  degrees produces a  $C_l$  of about 0.1) it is seen that variable- $\alpha$  case requires more work. This is true because of the control deflections required for the initial  $C_l$ , which were not present in the fixed  $\alpha$  case. Figure 4.10 shows, in agreement with Figure 4.8, that the larger the initial  $C_l$  is, the more beneficial the MTE case becomes in terms of required work.

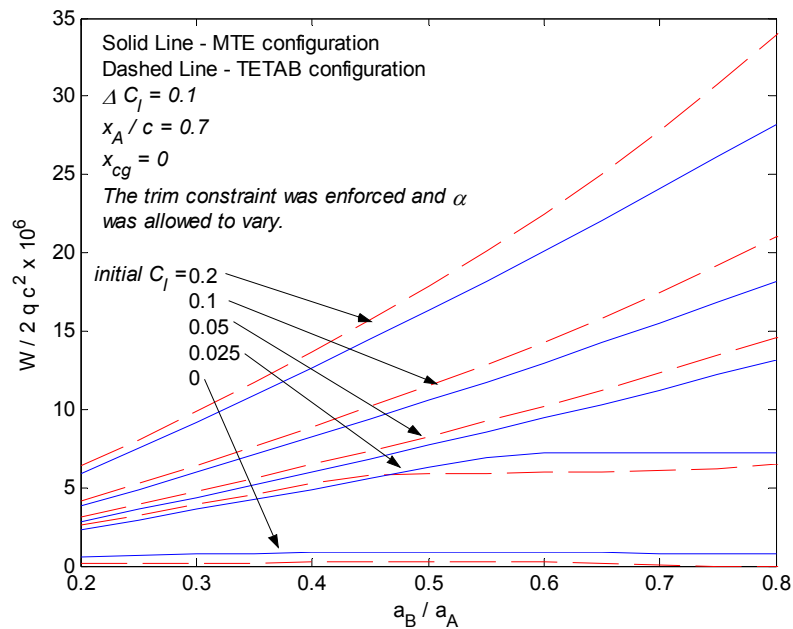


Figure 4.10: Minimum work values with an initial  $\alpha$  and allowing  $\alpha$  to vary

#### 4.4 Minimum Work Control Deflections for a Multiple $\Delta C_l$ 's

The results of the minimum work required for a single  $\Delta C_l$  in Section 4.2 and 4.3 are altered if a second  $\Delta C_l$  of opposite sign is considered in the optimization. Adding a second  $\Delta C_l$  allows the work calculated to be considered the work required for a complete flight path. Figure 4.11 shows an example of how a complex flight path can be represented with two  $C_l$  changes under the quasi-steady linear assumptions that have been made. It is desired here to investigate the influence the second  $\Delta C_l$  has on the work comparison between the LETE, MTE, and TETAB control surface configurations.

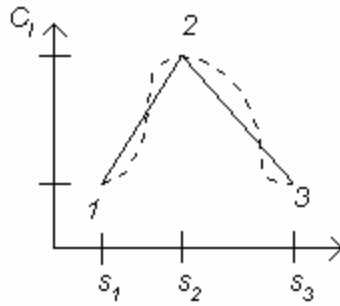


Figure 4.11: Variation of desired lift coefficients

As done in the single  $\Delta C_l$  case, it is helpful to consider the simplified problem of an initially flat airfoil at zero-degrees  $\alpha$ . It can be shown that the minimum aerodynamic work required for this airfoil to obtain a given  $C_l$  and then return to a  $C_l$  of zero is directly related to the single  $\Delta C_l$  case. Consider Figure 4.2, which shows for the single  $\Delta C_l$  case that if there is no region of zero work, then the minimum work deflections are obtained from Eq. (4.4). Eq. (4.4) solves for  $\delta_{A_2}$  when  $I_A$  equals zero and  $I_B$  is positive. This positive value of  $I_B$  at the end of the first  $\Delta C_l$  is represented in Figure 4.12 as the value of  $I_{A,12}$  at the end of the  $\tau_{12}$  line. From Eq. (2.17) it is seen that at the beginning of the second  $\Delta C_l$  the value of  $I_B$  will be equal in magnitude and opposite in sign to the value at the end of the first  $\Delta C_l$ . This is shown in Figure 4.12 and means that the work required for the second  $\Delta C_l$  will be zero. The final control deflections are zero and the problem is solved by determining the deflections for state 2 from Eq. 4.4.

If, as shown in Figure 4.1, there is a region of zero work for the first  $\Delta C_l$ , then there will be work required for the second  $\Delta C_l$ . In this case, the second  $\Delta C_l$  determines the control deflections and the problem is a reverse of the previous problem. Because of this symmetry, the minimum work control deflections are again found from Eq. (4.4). This means that for the minimum aerodynamic work for the two  $\Delta C_l$  case, a region of zero work will exist for one  $\Delta C_l$  and work will be required for the other  $\Delta C_l$ .

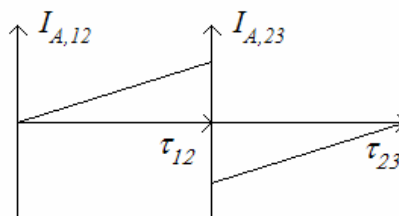


Figure 4.12: The influence of the second  $\Delta C_l$  on the minimum work

## 4.5 The Minimum Work for a LETE Configuration

The LETE configuration is a special case because the two control surfaces are not connected as they are in the TETAB and MTE cases. The influence of this on two  $\Delta C_l$  changes will be briefly discussed below.

Consider a leading and trailing edge flap combination with both flaps being 20% of the chord. Let  $C_{l,1} = 0$ ,  $C_{l,2} = 0.1$ ,  $C_{l,3} = 0$ , where the subscripts 1, 2, and 3 refer to the initial, middle, and final states as shown in Figure 4.11. Assume that both control surfaces are initially undeflected, meaning  $\delta_{LE,1}$  and  $\delta_{TE,1}$  equal zero, and that the airfoil remains at  $\alpha = 0$ . It is desired to find the leading and trailing edge deflections for states 2 and 3 that require the minimum total work. Figure 4.13 shows a surface plot of the work values for different combinations of  $\delta_{LE,2}$  and  $\delta_{LE,3}$ .

The deflections for minimum work were found to be

$$\delta_{LE,2} = -9.5^\circ$$

$$\delta_{TE,2} = 0.95^\circ$$

$$\delta_{LE,3} = -9.5^\circ$$

$$\delta_{TE,3} = -0.70^\circ$$

which result in  $W/2qc^2 = 4.17 \times 10^{-6}$ . This is considerably larger than the  $0.3 \times 10^{-6}$  or  $2 \times 10^{-6}$  values required for the TETAB and MTE cases with  $x_A = 0.6$ . But it is considerably less than the  $12 \times 10^{-6}$  required by a single flap spanning 30% of the chord. Figures 4.14 and 4.15 show the load distributions produced by the minimum work deflections for this case. It is seen in Figure 4.14 that no work is required to deflect the leading edge flap from state 1 to 2. If it was not required to go to state 3, the optimum deflection for state 2 would consist of just the leading edge flap deflection so that the no work was required. But since state 3 is considered, there is a tradeoff between the leading and trailing edge deflections.

The above discussion shows that although the LETE flap combination appears favorable from a work standpoint for a single  $\Delta C_l$ , if two  $\Delta C_l$ 's are considered, the configuration is found to require more work than the TETAB or MTE configurations.

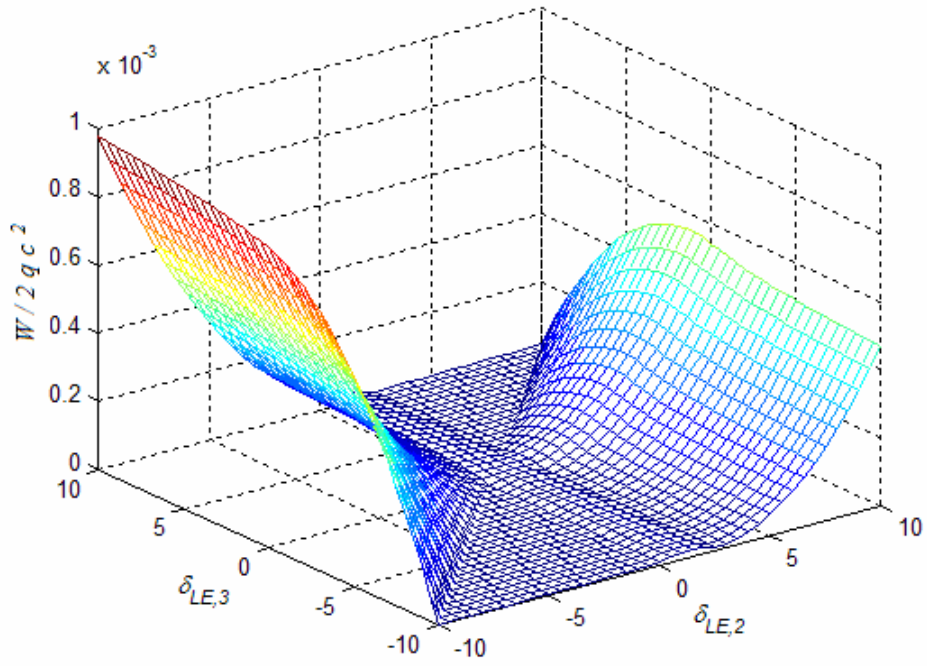


Figure 4.13: Work required to achieve  $C_{l,1} = 0$ ,  $C_{l,2} = 0.1$  and  $C_{l,3} = 0$

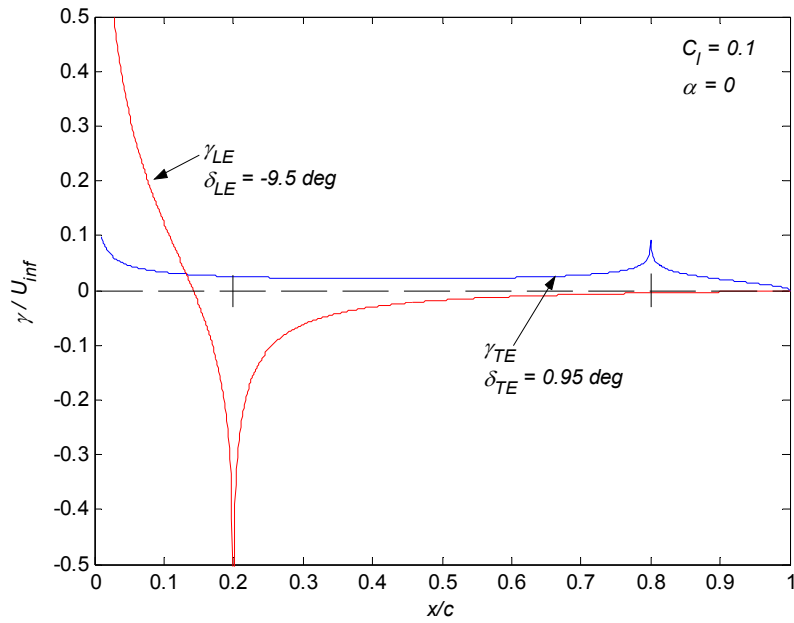


Figure 4.14 Load distributions at state 2

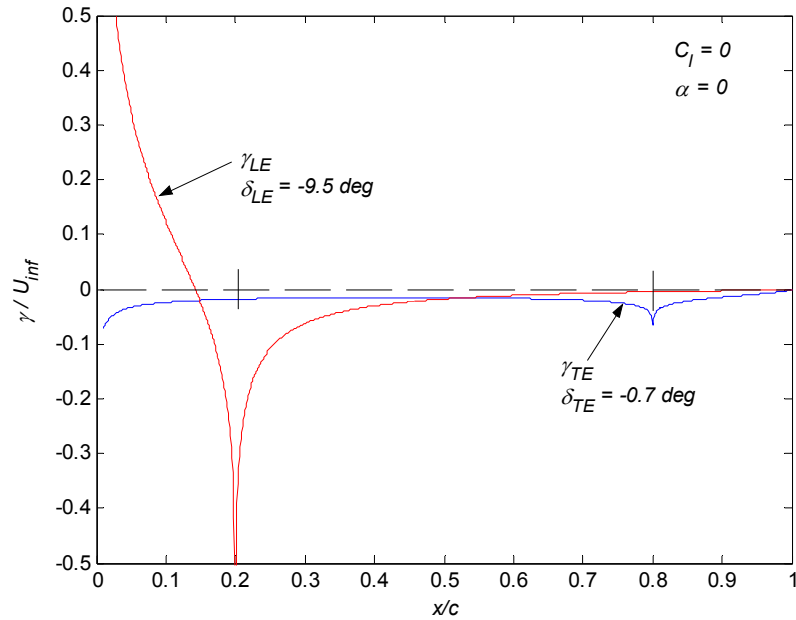


Figure 4.15: Load distributions at state 3

## 4.6 Chapter Summary

Chapter 4 presents a method for determining the control deflections that require the minimum aerodynamic work for a given  $\Delta C_l$ . This method is based on the work equations developed in Chapter 2 and the aerodynamic characteristics developed in Chapter 3. For an initially flat airfoil at zero- $\alpha$  with two control surfaces, Eq (4.4) was derived. This equation represents the minimum work control deflections for a given  $\Delta C_l$ . Figures 4.3 and 4.4 show that the TETAB configuration requires less work than the MTE configuration for cases where  $\alpha$  remains zero. Section 4.3 shows that there is certain  $\alpha$  past which the MTE case requires less work than the TETAB case. This is true because a given  $\delta$  for the MTE case produces much less  $\Delta z$  than for the TETAB case, which means that the  $\alpha$ -load distribution has a smaller influence on the minimum work for the MTE case. Section 4.4 discusses the minimum work for multiple  $\Delta C_l$ 's and shows that it is closely related to the minimum work for a single  $\Delta C_l$ . Section 4.5 investigates the leading-edge trailing-edge flap, which is shown to be considerably different than the two-segment trailing-edge devices.

# Chapter 5

## The Effect of Aeroelasticity on the Required Aerodynamic Work

### 5.1 Introduction

An important issue in the analysis of an aerodynamic control device is the influence of aeroelasticity on the effectiveness of the control device. This chapter will study this issue by examining the effect of aeroelasticity on the required aerodynamic work for a given change in lift. Section 5.2 will discuss the addition of static aeroelastic effects to the airfoil models developed in Chapter 3 as well as review the basic concepts of the active aeroelastic wing concept. Section 5.3 will compare the work required for single control surface morphing and conventional flaps. Section 5.4 will compare the work required for two-segment morphing (MTE) and conventional (TETAB) flaps. The benefits of the active aeroelastic wing concept will be shown to become clear upon studying the influence of dynamic pressure on the minimum work control deflections.

### 5.2 Aeroelastic Considerations

This section will review the modeling of a 1-DOF static aeroelastic airfoil, which will be used to extend the airfoil model of Chapter 3. The notation and technique will follow that of Forster *et al.* [2003], who conducted a similar study as discussed in Chapter 1.

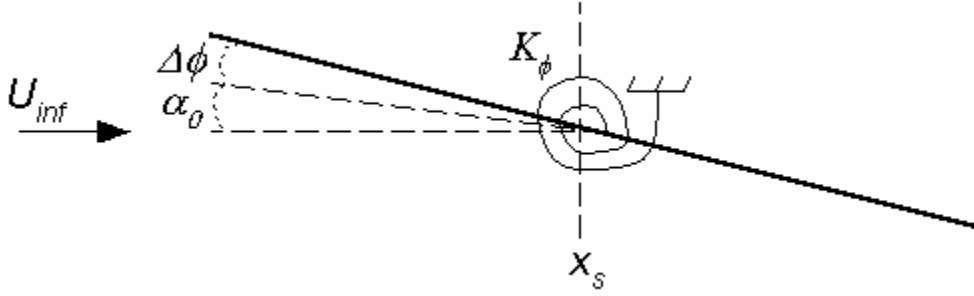


Figure 5.1: Flexible airfoil representation

Figure 5.1 shows the representation of an airfoil that is free to twist around a shear center ( $x_s$ ) with a spring constant  $K_\phi$ . The initial angle of attack is  $\alpha_0$ , which can be thought of as the equilibrium  $\alpha$  when no aerodynamic forces are applied. When aerodynamic forces are applied, the equilibrium  $\alpha$  is found by summing the pitching moments acting about  $x_s$ . This results in:

$$qc^2 \left[ eC_{l_\alpha} (\alpha_0 + \Delta\phi) + \sum_{n=1}^N (eC_{l_n} \beta_n + C_{M_n} \beta_n) \right] = K_\phi \Delta\phi \quad (5.1)$$

where  $e = x_s / c - 0.25$ . Solving Eq. (5.1) for  $\Delta\phi$  leads to

$$\Delta\phi = \frac{qc^2 \left[ eC_{l_\alpha} \alpha_0 + \sum_{n=1}^N (eC_{l_n} \beta_n + C_{M_n} \beta_n) \right]}{K_\phi - eC_{l_\alpha} qc^2} \quad (5.2)$$

where the equilibrium  $\alpha$  is now  $\Delta\phi + \alpha_0$ . The effect of aeroelasticity in the current 1-DOF static airfoil model is represented entirely by  $\Delta\phi$  in Eq (5.2).

Figure 5.2 shows, using an example presented by Forster *et al.* [2003], the effect of aeroelasticity on the initial (corresponding to  $\delta_{A,1}$  and  $\delta_{B,1}$ ) and final (corresponding to  $\delta_{A,2}$  and  $\delta_{B,2}$ ) load distributions. The difference between the initial state with aeroelastics and the initial state without aeroelastics is the additional load distribution due to  $\Delta\phi_1$ . It is seen that only the final state with aeroelastics is shown in Figure 5.2. The final state without aeroelastics is not shown because, as a result of  $\Delta\phi_2$  being very near zero, it is nearly the same as the final state with aeroelastics.

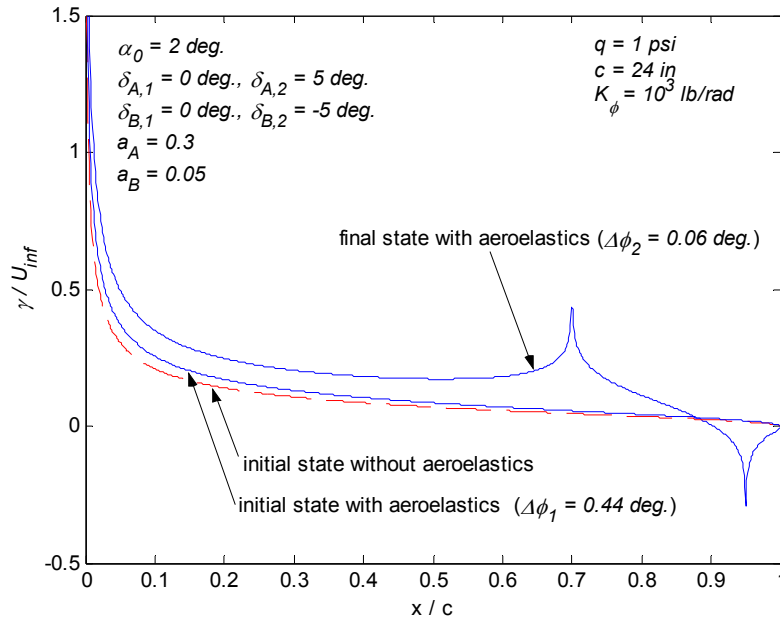


Figure 5.2: Example load distributions including aeroelastic effects

It is convention to define the dynamic pressure when the denominator of  $\Delta\phi$  becomes zero as the divergence dynamic pressure ( $q_D$ ). This is written as:

$$q_D = \frac{K_\phi}{ec^2 C_{l_\alpha}} \quad (5.3)$$

where it should be noted that this is independent of the control surfaces on the airfoil. The dynamic pressure of interest for control surfaces is the reversal dynamic pressure ( $q_R$ ), which is the dynamic pressure at which the flexible control effectiveness of a control surface is zero. The flexible control effectiveness ( $\tilde{C}_{l_\beta}$ ) can be written as

$$\tilde{C}_{l_\beta} = C_{l_\alpha} \Delta\phi_\beta + C_{l_\beta} \quad (5.4)$$

where  $C_{l_\beta}$  is the rigid control effectiveness and  $\Delta\phi_\beta$  is the  $\Delta\phi$  per unit deflection  $\beta$ . Combining Eqs. (5.2) and (5.4) and solving for the  $q$  that makes  $\tilde{C}_{l_\beta} = 0$  results in

$$q_R = -\frac{K_\phi C_{l_\beta}}{c^2 C_{l_\alpha} C_{M_\beta}} \quad (5.5)$$

where it should be noted that on a multiple control surface configuration, there is a separate  $q_R$  for each control surface. If the deflection of a control surface is intended to produce a rolling maneuver, the reversal dynamic pressure can be interpreted as the roll reversal dynamic pressure for the current 2-D airfoil model. Figures 5.3 and 5.4, taken from Anderson, *et al.* [1997], show

the loss in roll performance and the increase in the required aileron deflection as  $q_R$  is approached. It should be understood that although Figure 5.4 shows that the required aileron deflection becomes infinite at  $q_R$ , this dynamic pressure does not represent a boundary that cannot be passed. This is shown in Figure 5.5, where it is seen that the required aileron deflection is opposite in sign of that required before  $q_R$  for the single control surface case. As long as maneuvers are not attempted at  $q_R$  and the control system is programmed to account for the aileron reversal, it should be possible to perform maneuvers at dynamic pressures around and past  $q_R$  with a single control surface. The main problem with this, though, is that the increase in the required deflections causes an increase in the drag and required actuator work.

The loss in maneuverability mentioned above as  $q_R$  is approached has led to the development of the active aeroelastic wing (AAW), which uses multiple control surfaces to reduce the required control deflections at dynamic pressures around  $q_R$  [Miller 1994]. This is shown in Figure 5.5, which indicates the reduction in the required deflections for a leading edge – trailing edge flap combination over that required for a trailing edge flap only. If more than one control surface is being used to achieve a desired roll rate, then there must be some type of cost function to uniquely choose the deflections. In the case of Figure 5.5, Anderson used a “minimum control energy criteria” which is said to “minimize the overall control surface actuator command signals.” This is similar to minimizing Eq. (2.5) when  $\eta = 1$ , which implies an equal cost for positive and negative work. Minimizing Eq. (2.5) with  $\eta = 0$ , which is used throughout this paper, will in most cases lead to the trivial solution of deflecting just the leading edge flap.

It makes sense that in Figure 5.5 the trailing edge deflection goes to zero at the trailing edge  $q_R$ , because at this point its effectiveness is zero. Notice that there is no reversal dynamic pressure for the leading edge flap. This is verified by substituting the leading edge flap characteristics shown in Figure 3.9 into Eq. (5.5), which results in a negative  $q_R$ , meaning the velocity is imaginary. Section 5.4 will study cases with two-segment trailing edge flaps in which case both control surfaces have a reversal dynamic pressure.

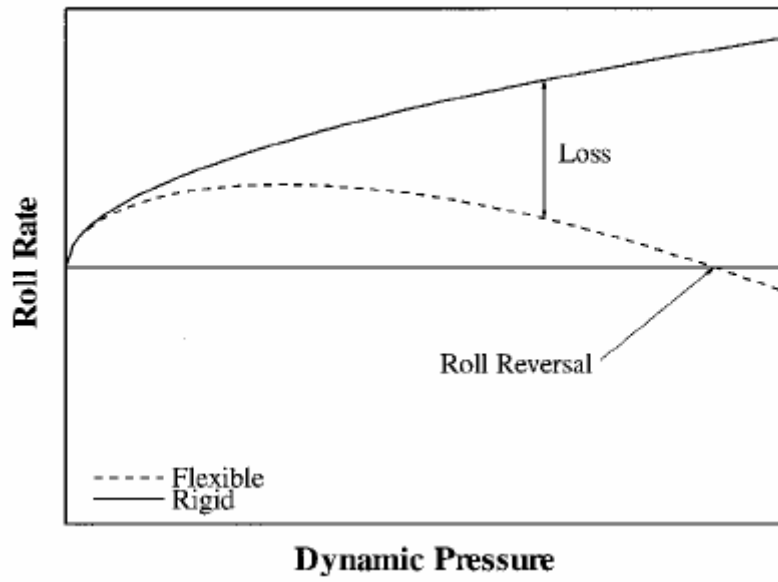


Figure 5.3: Roll rate achieved for a constant aileron deflection [Anderson, *et al.* 1997]

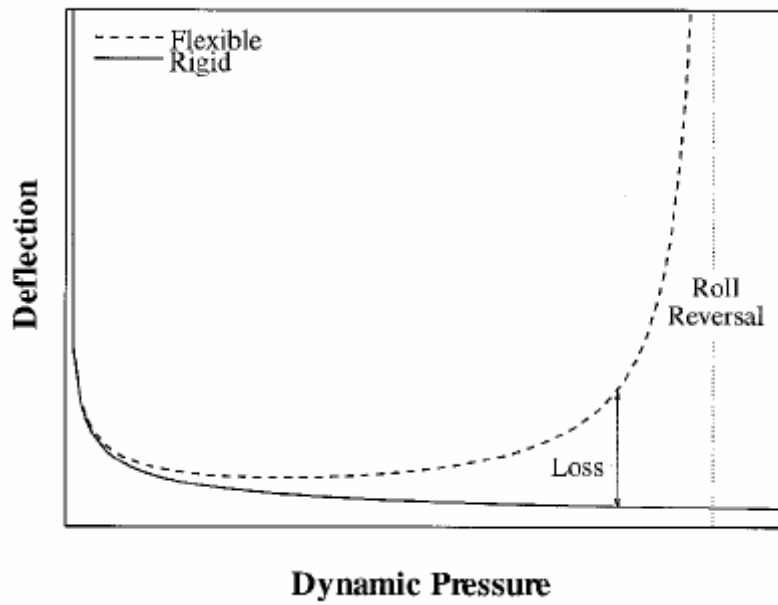


Figure 5.4: Aileron deflection required for a constant roll rate [Anderson, *et al.* 1997]

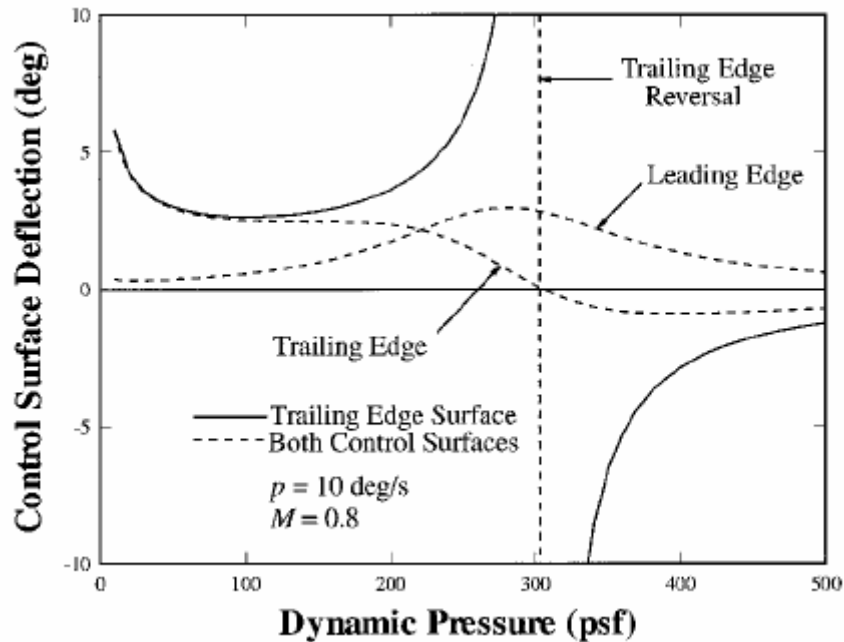


Figure 5.5: Control surface deflections required for a constant roll rate [Anderson, *et al.* 1997]

### 5.3 Required Work for Single Control Surface Cases

In Section 3.7 of Chapter 3, it was shown that a single-segment MTE device requires less work to achieve a  $\Delta C_l$  than a conventional flap. It is now desired to study the influence of aeroelasticity on this conclusion. Some aeroelastic differences between morphing and conventional cases are suspected because, as is seen in Figure 3.14, the lift is centered further back for the morphing case than for the conventional case therefore increasing the moment acting on the shear center.

The first case that will be examined is the work required for a single-surface morphing or conventional flap to achieve a lift ( $\Delta C_l q c$ ) of 0.5 lbs away from an initially flat airfoil at zero angle of attack. Notice that now we are comparing the work for a given change in lift, and not  $C_l$  as was done in Chapter 4. This is done because it is desired to compare the required work for different dynamic pressures, in which case the lift force corresponding to a given  $C_l$  is different. It should also be mentioned that a change in lift is used instead of a roll rate because it is a more basic quantity. For the current 2-D airfoil model, a change in lift can be transformed into a steady upward motion, which is the 2-D equivalent to a rolling motion, through the following equation [Weisshaar 2000]:

$$\frac{v}{U_\infty} = \frac{\Delta l}{qcC_{l_\alpha}} \quad (5.5)$$

where  $v$  represents the steady upward motion and  $\Delta l$  is the change in lift on the airfoil. Figure 5.6 shows the work required for the given change in lift for dynamic pressures less than  $q_R$  (the airfoil size and shape parameters are listed in the figure). It is shown that for low dynamic pressures, the conclusion reached in Section 3.7 that a morphing flap requires less work than a conventional flap still holds. But, for  $q/q_D > 0.085$ , the work required for the conventional flap becomes less than that required for the morphing flap. Figures 5.7 and 5.8 show the required control deflections and the resulting wing twist deformation for this case. As expected, the control deflections for the morphing and conventional cases follow the same trends. Comparing the magnitudes of the morphing and conventional deflections in Figure 5.7 is not very meaningful because it is dependent on how the deflection angles are defined. The magnitude of the wing deformation angle ( $\Delta\phi$ ) in Figure 5.8 is meaningful, though, and succeeds in showing why the morphing flap requires more work as  $q/q_D$  becomes large. The morphing flap produces larger negative  $\Delta\phi$  values, which means that more negative lift is created that must be compensated for with more control deflection, therefore increasing the required work. Figure 5.9 shows the same comparison as Figure 5.6 except that in this case  $\alpha_0$  is one degree instead of zero. This is shown to increase the range of dynamic pressures over which the morphing flap requires less work than the conventional flap. This influence of  $\alpha$  on the comparison between the work required for morphing and conventional flaps was also observed in Section 3.7.

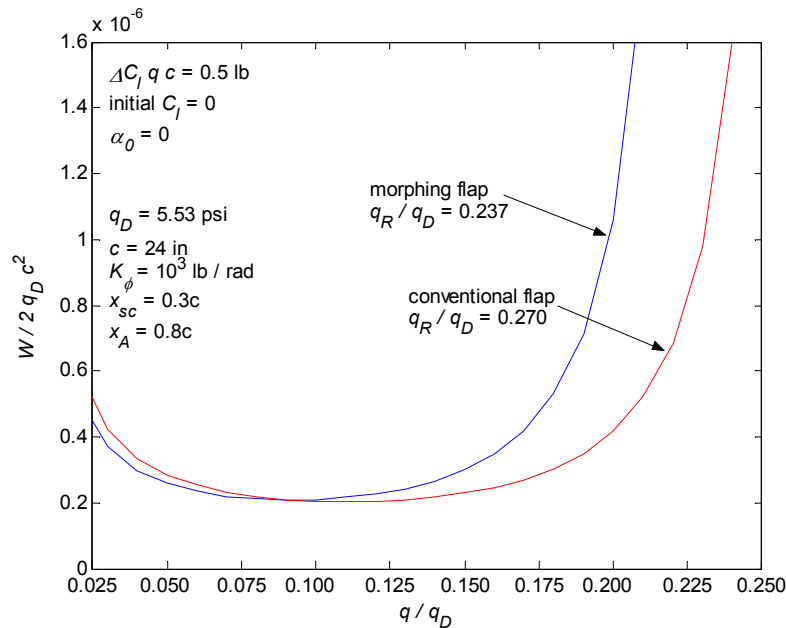


Figure 5.6: The effect of dynamic pressure on the required aerodynamic work for a given  $\Delta C_l q c$

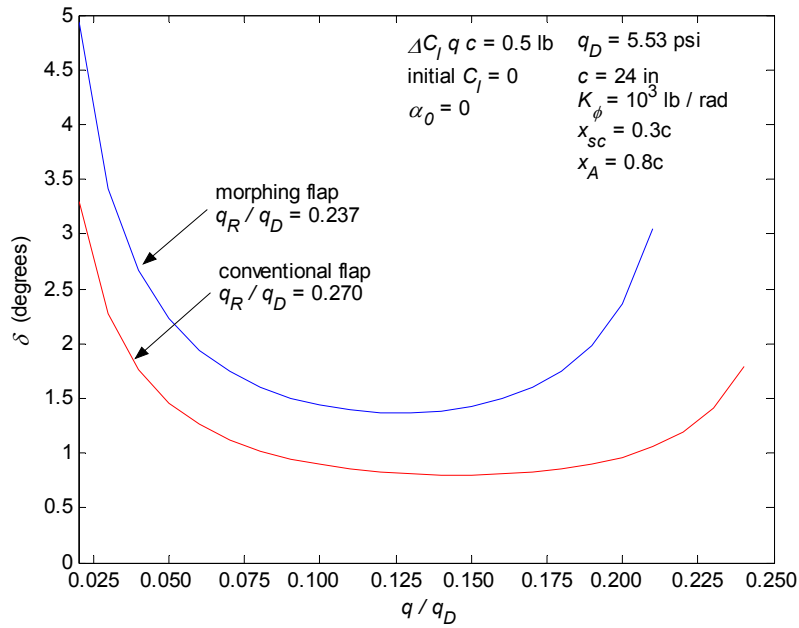


Figure 5.7: The effect of dynamic pressure on the deflection angle for a given  $\Delta C_l q c$

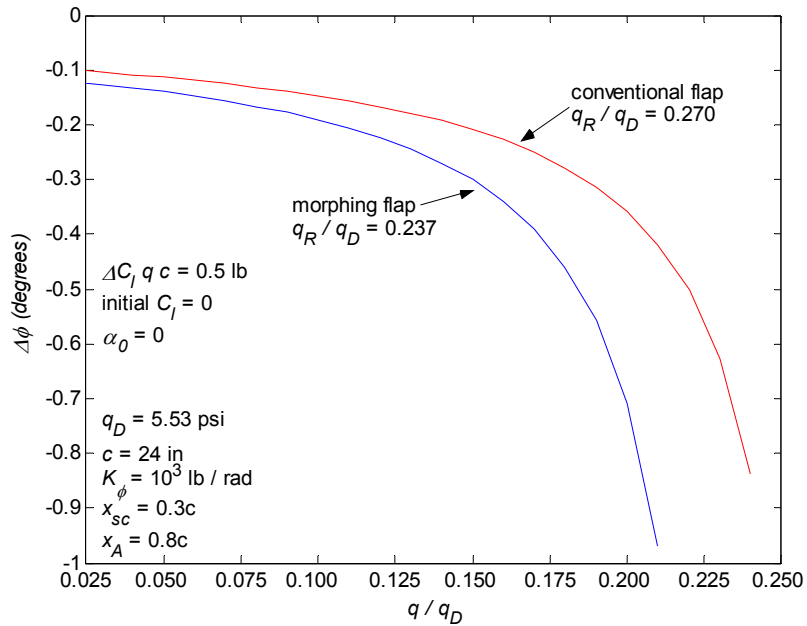


Figure 5.8: The effect of dynamic pressure on the wing deformation angle for a given  $\Delta C_l q c$

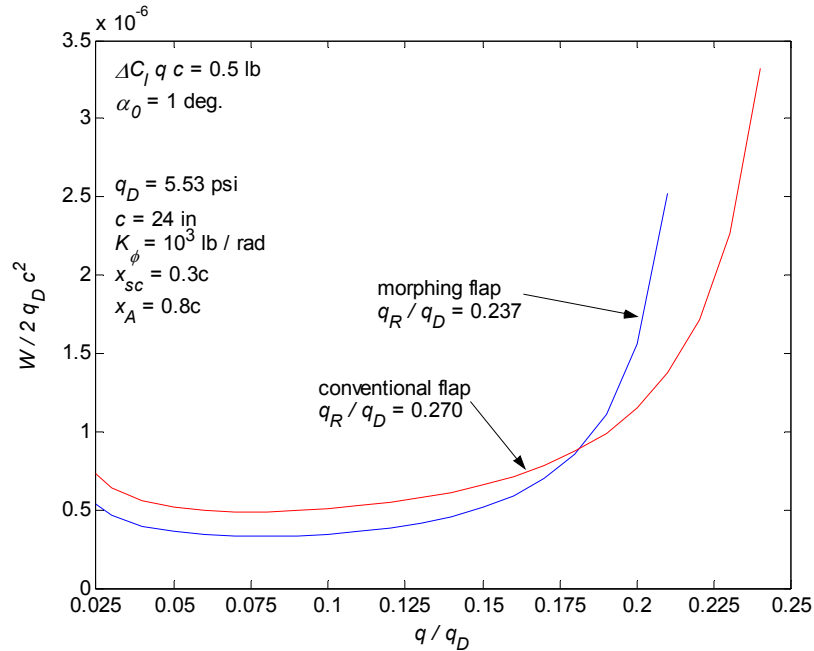


Figure 5.9: The effect of dynamic pressure on the work for a given  $\Delta C_l q c$  at  $\alpha_0 = 1$  degree

## 5.4 Required Work for Multiple Control Surface Cases

This section compares the minimum work control deflections for two-segment morphing and conventional flaps. This was studied in Sections 4.2 and 4.3 for rigid airfoils. Figure 5.10 shows the resulting minimum work values for the case where  $\alpha_0$  is one degree. This shows that unlike the single control surface case, where the morphing flap began to require more work than the conventional case as  $q_R$  was approached, the morphing flap continues to require less work past  $q_R$ . Figure 5.11 shows the change in the wing deformation angle as  $q/q_D$  varies. It is seen that past the  $q_R$  of the dominant control surface (flap A for the morphing and conventional case), the wing deformation angle becomes positive indicating the airfoil is generating lift by twisting the wing with control surface deflections. Figures 5.12 and 5.13 confirm this by showing negative control deflections past the  $q_R$  of control surface A ( $q_{R,A}$ ). Because the airfoil has a nonzero  $\alpha_0$ , the negative control deflections can be achieved with no work. Notice that in Figures 5.12 and 5.13 that  $\delta_A$  goes to zero at  $q_{R,A}$  but  $\delta_B$  does not go to zero at  $q_{R,B}$ . Why would a nonzero deflection be found for a control surface that creates no change in lift if it desired to minimize the work? The answer to this is that although at  $q_{R,B}$  control surface B is not capable of creating lift, it is useful for reducing the work required for control surface A. Figures 5.12 and 5.13 show that this is

exactly what is being done here, with the negative value of  $\delta_B$ , which requires no work because of the  $\alpha_0$ , reducing the work required for flap A.

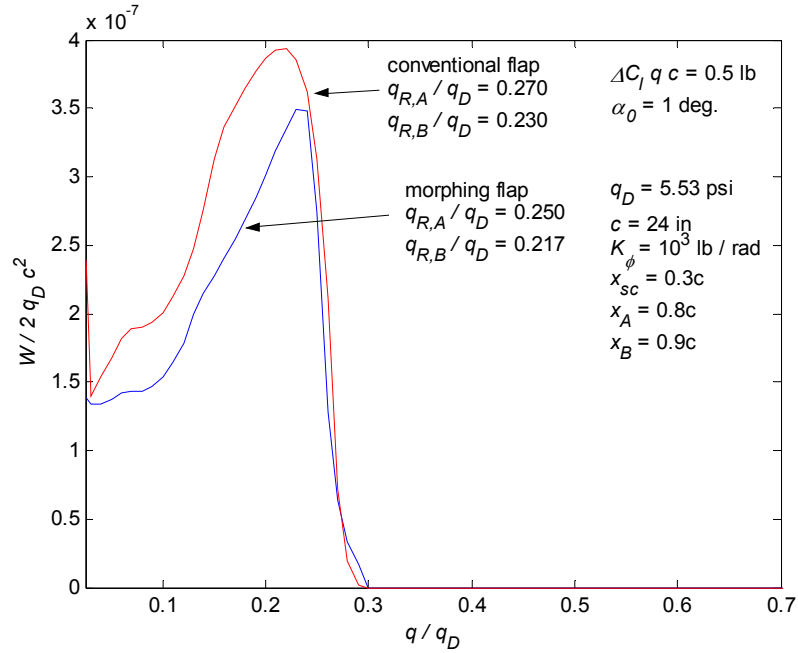


Figure 5.10: The effect of dynamic pressure on the required work with multiple control surfaces

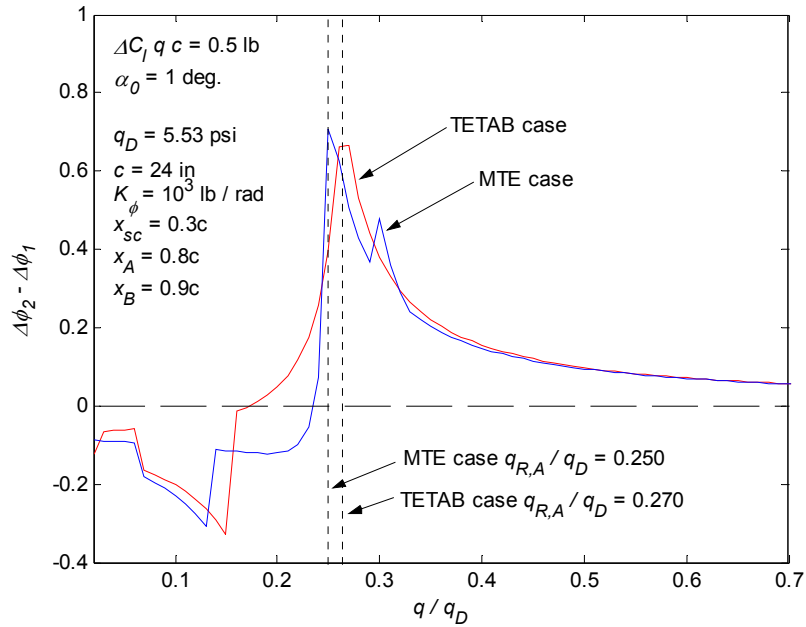


Figure 5.11: The effect of dynamic pressure on the deformation with multiple control surfaces

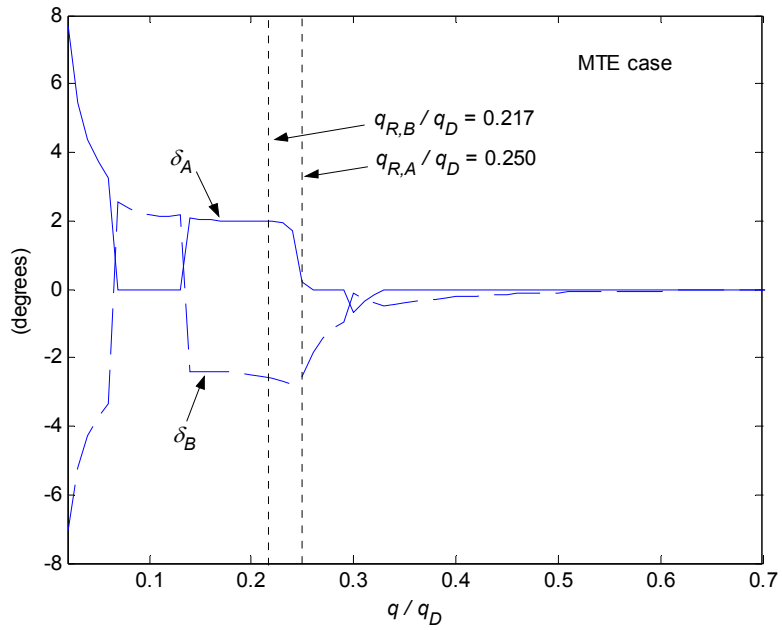


Figure 5.12: The effect of dynamic pressure on the minimum work control deflections

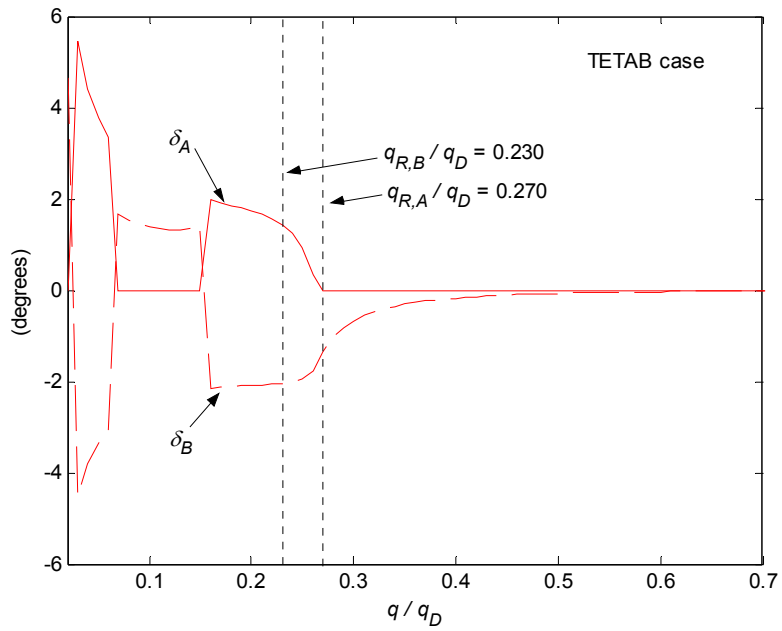


Figure 5.13: The effect of dynamic pressure on the minimum work control deflections

## 5.5 Chapter Summary

Chapter 5 presents the effect of a 1-DOF static aeroelastic model on the actuator work requirements for morphing and conventional flap airfoils. It is shown in Figures 5.6 and 5.9 that the work becomes very large as the reversal dynamic pressure ( $q_R$ ) is approached. At low dynamic pressures the morphing flap requires less work than the conventional flap. The dynamic pressure past which the conventional flap requires lower work is shown to depend on the initial lift acting on the airfoil.

A comparison of the minimum work required for two-segment morphing and conventional flaps is presented in Figure 5.10. This plot presents work values for dynamic pressures above and below  $q_R$ . The minimum work control deflections shown in Figures 5.12 and 5.13 indicate that around  $q_R$ , both control surfaces are used like with the leading and trailing edge configuration of the AAW.

# Chapter 6

## Conclusions

### 6.1 Brief Summary of Thesis

The first chapter provides an introduction to the concept of morphing aircraft. Past morphing concepts such as variable wing sweep and the AFTI/F-111 are discussed. It is emphasized that morphing allows for both the minimization of drag at multiple flight conditions as well improved maneuverability. A review of literature on the topic of aerodynamic work is presented. It is concluded that if aerodynamic work is to be used as a performance parameter for aerodynamic control devices, then a general theory must be developed that considers issues such as negative work and actuator placement. This task is the focus of Chapter 2.

Chapter 2 presents a method of calculating the mechanical work required from actuators to operate an aerodynamic control device. It is argued that it is really desired to calculate the energy “cost” of actuating an aerodynamic control device, and not the required mechanical work. This leads to calculation of the practical work ( $\mathcal{W}$ ), which is related to the straightforward work ( $\overline{\mathcal{W}}$ ) through Eq. (2.10). The term  $\eta$  in Eq. (2.10), which represents the difference in the cost of positive and negative work, defines the relationship between  $\overline{\mathcal{W}}$  and  $\mathcal{W}$ . The remainder of this study uses a value of  $\eta = 0$ , which implies that energy required by an actuator to perform negative work is zero. This is true because negative work means that the forces from the airstream and structure act in the same direction, therefore the forces required for initiating motion are supplied from the air-stream or the structure and not the actuator. An important consequence of treating negative and positive work as different quantities is that the structural and aerodynamic work

calculations cannot be performed independently. This is because the interaction of these two components determine when the work changes from positive to negative. The remainder of this thesis considered only the aerodynamic work component.

Chapter 3 applies thin airfoil theory to various control surface configurations to provide an aerodynamic model for the work calculation discussed in Chapter 2. Along with the usual calculation of the aerodynamic coefficients using the first three Fourier coefficients (Eqs. (3.3 - 3.8)), analytic solutions for the aerodynamic load distribution are found using Eq. (3.11). The determination of analytic equations for the aerodynamic load distribution is convenient for the application of the work equations developed in Chapter 2. These equations also provide insight into the effect of various control surface parameters on aerodynamic load distribution. Section 3.7 shows that less work is required to obtain a  $\Delta C_l$  with a single-surface morphing flap than with a conventional flap. Figures 3.13 – 3.15 show that this is true because the  $\Delta z$  required for the morphing flap is less than for the conventional flap. It is also shown that because the morphing flap requires less  $\Delta z$ , the influence of an  $\alpha$ -dependent load distribution on the work is less than that for a conventional flap.

Chapter 4 presents a method for determining the control deflections that require the minimum aerodynamic work for a given  $\Delta C_l$ . This method is based on the work equations developed in Chapter 2 and the aerodynamic characteristics developed in Chapter 3. For an initially flat airfoil at zero- $\alpha$  with two control surfaces, Eq (4.4) was derived. This equation represents the minimum work control deflections for a given  $\Delta C_l$ . Figures 4.3 and 4.4 show that the TETAB configuration requires less work than the MTE configuration for cases where  $\alpha$  remains zero. Section 4.3 shows that there is certain  $\alpha$  past which the MTE case requires less work than the TETAB case. This is true because a given  $\delta$  for the MTE case produces much less  $\Delta z$  than for the TETAB case, which means that the  $\alpha$ -load distribution has a smaller influence on the minimum work for the MTE case. Section 4.4 discusses the minimum work for multiple  $\Delta C_l$ 's and shows that it is closely related to the minimum work for a single  $\Delta C_l$ .

Chapter 5 presents the effect of a 1-DOF static aeroelastic model on the aerodynamic work requirements for morphing and conventional flap airfoils. It is shown in Figures 5.6 and 5.9, that for single-segment morphing and conventional flaps, the work becomes very large as the reversal dynamic pressure ( $q_R$ ) is approached. At low dynamic pressures the morphing flap requires less

work than the conventional flap. The dynamic pressure past which the conventional flap requires lower work is shown to depend on the initial lift acting on the airfoil. A comparison of the minimum work required for two-segment morphing and conventional flaps is presented in Figure 5.10. This plot presents work values for dynamic pressures above and below  $q_R$ . At nearly every value of  $q$ , the morphing flap required less work than the conventional flap. The minimum work control deflections shown in Figures 5.12 and 5.13 indicate that around  $q_R$ , both control surfaces are used in the same manner as the leading and trailing edge configuration of the active aeroelastic wing.

## 6.2 Contributions

This thesis provides a method for calculating the work to overcome aerodynamic forces required to deflect a general configuration of aerodynamic control devices. Past research in this area, as discussed in Section 1.3, has not confronted many of the issues required to compare the work required for general control surface configurations. The method developed here relates the aerodynamic and structural forces acting on the control surface as it is deflecting to the energy cost required for the actuator to perform the deflection. A contribution of this thesis is that it provides a clarification of what is really desired from a work analysis on an airfoil control surface. It is not the mechanical work required for a control surface deflection that is of interest, but really the energy cost of the actuator operating the control surface. Without getting into the details of the actuators, the calculation of the energy cost of an actuator is achieved through Eq. (2.10). The significance of this equation is that it accounts for a difference between the energy cost required by an actuator to perform negative work from that required to perform positive work. By turning to physiologists [Abbott, *et al*, 1952], who have studied the cost of negative work for animal muscles (which can be considered very advanced actuators), a value of  $\eta = 0$  was found to accurately represent most actuators. An important contribution of this work was recognizing that positive and negative work values should be treated differently in the calculation of the work required by a control surface. With the assumption of a linear aerodynamic and structural model, the details of calculating the energy cost for a general control surface configuration are presented. This is new in that it accounts for the difference between positive and negative work values, which allows for a simple and general method of calculating the actuator energy cost.

It appears that the equations obtained in Chapter 3 from thin airfoil theory for the load distributions for quadratic camberlines (including NACA camberlines) are absent from the literature. This may be because thin airfoil theory has been mainly used for the lift and pitching moment coefficients, which can be obtained from the simple calculation of the first three Fourier coefficients defined in Eqs. (3.3 – 3.5). And, it seems that the load distribution calculation is usually represented by the infinite series of Eq. (3.1) instead of the integral of Eq. (3.11). In any case, these analytic equations for the load distribution are valuable for the application of the work equations developed in Chapter 2, as well as many other aerodynamic analyses.

### **6.3 Future Work**

There are four main extensions to this work that would make it a more accurate representation of reality. The first of these is the use of unsteady thin airfoil theory to model the aerodynamic load distribution during the control surface motion. There does not seem to be a large amount of literature investigating the unsteady forces on an airfoil during the control surface motion. For example, what is the time-history of the hinge moment on a flap as it is deflecting from 0 to 5 degrees? The second extension of this work is the addition of a boundary layer calculation. This would allow for both viscous drag and flow separation to be predicted. The influence of different control surface configurations on the viscous drag and location of flow separation would be very interesting and useful. The addition of unsteady aerodynamics and viscous effects will likely result in load distributions that are no longer linear with respect to the control surface motion. This would require the work equations developed in Sections 2.3 and 2.4 to be generalized. The third extension of this work is the addition of a structural model. Although structural work terms are included in Chapter 2, the analysis of Chapters 4 and 5 consider only the aerodynamic work term. Extending this analysis to three-dimensional wings would allow for spanwise distributions of control surface deflections to be investigated. The aerodynamics would have to be modeled with a numerical method such as the vortex-lattice method instead of thin airfoil theory.

# References

Abbott, B. C., Bigland, B., and Ritchie, J. M., “The Physiological Cost of Negative Work,” *Journal of Physiology*, Vol. 117, July 1952, pp. 380-390.

Abbott, I. H., and Von Doenhoff, A. E., *Theory of Wing Sections*, Dover, 1959, pp. 385.

Allen, H. J., “General Theory of Airfoil Sections Having Arbitrary Shape or Pressure Distribution,” NACA Report No. 833, 1943.

Anderson, G., Forster, E., Kolonay, R., and Eastep, F., “Multiple Control Surface Utilization in Active Aeroelastic Wing Technology,” *Journal of Aircraft*, Vol. 34, July-August 1997, pp. 552-557.

Blikhan, R., and Cheng, J., “Energy Storage by Elastic Mechanisms in the Tail of Large Swimmers – a Re-evaluation,” *Journal of Theoretical Biology*, Vol. 168, 1994, pp. 315-321.

Bonnema, K. L, and Smith, S. B., “AFTI/F-111 Mission Adaptive Wing Flight Research Program,” AIAA Paper 88-2118, 1988.

Culick, F. E. C., “The Wright Brothers: First Aeronautical Engineers and Test Pilots,” *AIAA Journal*, Vol. 41, June 2003, pp. 985-1006.

Forster, E., Sanders, B., and Eastep, F., “Synthesis of a Variable Geometry Trailing Edge Control Surface,” AIAA Paper 2003-1717, April 2003.

Forster, E., Sanders, B., and Eastep, F., "Modeling and Sensitivity Analysis of a Variable Geometry Trailing Edge Control Surface," AIAA Paper 2003-1807, April 2003.

Fulghum, D. A., "Pentagon Eyes Quadrupling UAV Force by 2010," *Aviation Week and Space Technology*, February 17, 2003, pp. 35-36.

Gern, F. H., Inman, D. J., and Kapania, R. K., "Computation of Actuation Power Requirements for Smart Wings with Morphing Airfoils," AIAA Paper 2002-1629, April 2002.

Glauert, H., *The Elements of Aerofoil and Airscrew Theory*, 2<sup>nd</sup> Edition, Cambridge University Press, 1947.

Gradshteyn, I. S., and Ryzhik, I. M., *Tables of Integrals Series and Products*, Academic Press, New York and London, 1965, pp. 148.

Greff, E., "The Development and Design Integration of a Variable Camber Wing for Long/Medium Range Aircraft," *Aeronautical Journal*, Vol. 94, November 1990, pp. 301-312.

Henderson, J. A., Weisshaar, T. A., and Sanders, B. "Integrated Wing Design with Adaptive Control Surfaces," AIAA Paper 2001-1428, April 2001.

Herbst, W. B., and Krogull, B., "Design for Air Combat," *Journal of Aircraft*, Vol. 10, April 1973, pp 247-253.

Herbst, W. B., "Future Fighter Technologies," *Journal of Aircraft*, Vol. 17, August 1980, pp 561-566.

Herbst, W. B., "Dynamics of Air Combat," *Journal of Aircraft*, Vol. 20, July 1983, pp 594-599.

Kress, R. W., "Variable Sweep Wing Design," AIAA Paper 83-1051, 1983.

Johnston, C. O., *et al.* "A Model to Compare the Flight Control Energy Requirements of Morphing and Conventionally Actuated Wings," AIAA Paper 2003-1716, 2003.

Luiz Martins, A., and Catalano, F. M., "Aircraft Induced Drag Minimization Using a Constrained Optimization Method," ICAS-96-7.10.3, Italy 1996.

Luiz Martins, A., and Catalano, F. M., "Theoretical Study of a Mission Adaptive Wing," ICAS-96-7.3.3, Italy 1996.

Luiz Martins, A., and Catalano, F. M., "Drag Aerodynamic Optimization Study of a Mission Adaptive Wing for Transport Aircraft," AIAA Paper 97-2272, 1997.

Luiz Martins, A., and Catalano, F. M., "Drag Optimization for Transport Aircraft Mission Adaptive Wing," AIAA Paper 2000-0648, January 2000.

Miller, G. D., "An Active Flexible Wing Multi-Disciplinary Design Optimization Method," AIAA Paper 94-4412, 1994.

Monner, H. P., "Realization of an optimized wing camber by using formvariable flap structures," *Aerospace Sciences and Technology*, Vol. 5, 2001, 445-455.

Munk, M. M., "General Theory of Thin Wing Sections," NACA Report No. 142, 1923.

Nielson, K. S., "Locomotion: Energy Cost of Swimming, Flying, and Running," *Science*, Vol. 177, July 1972, pp. 222-228.

Pettit, G. W., Robertshaw, H. H., Gern, F. H., and Inman, D. J., "A Model to Evaluate the Aerodynamic Energy Requirements of Active Materials in Morphing Wings," 2001 ASME Design Engineering Technical Conference, September 2001.

Pinkerton, R. M., "Calculated and Measured Pressure Distributions over the Midspan Section of the NACA 4412 Airfoil," NACA Report No. 563, 1936.

Prock, B. C., Weisshaar, T. A., and Crossley, W. A., "Morphing Airfoil Shape Change Optimization with Minimum Actuator Energy as an Objective," AIAA Paper 2002-5401, September 2002.

Raymond, E. T., Chenoweth, C. C., *Aircraft Flight Control Actuation System Design*, Society of Automobile Engineers, 1993.

Renken, J. H., "Mission Adaptive Wing Camber Control Systems," AIAA Paper 85-5006, 1985.

Sanders B., Eastep, F. E., and Forster, E., "Aerodynamic and Aeroelastic Characteristics of Wings with Conformal Control Surfaces for Morphing Aircraft," *Journal of Aircraft*, Vol. 40, Jan.-Feb. 2003, pp. 94-99.

Smith, B. A., "AFTI/F-111 Flight Tests Demonstrate Potential of Mission Adaptive Wing," *Aviation Week and Space Technology*, November 24, 1986, pp. 40-41.

Smith, F. R., Harshberger, G. W., and Ujcik, V. G., "AFTI/F-111 Performance Flight Test Summary," SAE Paper 871881, 1987.

Smith, S. B., and Nelson, D. W., "Determination of the Aerodynamic Characteristics of the Mission Adaptive Wing," *Journal of Aircraft*, Vol. 27, Nov. 1990, pp. 950-958.

Spence, D. A., "The Lift on a Thin Airfoil with a Jet-Augmented Flap," *Aeronautical Quarterly*, Vol. 9, Aug. 1958, pp. 287-299.

Spillman, J. J., "The Use of Variable Camber to Reduce Drag, Weight and Costs of Transport Aircraft," *Aeronautical Journal*, Vol. 96, January 1992, pp. 1-9.

Stanewsky, E., "Aerodynamic Benefits of Adaptive Wing Technology," *Aerospace Sciences and Technology*, Vol. 4, 2000, pp. 439-452.

Stanewsky, E., "Adaptive Wing and Flow Control Technology," *Progress in Aerospace Sciences*, Vol. 37, 2001, pp. 583-667.

Szodruch, J., "The Influence of Camber Variation on the Aerodynamics of Civil Transport Aircraft," AIAA Paper 85-0353, 1985.

Theodorsen, T., "On the Theory of Wing Sections with Particular Reference to the Lift Distribution," NACA Report No. 383, 1931.

Tucker, V. A., "Aerodynamics and Energetics of Vertebrate Fliers," in *Swimming and Flying in Nature*, Vol. 2, Edited by Wu, Y. T., Brokaw, C. J., and Brennen, C., Plenum Press, 1975, pp. 845-867.

Tucker, V. A., and Parrott, G. C., "Aerodynamics of Gliding Flight in a Falcon and Other Birds," *Journal of Experimental Biology*, Vol. 52, 1970, pp. 345-367.

Waaland, I. T., "Technology in the Lives of an Aircraft Designer," 1991 Wright Brothers Lecture, AIAA Aircraft Design and Operations Meeting, 1991.

Weisshaar, T. A., "Control Effectiveness (Lecture 8)," AAE 556: Aeroelasticity, Purdue University, 2000, <http://roger.ecn.purdue.edu/~aae556/lecture8/lecture8.html>.

Wlezien, R. W., *et al.*, "The Aircraft Morphing Program," AIAA paper 98-1927, 1998.

# Appendix A

MATLAB code to calculate the aerodynamic work and aerodynamic properties of the MTE airfoil defined in Section 3.7.

```
%%%%%%%%%%%%%%%%%%%%%%%%%%%%%%%%%%%%%%%%%%%%%%%%%%%%%%%%%%%%%%%%%%%%%%%%%
% Input
%%%%%%%%%%%%%%%%%%%%%%%%%%%%%%%%%%%%%%%%%%%%%%%%%%%%%%%%%%%%%%%%%%%%%%%%%

% Considers the change from state 1 to state 2 and then to state 3. If only
% one change is of interest, make Cl3=Cl2, A_delta3=A_delta2, and
% alpha3=alpha2. Cl1 is implied through A_delta1, B_delta1, and alpha1.

% lift coefficient at state 2
Cl2=0.1;
% lift coefficient at state 3
Cl3=0.1;

% initial deflection of flap A (radians)
A_delta1=0*pi/180;

% initial deflection of flap B (radians)
B_delta1=0;

% deflection of flap A at state 2 (radians)
A_delta2=0;

% deflection of flap A at state 3 (radians)
A_delta3=0;
```

```

% angle of attack at state 1 (radians)
alpha1=0;

% angle of attack at state 2 (radians)
alpha2=0;

% angle of attack at state 3 (radians)
alpha3=0;

% start of flap A (x/c), see Figure 3.12
xA=.6;

% start of flap B (x/c), see Figure 3.12
xB=.8;

%%%%%%%%%%%%%%%%%%%%%%%%%%%%%%%%%%%%%%%%%%%%%%%%%%%%%%%%%%%%%%%%%%%%%%%%
%%%%%%%%%%%%%%%%%%%%%%%%%%%%%%%%%%%%%%%%%%%%%%%%%%%%%%%%%%%%%%%%%%%%%%%%
thetab1=acos(1-2*xA);
thetab2=acos(1-2*xB);

% Eq. (3.53) - per-radian of flap deflection A and B
a1_A = -1/(-2*xA + 2*xB);
a2_B = -(-1)/(-2 + 2*xB);
b1_A = -(1*xA)/(xA - xB);
b2_A = -(-1 + (1)*xB)/(-1 + xB);
b2_B = -((1)*xB)/(-1 + xB);
c1_A = -(1*xA^2)/(-2*xA + 2*xB);
c2_A = -(((1)*xB^2) + 1*(xA + xB - xA*xB))/(2*(-1 + xB));
c2_B = -(((1)*xB^2))/(2*(-1 + xB)) ;

% Eq. (3.54) - per-radian of flap deflection A and B
A0_A=-1/pi*((a1_A+b1_A)*(thetab2-thetab1)-a1_A*(sin(thetab2)-sin(thetab1))...
+b2_A*(pi-thetab2));
A1_A=2/pi*((a1_A+b1_A)*(sin(thetab2)-sin(thetab1))-a1_A/2*((thetab2-thetab1)...

```

```

+1/2*(sin(2*thetab2)-sin(2*thetab1)))+(b2_A)*(-sin(thetab2)));
A2_A=2/pi*(.5*(a1_A+b1_A)*(sin(2*thetab2)-sin(2*thetab1))-a1_A*((sin(thetab2)...
-sin(thetab1))/2+(sin(3*thetab2)-sin(3*thetab1))/6)-.5*(b2_A)*sin(2*thetab2));

A0_B=-1/pi*(a2_B*(pi-thetab2)+b2_B*(pi-thetab2)+a2_B*sin(thetab2));
A1_B=2/pi*((a2_B+b2_B)*(-sin(thetab2))-a2_B/2*((pi-thetab2)-.5*sin(2*thetab2)));
A2_B=2/pi*(-.5*(a2_B+b2_B)*sin(2*thetab2)+a2_B*(sin(thetab2)/2+sin(3*thetab2)/6));

```

```

% Eq. (3.6 - 3.8) - per-radian of flap deflection A and B

```

```

Cm_B=pi/4*(A2_B-A1_B);
Cl_B=pi*(2*A0_B+A1_B);

```

```

Cm_A=pi/4*(A2_A-A1_A);
Cl_A=pi*(2*A0_A+A1_A);

```

```

% Defined in Eq. (3.55)

```

```

SA=-(0.5-xA)/(xB-xA);
SB=-(xB-0.5)/(xB-1);
TA=0.5/(xB-xA);
TB=-0.5/(xB-1);
RA=-1;
RB=(0.5-xB)/(xB-1);

```

```

% Calculates the gamma distribution per-radian of flap deflection A and B

```

```

% (Eq. 3.55)

```

```

x=.001:.001:1-.001;
theta=acos(1-2*x);

```

```

gammaAb=2/pi*(TA*(thetab2-thetab1)*sin(theta)...
+(SA+TA*cos(theta)).*(log((sin(theta)*tan(thetab2/2)...
-cos(theta)+1)/(sin(theta)*tan(thetab2/2)+cos(theta)-1))...
-log((sin(theta)*tan(thetab1/2)-cos(theta)+1)/(sin(theta)*tan(thetab1/2)...

```

```

+cos(theta)-1))+log((sin(theta)*tan(thetab2/2)-cos(theta)...
+1)/(sin(theta)*tan(thetab2/2)+cos(theta)-1)));

gammaAa=-2/pi*(SA*(thetab2-thetab1)+TA*(sin(thetab2)-sin(thetab1))...
+RA*(pi-thetab2))*((1+cos(theta))/sin(theta));

gammaBb=2/pi*(TB*(pi-thetab2)*sin(theta)-(SB+...
TB*cos(theta)).*log((sin(theta)*tan(thetab2/2)-cos(theta)+...
1)/(sin(theta)*tan(thetab2/2)+cos(theta)-1)));

gammaBa=-2/pi*(-TB*(sin(thetab2))+RB*(pi-thetab2))*((1+...
cos(theta))/sin(theta));

%%%%%%%%%%%%%%%%%%%%%%%%%%%%%%%%%%%%%%%%%%%%%%%%%%%%%%%%%%%%%%%%%%%%%%%%
% Calculates the Q-terms defined in Eq. (2.18)
%%%%%%%%%%%%%%%%%%%%%%%%%%%%%%%%%%%%%%%%%%%%%%%%%%%%%%%%%%%%%%%%%%%%%%%%
x01=xA+.001:.001:xB-.001;
theta01=acos(1-2*x01);

fA1=-1/8*(1-cos(theta01)).^2./(xB-xA)-1/2*(1-cos(theta01))*xA/(xA-xB)-...
.5*xA^2/(xB-xA); % from Eq. (3.56)

% Integrals performed numerically
Q_A_A_a1=trapz(theta01,-2/pi*(SA*(thetab2-thetab1)+TA*(sin(thetab2)-sin(thetab1))...
+RA*(pi-thetab2))*((1+cos(theta01))/sin(theta01)).*(-1/8*(1-...
cos(theta01)).^2./(xB-xA)-1/2*(1-cos(theta01))*xA/(xA-xB)...
-.5*xA^2/(xB-xA))*0.5.*sin(theta01) );

Q_A_B_a1=trapz(theta01, -2/pi*(-TB*(sin(thetab2))+RB*(pi-thetab2))*((1+...
cos(theta01))/sin(theta01)).*(-1/8*(1-cos(theta01)).^2./(xB-xA)-1/2*(1-...
cos(theta01))*xA/(xA-xB)-.5*xA^2/(xB-xA))*0.5.*sin(theta01) );

Q_A_alpha1=trapz(theta01,2*(1)*((1+cos(theta01))/sin(theta01)).*(-1/8*(1-...
cos(theta01)).^2./(xB-xA)-1/2*(1-cos(theta01))*xA/(xA-xB)-...

```

$$.5 * xA^2 / (xB - xA) * 0.5 * \sin(\theta_01) );$$

$$Q\_A\_A\_b1 = \text{trapz}(\theta_01, 2/\pi * (TA * (\theta_{b2} - \theta_{b1}) * \sin(\theta_01) + \dots \\ (SA + TA * \cos(\theta_01)) * \log((\sin(\theta_01) * \tan(\theta_{b2}/2) - \cos(\theta_01) + \dots \\ 1) / (\sin(\theta_01) * \tan(\theta_{b2}/2) + \cos(\theta_01) - 1)) - \dots \\ \log((\sin(\theta_01) * \tan(\theta_{b1}/2) - \cos(\theta_01) + \dots \\ 1) / (\sin(\theta_01) * \tan(\theta_{b1}/2) + \cos(\theta_01) - 1))) + \dots \\ \log((\sin(\theta_01) * \tan(\theta_{b2}/2) - \cos(\theta_01) + \dots \\ 1) / (\sin(\theta_01) * \tan(\theta_{b2}/2) + \cos(\theta_01) - \dots \\ 1))) * (-1/8 * (1 - \cos(\theta_01)) .^2 / (xB - xA) - 1/2 * (1 - \dots \\ \cos(\theta_01)) * xA / (xA - xB) - .5 * xA^2 / (xB - xA) * 0.5 * \sin(\theta_01)));$$

$$Q\_A\_B\_b1 = \text{trapz}(\theta_01, 2/\pi * (TB * (\pi - \theta_{b2}) * \sin(\theta_01) - \dots \\ (SB + TB * \cos(\theta_01)) * \log((\sin(\theta_01) * \tan(\theta_{b2}/2) - \dots \\ \cos(\theta_01) + 1) / (\sin(\theta_01) * \tan(\theta_{b2}/2) + \cos(\theta_01) - \dots \\ 1))) * (-1/8 * (1 - \cos(\theta_01)) .^2 / (xB - xA) - 1/2 * (1 - \dots \\ \cos(\theta_01)) * xA / (xA - xB) - .5 * xA^2 / (xB - xA) * 0.5 * \sin(\theta_01)));$$

$$x02 = xB + .001 : .001 : 1 - .001;$$

$$\theta_02 = \arccos(1 - 2 * x02);$$

$$fA2 = -.5 * (1 - \cos(\theta_02)) + .5 * (xB + xA); \text{ \% from Eq. (3.56)}$$

$$fB = 1/8 * (1 - \cos(\theta_02)) .^2 / (xB - 1) - 1/2 * (1 - \cos(\theta_02)) * xB / (xB - 1) + \dots$$

$$.5 * xB^2 / (xB - 1); \text{ \% from Eq. (3.56)}$$

$$Q\_A\_A\_a2 = \text{trapz}(\theta_02, -2/\pi * (SA * (\theta_{b2} - \theta_{b1}) + TA * (\sin(\theta_{b2}) \dots \\ - \sin(\theta_{b1})) + RA * (\pi - \theta_{b2})) * ((1 + \cos(\theta_02)) / \sin(\theta_02)) * (-\dots \\ .5 * (1 - \cos(\theta_02)) + .5 * (xB + xA)) * 0.5 * \sin(\theta_02) );$$

$$Q\_A\_B\_a2 = \text{trapz}(\theta_02, -2/\pi * (-TB * (\sin(\theta_{b2})) + RB * (\pi - \theta_{b2})) * ((1 + \dots \\ \cos(\theta_02)) / \sin(\theta_02)) * (-.5 * (1 - \cos(\theta_02)) + .5 * (xB + xA)) * 0.5 * \sin(\theta_02));$$

$$Q\_A\_alpha2 = \text{trapz}(\theta_02, 2 * (1) * ((1 + \cos(\theta_02)) / \sin(\theta_02)) * (-.5 * (1 - \dots \\ \cos(\theta_02)) + .5 * (xB + xA)) * 0.5 * \sin(\theta_02) );$$

$$Q\_A\_A\_b2 = \text{trapz}(\theta_2, 2/\pi * (TA * (\theta_2 - \theta_1) * \sin(\theta_2) + \dots \\ (SA + TA * \cos(\theta_2)) * \log((\sin(\theta_2) * \tan(\theta_2/2) - \cos(\theta_2) + \dots \\ 1) / (\sin(\theta_2) * \tan(\theta_2/2) + \cos(\theta_2) - 1)) - \log((\sin(\theta_2) * \tan(\theta_1/2) - \dots \\ \cos(\theta_2) + 1) / (\sin(\theta_2) * \tan(\theta_1/2) + \cos(\theta_2) - 1))) + \dots \\ \log((\sin(\theta_2) * \tan(\theta_2/2) - \cos(\theta_2) + 1) / (\sin(\theta_2) * \tan(\theta_2/2) + \dots \\ \cos(\theta_2) - 1))) * (-.5 * (1 - \cos(\theta_2)) + .5 * (x_B + x_A))^{0.5} * \sin(\theta_2) );$$

$$Q\_A\_B\_b2 = \text{trapz}(\theta_2, 2/\pi * (TB * (\pi - \theta_2) * \sin(\theta_2) - (SB + \dots \\ TB * \cos(\theta_2)) * \log((\sin(\theta_2) * \tan(\theta_2/2) - \cos(\theta_2) + \dots \\ 1) / (\sin(\theta_2) * \tan(\theta_2/2) + \cos(\theta_2) - 1))) * (-.5 * (1 - \dots \\ \cos(\theta_2)) + .5 * (x_B + x_A))^{0.5} * \sin(\theta_2) );$$

$$Q\_B\_A\_a = \text{trapz}(\theta_2, -2/\pi * (SA * (\theta_2 - \theta_1) + TA * (\sin(\theta_2) - \dots \\ \sin(\theta_1)) + RA * (\pi - \theta_2)) * ((1 + \cos(\theta_2)) / \sin(\theta_2)) * (1/8 * (1 - \dots \\ \cos(\theta_2))^{.2} / (x_B - 1) - 1/2 * (1 - \cos(\theta_2)) * x_B / (x_B - 1) + .5 * x_B^2 / (x_B - \dots \\ 1)) * 0.5 * \sin(\theta_2) );$$

$$Q\_B\_B\_a = \text{trapz}(\theta_2, -2/\pi * (-TB * (\sin(\theta_2)) + RB * (\pi - \theta_2)) * ((1 + \dots \\ \cos(\theta_2)) / \sin(\theta_2)) * (1/8 * (1 - \cos(\theta_2))^{.2} / (x_B - 1) - \dots \\ 1/2 * (1 - \cos(\theta_2)) * x_B / (x_B - 1) + .5 * x_B^2 / (x_B - 1)) * 0.5 * \sin(\theta_2) );$$

$$Q\_B\_alpha = \text{trapz}(\theta_2, 2 * (1 * ((1 + \cos(\theta_2)) / \sin(\theta_2)) * (1/8 * (1 - \dots \\ \cos(\theta_2))^{.2} / (x_B - 1) - 1/2 * (1 - \cos(\theta_2)) * x_B / (x_B - 1) + .5 * x_B^2 / (x_B - \dots \\ 1)) * 0.5 * \sin(\theta_2) );$$

$$Q\_B\_A\_b = \text{trapz}(\theta_2, 2/\pi * (TA * (\theta_2 - \theta_1) * \sin(\theta_2) + \dots \\ (SA + TA * \cos(\theta_2)) * \log((\sin(\theta_2) * \tan(\theta_2/2) - \cos(\theta_2) + \dots \\ 1) / (\sin(\theta_2) * \tan(\theta_2/2) + \cos(\theta_2) - 1)) - \dots \\ \log((\sin(\theta_2) * \tan(\theta_1/2) - \cos(\theta_2) + \dots \\ 1) / (\sin(\theta_2) * \tan(\theta_1/2) + \cos(\theta_2) - 1))) + \dots \\ \log((\sin(\theta_2) * \tan(\theta_2/2) - \cos(\theta_2) + \dots \\ 1) / (\sin(\theta_2) * \tan(\theta_2/2) + \cos(\theta_2) - \dots \\ 1))) * (1/8 * (1 - \cos(\theta_2))^{.2} / (x_B - 1) - 1/2 * (1 - \dots$$

$$\cos(\text{theta02}) * xB / (xB - 1) + .5 * xB^2 / (xB - 1) * 0.5 * \sin(\text{theta02});$$

$$Q\_B\_B\_b = \text{trapz}(\text{theta02}, 2/\pi * (TB * (\pi - \text{thetab2}) * \sin(\text{theta02}) - (SB + TB * \cos(\text{theta02})) * \log((\sin(\text{theta02}) * \tan(\text{thetab2}/2) - \cos(\text{theta02}) + 1) / (\sin(\text{theta02}) * \tan(\text{thetab2}/2) + \cos(\text{theta02}) - 1))) * (1/8 * (1 - \cos(\text{theta02}))^2 / (xB - 1) - 1/2 * (1 - \cos(\text{theta02})) * xB / (xB - 1) + .5 * xB^2 / (xB - 1)) * 0.5 * \sin(\text{theta02}));$$

$$Q\_A\_A = \text{real}(Q\_A\_A\_a1 + Q\_A\_A\_b1 + Q\_A\_A\_a2 + Q\_A\_A\_b2);$$

$$Q\_A\_B = \text{real}(Q\_A\_B\_a1 + Q\_A\_B\_b1 + Q\_A\_B\_a2 + Q\_A\_B\_b2);$$

$$Q\_B\_A = \text{real}(Q\_B\_A\_a + Q\_B\_A\_b);$$

$$Q\_B\_B = \text{real}(Q\_B\_B\_a + Q\_B\_B\_b);$$

$$Q\_A\_alpha = Q\_A\_alpha1 + Q\_A\_alpha2;$$

%%  
 %%%

$$B\_delta2 = (Cl2 - Cl\_A * A\_delta2 - 2 * \pi * alpha2) / Cl\_B;$$

$$B\_delta3 = (Cl3 - Cl\_A * A\_delta3 - 2 * \pi * alpha3) / Cl\_B;$$

% Applies Eq. (2.19) for each control surface for both Cl changes 12 and 23

$$\text{tau0\_A12} = -(Q\_A\_A * A\_delta1 + Q\_A\_B * B\_delta1 + Q\_A\_alpha * alpha1) / (Q\_A\_A * (A\_delta2 - A\_delta1) + Q\_A\_B * (B\_delta2 - B\_delta1) + Q\_A\_alpha * (alpha2 - alpha1));$$

$$\text{tau0\_B12} = -(Q\_B\_A * A\_delta1 + Q\_B\_B * B\_delta1 + Q\_B\_alpha * alpha1) / (Q\_B\_A * (A\_delta2 - A\_delta1) + Q\_B\_B * (B\_delta2 - B\_delta1) + Q\_B\_alpha * (alpha2 - alpha1));$$

$$\text{tau0\_A23} = -(Q\_A\_A * A\_delta2 + Q\_A\_B * B\_delta2 + Q\_A\_alpha * alpha2) / (Q\_A\_A * (A\_delta3 - A\_delta2) + Q\_A\_B * (B\_delta3 - B\_delta2) + Q\_A\_alpha * (alpha3 - alpha2));$$

$$\text{tau0\_B23} = -(Q\_B\_A * A\_delta2 + Q\_B\_B * B\_delta2 + Q\_B\_alpha * alpha2) / (Q\_B\_A * (A\_delta3 - A\_delta2) + Q\_B\_B * (B\_delta3 - B\_delta2) + Q\_B\_alpha * (alpha3 - alpha2));$$

```

I_A_0_12=(Q_A_A*A_delta1+Q_A_B*B_delta1+Q_A_alpha*alpha1)*(A_delta2-A_delta1);
I_B_0_12=(Q_B_A*A_delta1+Q_B_B*B_delta1+Q_B_alpha*alpha1)*(B_delta2-B_delta1);
I_A_1_12=(Q_A_A*A_delta2+Q_A_B*B_delta2+Q_A_alpha*alpha2)*(A_delta2-A_delta1);
I_B_1_12=(Q_B_A*A_delta2+Q_B_B*B_delta2+Q_B_alpha*alpha2)*(B_delta2-B_delta1);

```

```

I_A_0_23=(Q_A_A*A_delta2+Q_A_B*B_delta2+Q_A_alpha*alpha2)*(A_delta3-A_delta2);
I_B_0_23=(Q_B_A*A_delta2+Q_B_B*B_delta2+Q_B_alpha*alpha2)*(B_delta3-B_delta2);
I_A_1_23=(Q_A_A*A_delta3+Q_A_B*B_delta3+Q_A_alpha*alpha3)*(A_delta3-A_delta2);
I_B_1_23=(Q_B_A*A_delta3+Q_B_B*B_delta3+Q_B_alpha*alpha3)*(B_delta3-B_delta2);

```

```

% Applies Eq. (2.20) and (2.21)

```

```

if I_A_0_12<=0 & I_A_1_12 <=0

```

```

W_A_12=(Q_A_A*(A_delta2+A_delta1)+Q_A_B*(B_delta2+B_delta1)+Q_A_alpha*(alpha2+..
.
alpha1))*(A_delta2-A_delta1)/2;

```

```

elseif I_A_0_12>=0 & I_A_1_12 >=0

```

```

W_A_12=0;

```

```

elseif I_A_0_12<=0 & I_A_1_12 >=0

```

```

W_A_12=(Q_A_A*((A_delta2-A_delta1)*tau0_A12^2/2+A_delta1*tau0_A12)+...
Q_A_B*((B_delta2-B_delta1)*tau0_A12^2/2+B_delta1*tau0_A12)+...
Q_A_alpha*((alpha2-alpha1)*tau0_A12^2/2+alpha1*tau0_A12))*(A_delta2-A_delta1);

```

```

else

```

```

W_A_12=(Q_A_A*((A_delta2-A_delta1)*(1-tau0_A12^2)/2+A_delta1*(1-tau0_A12))...
+Q_A_B*((B_delta2-B_delta1)*(1-tau0_A12^2)/2+B_delta1*(1-tau0_A12))+...
Q_A_alpha*((alpha2-alpha1)*(1-tau0_A12^2)/2+...
alpha1*(1-tau0_A12)))*(A_delta2-A_delta1);

```

```

end

```

```

if I_B_0_12<=0 & I_B_1_12 <=0

```

```

W_B_12=(Q_B_A*(A_delta2+A_delta1)+Q_B_B*(B_delta2+B_delta1)+...
Q_B_alpha*(alpha2+alpha1))*(B_delta2-B_delta1)/2;

```

```

elseif I_B_0_12 >= 0 & I_B_1_12 >= 0
    W_B_12 = 0;
elseif I_B_0_12 <= 0 & I_B_1_12 >= 0
    W_B_12 = (Q_B_A * ((A_delta2 - A_delta1) * tau0_B12^2 / 2 + A_delta1 * tau0_B12) + ...
    Q_B_B * ((B_delta2 - B_delta1) * tau0_B12^2 / 2 + B_delta1 * tau0_B12) + ...
    Q_B_alpha * ((alpha2 - alpha1) * tau0_B12^2 / 2 + alpha1 * tau0_B12)) * (B_delta2 - B_delta1);
else
    W_B_12 = (Q_B_A * ((A_delta2 - A_delta1) * (1 - tau0_B12^2) / 2 + A_delta1 * (1 - tau0_B12)) + ...
    Q_B_B * ((B_delta2 - B_delta1) * (1 - tau0_B12^2) / 2 + B_delta1 * (1 - tau0_B12)) + ...
    Q_B_alpha * ((alpha2 - alpha1) * (1 - tau0_B12^2) / 2 + alpha1 * (1 - ...
    tau0_B12))) * (B_delta2 - B_delta1);
end

if I_A_0_23 <= 0 & I_A_1_23 <= 0
    W_A_23 = (Q_A_A * (A_delta3 + A_delta2) + Q_A_B * (B_delta3 + B_delta2) + ...
    Q_A_alpha * (alpha3 + alpha2)) * (A_delta3 - A_delta2) / 2;
elseif I_A_0_23 >= 0 & I_A_1_23 >= 0
    W_A_23 = 0;
elseif I_A_0_23 < 0 & I_A_1_23 >= 0
    W_A_23 = (Q_A_A * ((A_delta3 - A_delta2) * tau0_A23^2 / 2 + A_delta2 * tau0_A23) + ...
    Q_A_B * ((B_delta3 - B_delta2) * tau0_A23^2 / 2 + B_delta2 * tau0_A23) + ...
    Q_A_alpha * ((alpha3 - alpha2) * tau0_A23^2 / 2 + alpha2 * tau0_A23)) * (A_delta3 - A_delta2);
else
    W_A_23 = (Q_A_A * ((A_delta3 - A_delta2) * (1 - tau0_A23^2) / 2 + ...
    A_delta2 * (1 - tau0_A23)) + Q_A_B * ((B_delta3 - B_delta2) * (1 - ...
    tau0_A23^2) / 2 + B_delta2 * (1 - tau0_A23)) + Q_A_alpha * ((alpha3 - alpha2) * (1 - ...
    tau0_A23^2) / 2 + alpha2 * (1 - tau0_A23))) * (A_delta3 - A_delta2);
end

if I_B_0_23 <= 0 & I_B_1_23 <= 0
    W_B_23 = (Q_B_A * (A_delta3 + A_delta2) + Q_B_B * (B_delta3 + B_delta2) + ...
    Q_B_alpha * (alpha3 + alpha2)) * (B_delta3 - B_delta2) / 2;
elseif I_B_0_23 >= 0 & I_B_1_23 >= 0
    W_B_23 = 0;

```

```

elseif I_B_0_23 <= 0 & I_B_1_23 >= 0
    W_B_23 = (Q_B_A * ((A_delta3 - A_delta2) * tau0_B23^2 / 2 + A_delta2 * tau0_B23) + ...
    Q_B_B * ((B_delta3 - B_delta2) * tau0_B23^2 / 2 + B_delta2 * tau0_B23) + ...
    Q_B_alpha * ((alpha3 - alpha2) * tau0_B23^2 / 2 + alpha2 * tau0_B23)) * (B_delta3 - B_delta2);
else
    W_B_23 = (Q_B_A * ((A_delta3 - A_delta2) * (1 - tau0_B23^2) / 2 + A_delta2 * (1 - ...
    tau0_B23)) + Q_B_B * ((B_delta3 - B_delta2) * (1 - tau0_B23^2) / 2 + B_delta2 * (1 - ...
    tau0_B23)) + Q_B_alpha * ((alpha3 - alpha2) * (1 - tau0_B23^2) / 2 + alpha2 * (1 - ...
    tau0_B23))) * (B_delta3 - B_delta2);
end

% The total practical work is:
W = (W_A_12 + W_A_23 + W_B_12 + W_B_23);

```